

UC Irvine

UC Irvine Electronic Theses and Dissertations

Title

Expansion of the bioluminescence toolkit for in vivo imaging

Permalink

<https://escholarship.org/uc/item/16c295pd>

Author

McCutcheon, David Clark

Publication Date

2015

Peer reviewed|Thesis/dissertation

UNIVERSITY OF CALIFORNIA,
IRVINE

Expansion of the bioluminescence toolkit for *in vivo* imaging

DISSERTATION

submitted in partial satisfaction of the requirements
for the degree of

DOCTOR OF PHILOSOPHY

in Chemistry

by

David Clark McCutcheon

Dissertation Committee:
Assistant Professor Jennifer A. Prescher, Chair
Associate Professor Elizabeth R. Jarvo
Professor Gregory A. Weiss

2015

Select figures and text from Chapter 1 © 2015 Springer-Verlag Berlin Heidelberg
Select figures and text from Chapter 2 © 2012 American Chemical Society
Select figures and text from Chapter 2 © 2015 Royal Society of Chemistry
Select figures and text from Chapter 3 © 2012 American Chemical Society
All other materials © 2015 David Clark McCutcheon

DEDICATION

To

my mother

Thank you for sending me down the right path

Small actions have profound effects.

For the simple act of returning a duffle bag full of suspicious chemicals to your adolescent son, shaped his future for years to come.

I am eternally grateful for your love and support.

I love you.

Your son, Charles.

TABLE OF CONTENTS

	Page
LIST OF FIGURES	iv
LIST OF SCHEMES	vi
CURRICULUM VITAE	vii
ABSTRACT OF THE DISSERTATION	x
CHAPTER 1: Optical tools to study biological processes	1
CHAPTER 2: Rapid and scalable assembly of firefly luciferase scaffolds	26
CHAPTER 3: Expedient synthesis of electronically modified luciferins	50
CHAPTER 4: Expedient synthesis of sterically modified luciferins	71
APPENDIX : NMR spectra	100

LIST OF FIGURES

	Page
Figure 1-1 Considerations for fluorescence imaging	3
Figure 1-2 Common optical probes used for tracking cell communication and function	6
Table 1-1 Luciferin and luciferases commonly used in bioluminescence imaging	6
Figure 1-3 Luciferase probes can be used to track cell populations and gene expression patterns in vivo	12
Figure 1-4 BRET probes can report on immune cell function	13
Figure 1-5 Collection of modified luciferin analogs that may be suitable for bioluminescence imaging	16
Figure 1-6 Immune cell interactions can be visualized with proximity reporters	19
Figure 2-1 Firefly luciferase (Fluc) catalyzes the oxidation of D-luciferin	28
Figure 2-2 Retrosynthetic analysis of D-luciferin	29
Figure 3-1 Retrosynthetic analysis of nitrogenous luciferin analogs	52
Figure 3-2 N-H tautomerization of benzimidazole	55
Figure 3-3 Light production from nitrogenous luciferin analogs	57
Table 3-1 Fluorescence emission for nitrogenous luciferin analogs	57
Figure 3-4 Prolonged bioluminescent light emission with nitrogenous analogs	58
Figure 3-5 Cellular imaging with luciferin analogs	59
Figure 3-6 Time-dependent light emission measured for nitrogenous analogs	60
Figure 4-1 Approach to develop orthogonal luciferin-luciferase pairs	71
Figure 4-2 Side chains within the Fluc active site are closest in proximity to the 4' and 7'-positions	75

Figure 4-3 Side reactivity of <i>o</i> -hydroxybenzaldehyde derivatives to form trioxa[3.3.1]nonanes	76
Figure 4-4 Retrosynthetic approach to sterically modify the 7'-position of luciferin using a modified Mannich reaction	78
Figure 4-5 Preliminary attempts to access 4'-sterically perturbed luciferin analogs by manipulation of existing functionality post-benzothiazole formation	80
Figure 4-6 Retrosynthetic S _N 2 approach to sterically modify the 4'-position of luciferin	81
Figure 4-7 Bioluminescence of a series of sterically perturbed luciferin analogs	83
Figure 4-8 Effect of pH on the bioluminescence of a series of 7'-benzylamino luciferin	84
Figure 4-9 Chemiluminescence reaction used to gauge luciferin light emitting ability	86
Figure 4-10: Chemiluminescence of a series of sterically perturbed luciferin analogs	86

LIST OF SCHEMES

	Page
Scheme 2-1 Intial synthetic route to D-luciferin	30
Scheme 2-2 Improved synthesis of D-luciferin	31
Scheme 2-3 Mild and efficient synthesis of monoaryl - dithiooxamide	32
Scheme 2-4 Synthesis of D-luciferin via Appel's salt condensation and thermolysis	33
Scheme 2-5 Synthesis of aminoluciferin	35
Scheme 3-1 Synthesis of nitrogenous luciferin scaffolds	53
Scheme 3-2 Synthesis of methylated benzimidazole analog	55
Scheme 4-1 Synthesis of 7'-formyl and 7'-hydroxymethyl luciferin	77
Scheme 4-2: Synthetic route to sterically encumbered 7'-benzylamino luciferin analogs	78
Scheme 4-3: Synthetic route to sterically encumbered 4'-benzylamino luciferins	82

CURRICULUM VITAE

David C. McCutcheon

Post-Doctoral Researcher
Chemistry, Engineering & Medicine for Human Health (ChEM-H)
Medicinal Chemistry Knowledge Center
Stanford University; Stanford, CA 94305-4125

Email: David.McCutch@gmail.com

EDUCATION AND TRAINING

Stanford University ; Stanford CA	2015–2017
University of California-Irvine ; Irvine, CA <i>Ph.D. Chemistry</i>	2008–2015
Youngstown State University ; Youngstown, OH <i>M.S. Chemistry</i>	2006–2008
Edinboro University of Pennsylvania ; Edinboro, PA <i>B.S. Chemistry (A.C.S. certified)</i>	2000–2005

RESEARCH EXPERIENCE

Stanford University ; Stanford, CA Post-Doctoral research Advisor: Mark Smith, PhD. and Professor Chaitan Khosla <u>Research</u> : Synthesis and structure-activity elucidation of novel therapeutics	2015–2017
University of California-Irvine ; Irvine, CA Doctoral research Advisor: Professor Jennifer A. Prescher <u>Research</u> : Expansion of the bioluminescence toolkit for <i>in vivo</i> imaging	2010–2015
University of California-Irvine ; Irvine, CA Doctoral research Advisor: Professor Scott D. Rychnovsky <u>Research</u> : Towards the total synthesis of amphidinol-3	2008–2010
Youngstown State University ; Youngstown, OH Masters research Advisor: Professor Peter Norris <u>Research</u> : Synthesis of UDP- <i>N</i> -acetyl-L-fucosamine analogs as inhibitors of the bacterial polysaccharide capsule	2006–2008
Case Western Reserve University ; Cleveland, OH Research assistant Advisor: Professor Anthony Berdis <u>Research</u> : Non-natural nucleotide incorporation during DNA replication	2005–2006

RESEARCH EXPERIENCE

Case Western Reserve University; Cleveland, OH 2003
Summer Undergraduate Research in Pharmacology
Advisor: Clark W. Distelhorst, M.D.
Research: Modulatory effects of dexamethasone and psychosine on T-cell death-associated gene-8 expression

PUBLICATIONS

[* denotes equal contribution]

11. McCutcheon, D. C.*; Steinhardt, R. C.*; Prescher, J. A. Chemistries for visualizing cell-cell communication. In “Visualizing chemical communication among migratory cells in vivo,” Eds (Springer): Contag, C. H. and Prescher, J. A. *In Review*.
10. McCutcheon, D. C.*; Porterfield, W. B. *; Jones, K. A.; Paley, M. A.; Rathbun, C.; Prescher, J. A. New luciferase-luciferin pairs for multi-parameter imaging. *In Preparation*.
9. Steinhardt, R. C.; Krull, B. T.; McCutcheon, D. C.; Rathbun, C.; Furche, F.; Prescher, J. A. Building better bioluminescent reporters via ab initio calculations. *In Preparation*.
8. McCutcheon, D. C.; Porterfield, W. B.; Prescher, J. A. Rapid and scalable assembly of firefly luciferase substrates. *Org. Biomol. Chem.* **2015**, *16*, 39.
7. Porterfield, W. B.; Jones, K. A.; McCutcheon, D. C.; Prescher, J. A. Imaging cell-cell contacts with “caged luciferins”. *In Revision*.
6. Steinhardt, R. C.; O’Neill J. M.; McCutcheon, D. C.; Paley, M. A.; Prescher, J. A. Rapid access to functionalized luciferins via click chemistry. *In Revision*.
5. McCutcheon, D. C.; Norris, P.; Zeller, M. 1,3,4-Tri-*O*-acetyl-2-*N*-(trifluoroacetyl)-*b*-L-fucose. *Acta Crystallogr., Sect. E: Struct. Rep. Online* **2013**, *70*, o134.
4. McCutcheon, D. C.; Paley, M. A.; Steinhardt, R. C.; Prescher, J. A. Expedient synthesis of electronically modified luciferins for bioluminescence imaging. *J. Am. Chem. Soc.* **2012**, *134*, 7604. *This work was featured in Angewandte Chemie.*
3. Alhassan, A.-B.; McCutcheon, D. C.; Zeller, M.; Norris, P. Azidonitration of di-*O*-acetyl-L-fucal: X-ray crystal structures of intermediate azidodeoxysugars and of the bacterial aminosugar *N*-acetyl-L-fucosamine. *J. Carbohydr. Chem.* **2012**, *31*, 371.
2. McCutcheon, D. C.; Norris, P.; Zeller, M. 3,4-Di-*O*-acetyl-2-azidodeoxy-1-*O*-nitro- α -L-fucose. *Acta Crystallogr., Sect. E: Struct. Rep. Online* **2007**, *63*, o3484.
1. Berdis, A. J.; McCutcheon, D. The use of non-natural nucleotides to probe template-independent DNA synthesis. *ChemBioChem* **2007**, *8*, 1399.

TEACHING EXPERIENCE

University of California-Irvine, Department of Chemistry; Irvine, CA

Prescher Lab Safety Officer

2010–2015

Graduate Student Instructor

Chemical Biology Lab (for advanced undergraduates)

Spring 2012, Winter 2013

Organic Synthesis Lab (for advanced undergraduates)

Spring 2010

Organic Chemistry Lab (for undergraduates)

Spring 2009, Fall 2009

Mentored: Brendan Zhang, graduate researcher

Fall 2013–Spring 2015

Jessica O'Neill, undergraduate researcher

Fall 2011–Spring 2013

Interned at Takeda Pharmaceutical Company

Youngstown State University, Department of Chemistry; Youngstown, OH

Graduate Student Instructor

Organic Chemistry Lab (for undergraduates),

Fall 2006, Fall 2007, Spring 2008

Biochemistry Lab (for undergraduates)

Spring 2007

Edinboro University of Pennsylvania, Department of Chemistry; Edinboro, PA

Laboratory Peer Mentor

Office for Students with Disabilities

General Chemistry (for undergraduate students)

Fall 2002, Spring 2003, Fall 2003

Biochemistry (for undergraduate students)

Fall 2003, Spring 2004

HONORS AND AWARDS

2012-2013

Allergan Scholar Fellowship

2015

University of California-Irvine Dissertation Fellowship

PRESENTATIONS

7. Modular synthesis of luciferin analogs for multi-component bioluminescence imaging. Gordon Research Conference (GRC) on Heterocycles, Salve Regina University, Newport, RI **2014**. (poster)
6. Expansion of the bioluminescence toolkit. 3rd annual Vertex Day Lecture, University of California, Irvine, Vertex Pharmaceuticals, Irvine, CA, **2013**. (oral)
5. Expedient synthesis of luciferin analogs for orthogonal bioluminescence imaging. University of California, Irvine, Pharmaceutical Science Department, Irvine, CA, **2012**. (poster)
4. Expedient synthesis of luciferin analogs for orthogonal bioluminescence imaging. University of California, Irvine, Institute for Immunology, Irvine, CA, **2012**. (poster)
3. Expedient synthesis of luciferin analogs for orthogonal bioluminescence imaging. National Meeting of the American Chemical Society, San Deigo, CA, **2012**. (poster)
2. Synthesis of *N*-2-modified analogs of *N*-acetyl-L-fucosamine. 40th Central Regional Meeting of the American Chemical Society, Columbus, OH, **2008**. (poster)
1. Towards mimics of UDP-*N*-acetyl-L-fucosamine. 39th Central Regional Meeting of the American Chemical Society, Covington, KY, **2007**. (poster)

ABSTRACT OF THE DISSERTATION

Expanding the bioluminescence toolkit for *in vivo* imaging

By

David Clark McCutcheon

Doctor of Philosophy in Chemistry

University of California, Irvine, 2015

Professor Jennifer A. Prescher, Chair

Bioluminescence imaging is among the most popular methods for visualizing biological processes *in vitro*, in live cells, and even in whole organisms. At the core of this technology are enzymes (luciferases) that catalyze the oxidation of small-molecule substrates (luciferins) to release visible light. Since cells and tissues do not normally emit significant numbers of visible photons, bioluminescence provides extremely high signal-to-noise ratios, making it well-suited for sensitive imaging applications. Indeed, this technology is routinely used to monitor cell trafficking networks, gene expression patterns, and drug delivery mechanisms *in vivo*. Despite its remarkable versatility, bioluminescence has been largely limited to monitoring one cell type or biological feature at a time. This is because only a handful of luciferases are suitable for biological work and, of these, nearly all utilize the same substrate (D-luciferin). Retooling bioluminescence technology for multicomponent imaging requires access to larger collections of light-emitting luciferins. Such molecules could potentially provide different colors of bioluminescent light or be utilized by novel luciferase variants. Unfortunately, luciferins have been notoriously difficult to produce, owing to a lack of rapid and reliable syntheses for these richly functionalized molecules. This dissertation develops and expedient method to prepare D-luciferin, along with new classes of light-emitting analogs.

CHAPTER 1: Optical tools to study biological processes

1.1 Introduction

Technologies have emerged within the imaging community that enable the non-destructive, real-time observation of dynamic cellular movements *in vivo*. Among the most popular of these approaches involve optical reporters [1–5]. Optical imaging tools are uniquely suited to visualize cellular communication in living organisms. These tools produce visible light that can report on cell motions and other behaviors [6–8]. Visible light is desirable for many *in vivo* applications owing to its non-toxicity (and thus biocompatibility). Wavelengths in the 380–750 nm realm (UV-vis) have been used for decades in cell microscopy experiments and *in vitro* assays to measure gene expression levels (Figure 1-1A). For imaging in live animals, though, more red-shifted light (>650 nm) is desirable. These wavelengths are less prone to absorption and scatter by endogenous chromophores and light, and can pass through tissues to be detected by sensitive cameras [9,10]. Mammalian tissues themselves emit few endogenous photons. Thus, optical probes can selectively report on a variety of cellular features. These probes—and how they have been used to understand biological processes—are the focus of this chapter.

For imaging *in vivo*, most optical agents can be categorized as fluorescent or bioluminescent probes. Fluorescent probes emit light following absorption of incident photons (Figure 1-1B), and can be further sub-divided into two classes: small molecules (fluorophores) and fluorescent proteins (FPs, Figure 1-1C). The bulk of FPs contain an internal chromophore produced from native amino acids upon protein folding [11]. For some FPs, the emission spectra are broad enough to include wavelengths that can escape tissue.

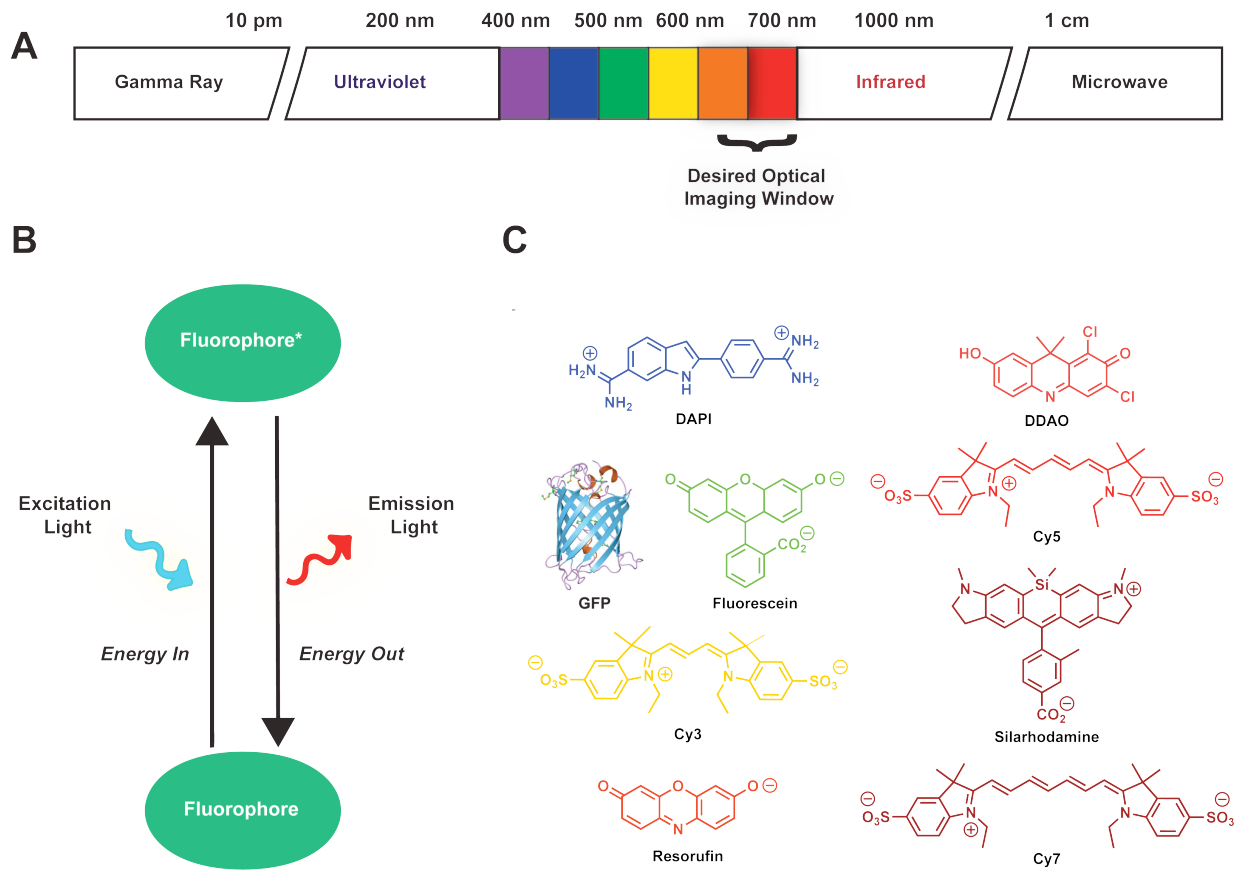


Figure 2-1: Considerations for fluorescence imaging. **(A)** The electromagnetic spectrum, with the desired window for *in vivo* optical imaging highlighted. **(B)** Fluorescent probes require excitation energy to emit light. Upon irradiation, the probes are electronically excited; relaxation to the ground state results in photon emission. **(C)** Examples of common fluorescent probes used for biological imaging.

Pushing these emission wavelengths farther into the red region is important for improved sensitivity and biocompatibility. Over the years, both targeted and random mutagenesis have been used to diversify the palette of fluorescent proteins [4,11–13]. Some fluorescent proteins now excite and emit light in the red/near-infrared regime and are broadly useful for noninvasive imaging in whole organisms.

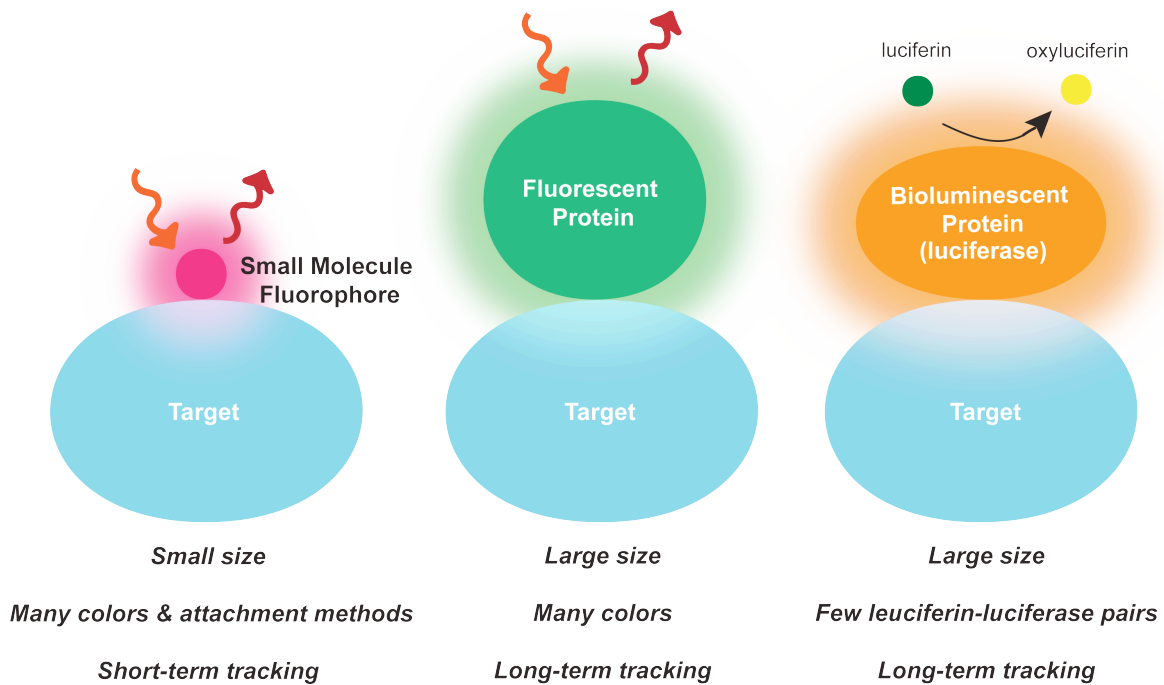
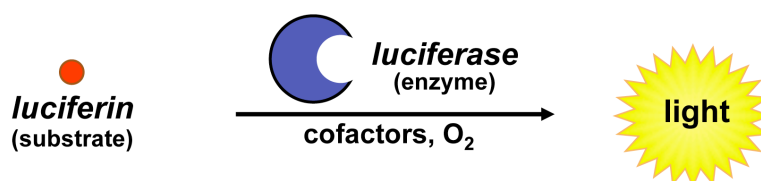
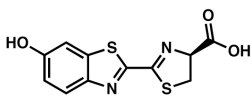
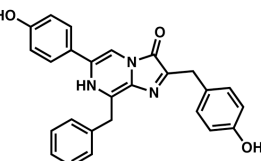
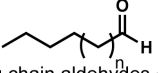
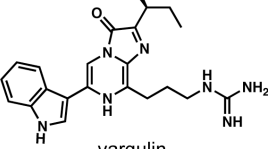


Figure 1-2: Common optical probes used for tracking cell communication and function. These include small molecule fluorophores, fluorescent proteins, and bioluminescent proteins (luciferases). Signature features of these probes are also listed.

A complementary set of optical imaging probes comprises bioluminescent enzyme-substrate pairs. Like fluorescence imaging, bioluminescence imaging (BLI) has been useful for examining cellular and biological features in live organisms. BLI relies on a class of enzymes (luciferases) that catalyze light emission using small molecule substrates (Figure 1-2). Several luciferase-luciferin pairs have been identified in nature. The most popular for *in vivo* imaging derive from the North American firefly, *Photinus pyralis* (Fluc) [3,14]. Fluc catalyzes the oxidation of the small molecule D-luciferin, and emits yellow-green light. Other well known luciferases derive from marine organisms, including *Renilla reniformis* (Rluc) and *Gaussia princeps* (Gluc). These enzymes catalyze the release of blue-green light using the small molecule coelenterazine (Table 1-1) [3,14]. Continued efforts to identify new luciferase-luciferin pairs in nature, and engineer non-natural ones, will expand the bioluminescent spectra. However, the variations in wavelength are not as dramatic as those for fluorescent molecules and dyes. This has somewhat limited the applicability of BLI for multi-component imaging [2,3].

Table 1-1: Luciferin and luciferases commonly used in bioluminescence imaging. Table 1-1 is reproduced with permission from Paley, M. A.; Prescher, J. A. *MedChemComm* **2014**, *5*, 255.



luciferase	luciferin	peak emission (nm) *	approximate size (kD)	comments
firefly luciferase (Fluc)	 D-luciferin	562	61	Largest percentage of >600 nm light emitted among classes of luciferases. Primarily used intracellularly due to requirement for ATP.
click beetle green (CB green)		537	61	
click beetle red (CB red)		613	61	
<i>Renilla reniformis</i> (Rluc/Rluc8)	 coelenterazine (CTZ)	482/487	36	All can be used extracellularly. Mutant versions (e.g., Rluc8/Rluc8.6/Gluc4) offer brighter and/or more sustained emission.
<i>Gaussia princeps</i> (Gluc)		482	20	
<i>Aequorea victoria</i> (Aequorin)		470	22	
Lux AB	 long chain aldehydes + FMN cofactor	480	A: 42 B: 47	Mostly limited to use in bacteria; lux operon (<i>luxCDABE</i>) encodes for all components necessary for light emission.
<i>Vargula hilgendorfii</i> (Vluc)	 vargulin	462	62	Recently characterized bioluminescent system; can be used in tandem with other luciferase-luciferin pairs.

1.2 Considerations for selecting an optical imaging modality

The photons produced by either fluorescent or bioluminescent probes must ultimately must be registered by a detector. Modern instrumentation offers a large linear range of photon detection [9] allowing very faint events [15] to be visualized in concert with relatively bright ones. In whole animal models, the number of photons reaching detector is influenced by overlying tissue and blood. Endogenous chromophores in these tissues and blood can both absorb and scatter light from the reporters. In general, the light reaching the detector falls off on a logarithmic scale with depth [9,10]. Transparent organisms avoid this problem; however, it can be limiting in studies that require mammalian tissues/organisms. In these latter cases, mathematical models can begin to deconvolute the diffusion of light within tissue [9,16]. Based on these considerations, the ideal range for light transmission through tissue is in the near infrared range (650 - ~950 nm). Shorter wavelengths are absorbed by endogenous chromophores (melanin, hemoglobin, etc.) Longer wavelengths are absorbed by water.

Fluorescence microscopy can be reliably used to visualize cells over hundreds of micrometers, enabling studies of cell-to-cell contact in explanted tissues and small distances in live animals [17,18]. Fluorescence imaging over longer distances or depths remains difficult, though, owing to autofluorescence issues. Fluorescence microscopy also requires that investigators know where to look, that is, where and when to shine the excitation light. The continued development of far-red emitting FPs is easing this requirement [19,20].

Imaging with bioluminescent probes, by contrast, does not rely on excitation light and can often be a better choice for imaging in thick tissues and animals. BLI has a very high signal-to-noise ratio, due to virtually no photons being produced in mammalian tissue. The most commonly used luciferases (from the insect family) release light in the 600-650 nm range.

While not absorbed well by hemoglobin, the wavelengths are still subject to the diffusive effect of scattering that occurs as light descends deeper into tissue. The deeper the imaging source, the poorer the resolution. Thus BLI and noninvasive macroscopic imaging, in general, is a tradeoff between sensitivity and resolution.

The current depth limit of bioluminescence imaging (BLI) using firefly luciferases/luciferins is ~1-2 cm, and it is possible to use this technology without knowing the location of the imaging target *a priori*. BLI also requires an exogenous substrate and this can be limiting, based on cost and accessibility, as well as the bioavailability of the substrate. Bioluminescent probes are typically used for macroscale imaging in whole animals (due to low background signals), but are weak emitters. By contrast, fluorescent probes are more suitable for microscopic imaging owing to their requirement for excitation light. In fact, fluorescent and bioluminescent tools are often used in tandem to gain information across all length scales.

Optical reporters must often track with the cells of interest, requiring chemical or genetic “attachment” to the imaging target. Historically, small molecule fluorophores have been used to track cells for short-term imaging. These tools span a large spectrum of excitation and emission wavelength combinations [21]. For reasons mentioned above, those fluorophores whose excitation and emission wavelengths occur in the NIR tissue transmission window are particularly useful for *in vivo* imaging [22–24]. In addition to the traditional small organic molecules, fluorescent nanoparticles and quantum dots may also be used for *in vivo* imaging applications [18, 25, 26]. Collectively, these tools can be appended covalently or non-covalently (DiI, DiR, etc.) to cell surfaces. For cell-targeting probes, the dyes are often attached to antibodies via bioconjugation chemistries [27,28].

When the reporter probe needs to be used for long-term, serial tracking, genetic “attachment” is often more desirable. Genes encoding fluorescent or bioluminescent proteins can be incorporated into cells and animals, and the optical signatures of their encoded proteins can “report” on desired biological process. Such genetic strategies can be used to mark cells or proteins for long-term visualization and monitor molecular events. Importantly, genetic tags propagate with cell division, providing stable sources of signal for longitudinal studies [29,30]. Genetic reporters can also be cloned into promoter regions of genes [31]. In these cases, reporter production mimics the transcription of the native gene in response to a cellular process. Several transgenic mice expressing these reporters are also readily available from commercial vendors.

1.3 Macroscale visualization of immune function with bioluminescent tools

Despite numerous advances in optical imaging over the past fifty years, our ability to resolve molecular and microscopic events in tissues and whole organisms remains limited. This is primarily due to the scattering of visible light by lipids and other biomolecules in opaque tissues, a phenomenon that broadens the area of signal perceived by the detector. Scattering can be partially ameliorated with physical methods, including mechanical disruption and dissolution [32], but these procedures are typically not compatible with serial imaging experiments requiring intact, living tissues. Intravital microscopy circumvents the need for disrupting tissue structures by placing the optical source and detector near the tissue of interest. Surgically implanted windows can further reduce interference from overlying tissues and resolve issues due to autofluorescence [17]. While providing unrivaled insight into microscopic cell interactions in living tissues, these techniques are invasive and not readily accessible to all researchers. Furthermore, these techniques require *a priori* knowledge of when and where to image. Where

fluorescence imaging techniques fall short, bioluminescence enables the imaging of long-distance and prolonged biological events *in vivo*.

Bioluminescence imaging (BLI) with luciferase-luciferin pairs is more suited to monitor biological processes in intact animals. Indeed, luciferase-labeled cells have been used to monitor cell trafficking patterns in diverse fields. Similar to microscopic imaging with FPs, several facets of immunology and methods for disease treatment have been monitored *in vivo* using BLI [33,34]. Improved luciferase reporters are enabling even more sensitive imaging in mouse models. Rabinovich and coworkers recently reported that as few as ten T-cells expressing an optimized luciferase can be imaged in some mouse models post-implantation [35]. This exquisite sensitivity has been capitalized on to track other immune cell classes, including NK cells homing to tumor stroma BLI [36]. Recently, the Negrin group examined the roles of regulatory T cells (Tregs) and natural killer T (NKT) in immune function (Figure 1-3A). Using adoptive transfer of luciferase-labeled CD4(+)NKT cells in a murine model of allogeneic hematopoietic cell transplantation (HCT) the authors monitored the migration of the cells first to lymphoid tissues then to graft-versus-host disease (GVHD) target tissues. GVHD entails donor cells attacking host tissue following transplantation. The study found that adoptively transferred NKT cells survive over 100 days and, unlike conventional T cells, do not cause significant GVHD-related morbidity or mortality. Furthermore, mixing in just 10,000 NKT cells to large boluses of T cells suppressed GVHD, demonstrating clinical potential in reducing GVHD in HCT [37]. While macroscale views of these cells could be readily gleaned, dissection and *ex vivo* analyses (with conventional fluorescent probes) were necessary to capture microscopic information.

The ability to sensitively visualize immune cell homing has similarly proved to be a tremendous boon to adoptive cell transfer studies in preclinical cancer models. These therapies

involve isolating a patient's white blood cells and engineering the cells *ex vivo* to improve their tumor-killing and homing efficacies. The modified cells are then re-introduced into the patient [33]. In a recent example, Tsukahara *et al.* utilized BLI to examine chimeric T cell engineering and its relevance to adoptive cell transfer. Human T cells were engineered to express CD19 receptors. CD19 is a cell surface protein that assembles with the B cell antigen receptor in order to decrease the threshold for antigen receptor-dependent stimulation. When these cells reinfused into mice bearing CD19⁺Fluc⁺ tumors, tumor proliferation was markedly reduced as judged by bioluminescence imaging [38].

Unlike fluorescence technologies, bioluminescence has been largely limited to monitoring one cell type or biological feature at a time. Only a handful of distinct luciferase-luciferin pairs have been optimized for use in heterologous organisms. While these bioluminescent probes often emit different colors of light, they remain difficult to distinguish in living organisms, where the depth of the source and various tissue properties influence the “color” of light observed by the detector. Luciferases that catalyze light emission with chemically distinct molecules can be more readily discerned, and some have been used in tandem. In one example, T-cells expressing Gluc could be readily visualized accumulating within Fluc-expressing tumor cells [39]. Sequential application of coelenterazine and luciferin (the Gluc and Fluc substrates, respectively) enabled both populations of cells to be imaged simultaneously. Similar bioluminescent pairs have been used to track T reg and effector T cell functions [40], differential tumor growth [41], MSC interactions with tumor stroma, and interaction of the immune system with fungal infections such as *Aspergillus* and *Candida* [42–45]. While fruitful, these studies still remain arduous, as substrates must often be supplied sequentially and given ample time to clear.

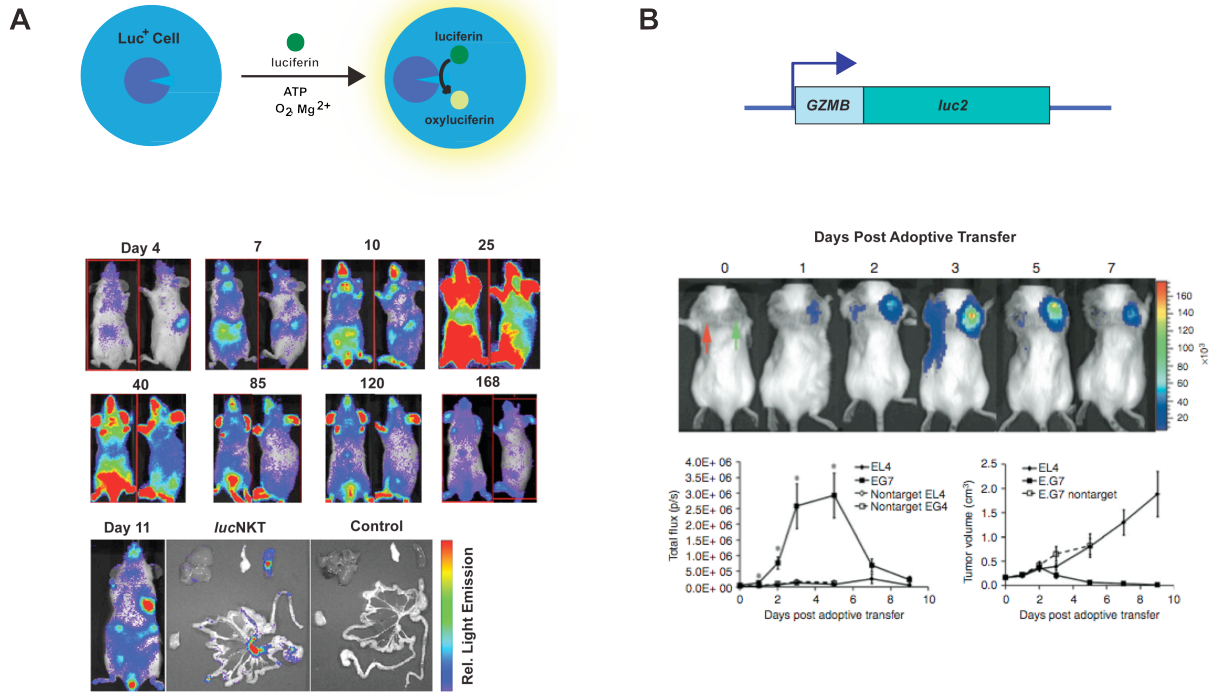


Figure 1-3: Luciferase probes can be used to track cell populations and gene expression patterns in vivo. **(A)** In graft-versus-host disease (GVHD) models, NKT (luc^+) cells were observed in the spleen and lymph nodes, then the skin and other organs. The total photons emitted from the luc^+ cells peaked at day 25, and then declined steadily. Imaging of excised organs indicated NKT cells trafficked to the spleen and mesenteric lymph nodes on day 11. **(B)** Bioluminescence imaging was used to monitor T cell effector function in response to tumor antigens in vivo. T cell activation was monitored using a $luc2$ reporter gene, driven by a granzyme B promoter. Mice were implanted with two cancer cell lines, EL4 (thyroma cell line) and its derivative EG7 (EL4 cells stably express chicken OVA cDNA). An adoptive T cell transfer was performed on the tumor bearing mice, with $CD8^+$ T cells responsive to OVA. Bioluminescent signal in the EG7 tumor was more robust than in the non-targeted EL4 tumor. Peak signal intensity from the target tumor coincided with tumor regression. OVA: ovalbumin. Image (A) is reproduced with permission from (Leveson-Gower et al. *Blood* **2011**, *117*, 3220-3229.). Image (B) is reproduced with permission from (Patel et al. *Cancer Res.* **2010**, *70*, 10141-10149.)

Similar to fluorescence imaging, BLI has been applied to studies of gene expression patterns [46]. Various promoters have been used to drive luciferase expression, including those involved in T cell activation [47] and B cell proliferation in addition to tumor progression [48], and other pathologies [49]. In a recent example, T cell activation was monitored via transfection of a Granzyme B promoter-luciferase reporter construct (Figure 1-3B). Granzyme B was used because of its known correlation with T cell activation. It should be noted that the researchers subsequently had to apply two rounds of signal amplification in order to detect the luciferase signal in a BLI platform. Researchers were then able to observe T cell activation in response to an antigenic tumor, the peak of which correlated with tumor regression [47]. In all cases, BLI provided a facile readout of gene expression levels across entire organisms.

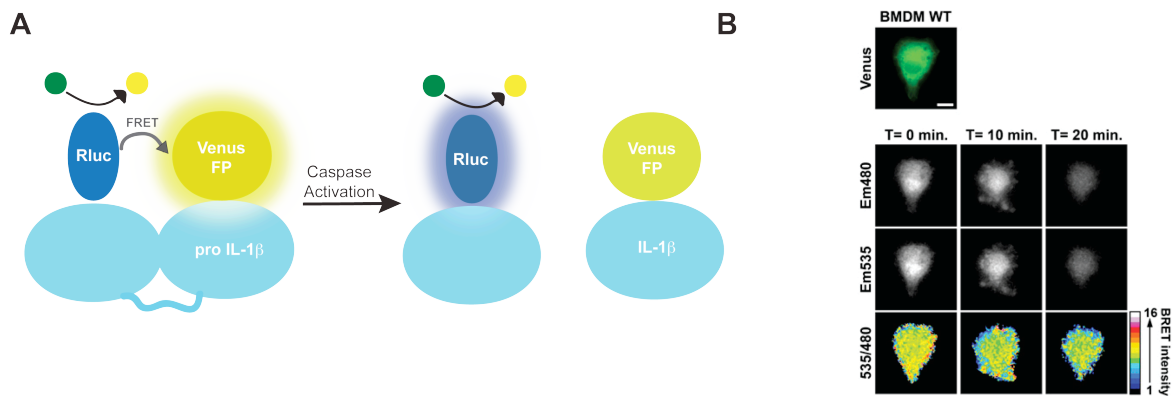


Figure 1-4: BRET probes can report on immune cell function. (A) A BRET sensor for IL-1 β formation (mediated by caspase activity) was devised. Before pro IL-1 β is cleaved, the two parts of the pro protein, labeled with Rluc and Venus fluorescent protein, are in close proximity. In this scenario, Rluc serves as the excitation source for Venus fluorescence. Once the pro protein is cleaved to mature IL-1 β , Rluc is no longer in close enough proximity to Venus fluorescent protein, and Rluc light emission is observed. (B) The BRET sensor was used to image IL-1 β processing in primary bone-marrow derived macrophages (BMDM). Macrophages were monitored at 480 nm (Rluc emission) and 535 nm (Venus emission), after being administered the Rluc substrate, coelenterazine. The bottom row is a pseudo colored for the 480/535 BRET ratio. Image (B) is reproduced with permission from (Compan et al. *J. Immunol.* **2012**, 189, 2131-2137.).

While less common, BLI can also be used to track individual proteins and other biomolecules relevant to immune function. In one example, the Serganova lab monitored the abundance of HIF-1 α , a transcription factor that is overexpressed in many human cancers, using a Fluc fusion. The chimeric protein enabled sensitive imaging of the abundance and stability of HIF-1 α *in cellulo* and in xenograph models [50]. Luciferase fusions have also been used to interrogate the canonical Wnt signaling pathway. The Wnt pathway regulates various aspects of development, including immune cell differentiation and becomes dysregulated in a variety of cancers [51]. In this network, β -catenin (β -cat) acts as a transcriptional activator of numerous host transcription factors. Usually marked for degradation, β -cat stabilization enables propagation of Wnt signaling. To study the posttranslational stabilization of β -cat, Naik *et al.* developed two bioluminescent fusion reporters, a β -cat click beetle luciferase (β -cat-CBG) and β -cat firefly luciferase (β -cat-FLuc). The researchers were able to observe modulators of β -cat activity and global β -cat levels, as well as processing, and downstream transcriptional activity by using further reporters [52].

Beyond direct detection, biomolecules can be visualized using bioluminescent sensors. Many of these exploit BRET in which bioluminescent emission excites a longer-wavelength fluorophore (Figure 1-4A). Analogous to FRET, the emission spectrum of the luciferase must overlap with the excitation of the fluorophore or FP. When the two light emitting molecules are in close proximity, the emission of the longer wavelength fluorophore is observed. Using an optimized version of Rluc (Rluc8) and a yellow-fluorescent protein (Venus) linked by pro-IL-1 β , the Pelegrin group developed a BRET sensor for caspase-1 activity (Figure 1-4B). Caspase-1 modulates several inflammatory signaling molecules, including the proapoptotic chemokine IL-1 β in macrophages and other immune cells. IL-1 β becomes activated upon caspase-1 cleavage

of the proprotein form (pro-IL-1 β). When the BRET sensor was expressed in cells with low levels of active caspase, the BRET pair remained in close proximity evidenced by the emission of yellow light. The blue photons emitted by Rluc8 acting upon coelentrazine are absorbed by venus which emits lower energy yellow light. In contrast when the BRET sensor is cleaved by caspase-1, Rluc is free to diffuse away from Venus and blue light is observed upon coelentrazine administration. The ratio of blue to yellow light in each case is a measure of caspase-1 activity and IL-1 β activation, which indicates changes in the inflammatory response [53].

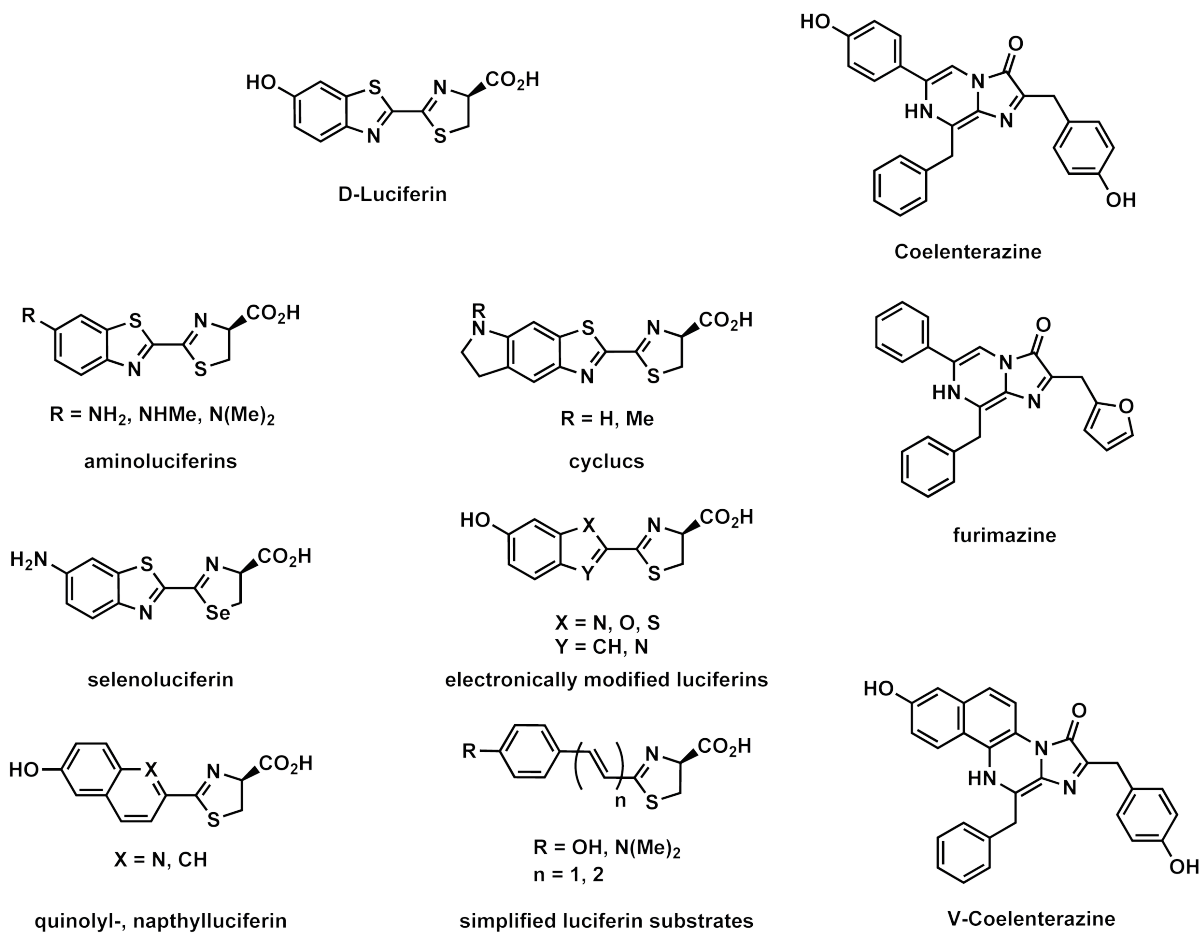


Figure 1-5 Collection of modified luciferin analogs that may be suitable for bioluminescence imaging.

1.4 Next-generation tools for imaging cell communication

The need to monitor cells at all length scales to capture chemical communication is driving the development of new tools and technologies. Work in the fluorescence realm is already well under way. As noted above, brighter, more photostable, and red-shifted FPs are being produced [12,20,54], along with metabolite-responsive FP's [55,56]. New chemistries to efficiently produce dyes and attach them to cells and other imaging targets are also being reported [21,22,57]. New fluorescence imaging technologies based on reconstitution of split GFP or enzymatic tagging of transcellular interactions have enabled rapid identification of direct cell contact in synapses [57–59].

In the bioluminescence realm, new luciferins and luciferases are also being engineered to track multiple cell types and for more sensitive imaging. The majority of this work to date has focused on identifying new luciferases, although many remain poorly characterized. Continued optimization of these luciferases for expression and stability is also increasing their sensitivity for use *in vivo*. Within well-characterized luciferase families, standard molecular biology techniques are being used to optimize reaction kinetics and, in some cases, provide altered colors or other desirable characteristics such as prolonged light emission [60–62].

More recently, focus has turned to the luciferin itself. The luciferin small molecule is the bioluminescent light-emitter, thus efforts to modify its structure and enzyme utilization are thus attractive. Urano and coworkers developed several new luciferin derivatives by appending fluorophores to the aromatic core [63] (Figure 1-5). Upon luciferase utilization, BRET interactions with the pendant fluorophore red shift the light emission. The Miller and Prescher labs have similarly explored nitrogenous luciferins [64,65]. Moerner and Urano have also developed different heterocyclic analogs [66]. Most have altered emission spectra, and are on par

with D-luciferin in terms of enzyme utilization. One of the cyclic amino luciferin derivatives exhibits enhanced bioavailability in mouse models. All strategies rely on efficient access to luciferins. To this end, we have developed a method to quickly access novel luciferin scaffolds [65,67].

Despite these efforts to identify improved luciferins, multispectral imaging with BLI remains difficult. As mentioned above, light emission in rodent models is skewed by tissue depth, complicating the interpretation of wavelength. Thus, multi-component bioluminescence imaging and efforts to map cell-cell contacts with distinct luciferase and luciferin pairs are complicated. In recent years, alternative methods to capture these events have been reported. For example, “split” versions of luciferase have been used to map cell interactions and detect chemokine receptor-ligand interactions. The Prescher group extended this technology to probing direct cell-cell contacts in living systems [68].

In a related strategy, the Prescher lab has crafted bioluminescent tools that produce light only when two cells interact. These tools comprise “caged” probes—luciferins outfitted with appendages (i.e., “cages”) that preclude binding to luciferase [69]. In the presence of “activator” cells capable of removing the cage (e.g., via selective enzymatic activity), active luciferin is liberated and available for use by luciferase-expressing (“reporter”) cells (Figure 1-6A). Reporter cells nearest the activator cells consume the most substrate; thus, light intensity correlates with the proximity of the two populations. A galactose-caged luciferin (Lugal) was synthesized to monitor the proximity between β -galactosidase (β -gal)-expressing activator cells and luciferase-expressing reporter cells in tumor models. When activator cells were localized to sites of metastases, Lugal administration signaled the invasion of luciferase-expressing tumor cells in mice (Figure 1-6B) [70]. This study enabled sensitive imaging of cell-cell interactions

not possible with traditional toolsets. Further extensions of “caged” luciferin technology and other methods to visualize cellular interactions promise to refine our views of organismal biology and disease.

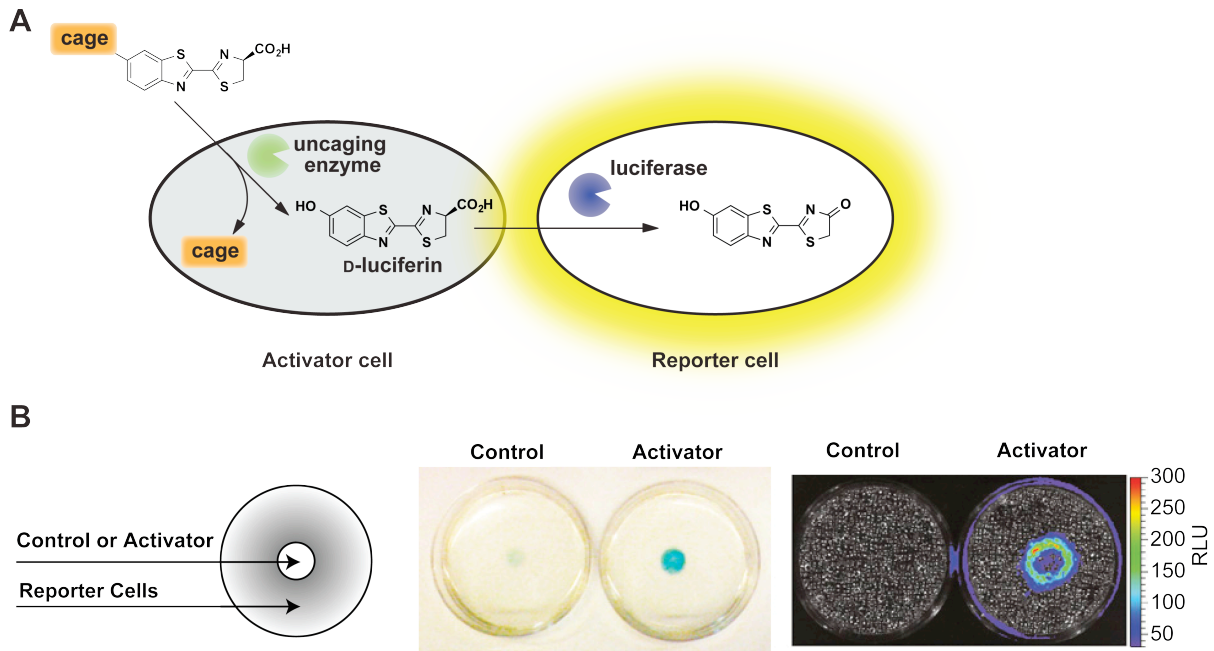


Figure 1-6: Immune cell interactions can be visualized with proximity reporters. **(A)** A proximity probe (“caged” luciferin) enters an activator cell, where it is liberated by an uncaging enzyme. Free luciferin can diffuse out of the cell. If a luc⁺ reporter cell is nearby, the uncaged substrate can be used to produce light. Robust light production is only observed when the activator and reporter cells are in close proximity. **(B)** An in vitro assay of the uncaging process. Activator or control cells in matrigel were plated in the center of a Petri dish. Luciferase reporter cells were plated in a monolayer surrounding the activator or control cells. The plates were incubated with a reporter substrate that shows location of uncaging enzyme activity (center). The caged luciferin was administered, and BLI was performed on the plates. Light emission was shown to correlate with the proximity of reporter cells to activator cells. Images were reproduced with permission from (Sellmyer et al. *Proc. Natl. Acad. Sci. USA.* **2013**, *110*, 8567-8572.)

1.5 Objectives of this study

Imaging technologies have revolutionized our understanding of living systems by enabling researchers to visualize biological features in real time. Despite its versatility, BLI is limited due to the paucity of available tools for multicomponent imaging applications. This is due, in part, to the lack of a generalizable synthetic method to rapidly access luciferin-like compounds. While contemporary syntheses may be used to produce D-luciferin, they employ conditions and reagents that make derivatization difficult. The ability to quickly attain large quantities of luciferin analogs is paramount to develop new bioluminescence tools. To this end, my dissertation work focused on expanding the number of tools for bioluminescence imaging.

I aimed to:

1. Develop a general synthetic route to access the D-luciferin heteroaromatic core.
2. Synthesize electronically perturbed analogs and characterize their bioluminescent properties with firefly luciferase.
3. Synthesize sterically perturbed luciferin analogs for multi-component bioluminescence imaging.
4. Enable the screening of mutant luciferases libraries.

References

- (1) Luker, G. D.; Luker, K. E. Optical imaging: current applications and future directions . *J. Nucl. Med.* **2008**, *49*, 1-4.
- (2) Prescher, J. A.; Contag, C. H. Guided by the light: visualizing biomolecular processes in living animals with bioluminescence. *Curr. Opin. Chem. Biol.* **2010**, *14*, 80-89.
- (3) Paley, M. A.; Prescher, J. A. Bioluminescence: a versatile technique for imaging cellular and molecular features. *MedChemComm* **2014**, *5*, 255-267.
- (4) Day, R. N.; Davidson, M. W. The fluorescent protein palette: tools for cellular imaging. *Chem. Soc. Rev.* **2009**, *38*, 2887-2921.
- (5) Hilderbrand, S. A.; Weissleder, R. Near-infrared fluorescence: application to in vivo molecular imaging. *Curr. Opin. Chem. Biol.* **2010**, *14*, 71-79.
- (6) Hochgrasfe, K.; Mandelkow, E-M. Making the brain glow: in vivo bioluminescence imaging to study neurodegeneration. *Mol. Neurobio.* **2013**, *47*, 868-882.
- (7) Gross, S.; Piwnica-Worms, D. Spying on cancer: molecular imaging in vivo with genetically encoded reporters. *Cancer Cell* **2005**, *7*, 5-15.
- (8) Germain, R. N.; Robey, E.A.; Cahalan, M. D. A Decade of Imaging Cellular Motility and Interaction Dynamics in the Immune System. *Science* **2012**, *336*, 1676-1681.
- (9) Rice, B. W.; Cable, M. D.; Nelson, M. B. In vivo imaging of light-emitting probes. *J. Biomed. Opt.* **2001**, *6*, 432-440
- (10) Cheong, W.F.; Prahl, S.A.; Welch, A. J. (1990) A review of the optical properties of biological tissues. *IEEE J. Quantum Electron.* of **1990**, *26*, 2166-2185.
- (11) Chudakov, D. M.; Matz, M. V.; Lukyanov, S.; Lukyanov, K. A.; Fluorescent Proteins and Their Applications in Imaging Living Cells and Tissues. *Physiol. Rev.* **2010**, *90*, 1103-63.
- (12) Shaner, N. C.; Steinbach, P. A. Tsien, R. Y. A guide to choosing fluorescent proteins. *Nat. Methods* **2005**, *2*, 905-909.
- (13) Yu, D.; Gustafson, W. C.; Han, C.; Lafaye, C. I. Noirclerc-Savoie, M.; Ge, W-P. Thayer, D. A.; Huang, H.; Kornberg, T. B.; Royant, A.; Jan, L. Y.; Jan, Y. N. Weiss, W. A.; Shu, X. An improved monomeric infrared fluorescent protein for neuronal and tumour brain imaging. *Nat. Commun.* **2014**, *5*, 1-7.
- (14) Adams Jr., S. T.; Miller, S. C. Beyond D-luciferin: expanding the scope of bioluminescence imaging in vivo. *Curr. Opin. Chem. Biol.* **2014**, *21*, 112-120.

- (15) Kim, J. B.; Urban, K.; Cochran, E.; Lee, S.; Ang, A.; Rice, B.; Bata, A.; Campbell, K.; Coffee, R.; Gorodinsky, A.; Lu, Z.; Zhou, H.; Kishimoto, T. K.; Lassota, P. Non-invasive detection of a small number of bioluminescent cancer cells in vivo. *PLoS One* **2010**, *5*, e9364.
- (16) Qiu, Y.; Palankar, R.; Echeverra, Ma. Medvedev, N.; Moya, S. E.; Delcea, M. Design of hybrid multimodal poly (lactic-co-glycolic acid) polymer nanoparticles for neutrophil labeling, imaging and tracking. *Nanoscale* **2013**, *5*, 12624-12632.
- (17) Pittet, M. J.; Weissleder, R. Intravital imaging. *Cell* **2011**, *147*, 983-991.
- (18) Weissleder, R.; Nahrendorf, M.; Pittet, M. J. Imaging macrophages with nanoparticles. *Nat. Mater.* **2014**, *13*, 125-138.
- (19) Nienhaus, K.; Nienhaus, G. U. Fluorescent proteins for live-cell imaging with super-resolution. *Chem. Soc. Rev.* **2014**, *43*, 1088-1106.
- (20) Chu, J.; Haynes, R. D.; Corbel, S. Y.; Li, P. Gonzalez-Gonzalez, E.; Burg, J. S.; Ataie, N. J.; Lam, A. J. Cranfill, P. J.; Baird, M. A.; Davidson, M. W.; Ng, H-L.; Garcia, K. C.; Contag, C. H.; Shen, K.; Blau, H. M.; Lin, M. Z. Non-invasive intravital imaging of cellular differentiation with a bright red-excitable fluorescent protein. *Nat. Methods* **2014**, *11*, 572-578.
- (21) Lavis, L. D.; Raines, R. T. Bright Ideas for Chemical Biology. *ACS Chem. Biol.* **2008**, *3*, 142-155.
- (22) Lavis, L. D.; Raines, R. T. Bright Building Blocks for Chemical Biology. *ACS Chem. Biol.* **2014**, *9*, 855-866.
- (23) Lu, H.; Mack, J.; Yang, Y.; Shen, Z. Structural modification strategies for the rational design of red/NIR region BODIPYs. *Chem. Soc. Rev.* **2014**, *43*, 4778-4823.
- (24) Adams, K. E.; Ke, S.; Kwon, S.; Liang, F.; Fan, Z.; Lu, Y.; Hirschi, K.; Mawad, M. E.; Barry, M. A.; Sevick-Muraca, E. M. Comparison of visible and near-infrared wavelength-excitable fluorescent dyes for molecular imaging of cancer. *J. Biomed. Opt.* **2007**, *12*, 024017.
- (25) Yao, J.; Yang, M.; Duan, Y. Chemistry, biology, and medicine of fluorescent nanomaterials and related systems: New insights into biosensing, bioimaging, genomics, diagnostics, and therapy. *Chem. Rev.* **2014**, *114*, 6130-6178.
- (26) Peng, F.; Su, Y.; Zhong, Y.; Fan, C.; Lee, S. T.; He, Y. Silicon nanomaterials platform for bioimaging, biosensing, and cancer therapy. *Acc. Chem. Res.* **2014**, *47*, 612-623.

- (27) Kalia, J.; Raines, R. T. Advances in bioconjugation. *Curr. Org. Chem.* **2010**, *14*, 138-147.
- (28) Biju, V. Chemical modifications and bioconjugate reactions of nanomaterials for sensing, imaging, drug delivery and therapy. *Chem. Soc. Rev.* **2014**, *43*, 744-764.
- (29) Contag, C. H.; Jenkins, D.; Contag, P. R.; Negrin, R. S. Use of reporter genes for optical measurements of neoplastic disease in vivo. *Neoplasia* **2000**, *2*, 41-52.
- (30) Mandl, S.; Schimmelpfennig, C.; Edinger, M.; Negrin, R. S.; Contag, C. H. Understanding immune cell trafficking patterns via in vivo bioluminescence imaging. *J. Cell Biochem. Suppl.* **2002**, *39*, 239-248.
- (31) Bhaumik, S.; Lewis, X. Z.; Gambhir, S. S. Optical imaging of Renilla luciferase, synthetic Renilla luciferase, and firefly luciferase reporter gene expression in living mice. *J. Biomed. Opt.* **2004**, *9*, 578-586.
- (32) Chung, K.; Wallace, J.; Kim, S. Y.; Kalyanasundaram, S.; Andalman, A. S.; Davidson, T. J.; Mirzabekov, J. J.; Zalocusky, K. A.; Mattis, J.; Denisin, A. K.; Pak, S.; Bernstein, H.; Ramakrishnan, C.; Grosenick, L.; Gradinaru, V.; Deisseroth, K. Structural and molecular interrogation of intact biological systems. *Nature* **2013**, *497*, 332-337.
- (33) Badr, C. E.; Tannous, B. A. Bioluminescence imaging: progress and applications. *Trends Biotechnol.* **2011**, *29*, 624-633.
- (34) Cao, Y-A.; Wagers, A. J.; Beilhack, A.; Dusich, J.; Bachmann, M. H.; Negrin, R. S.; Weissman, I. L.; Contag, C. H. Shifting foci of hematopoiesis during reconstitution from single stem cells. *Proc. Natl. Acad. Sci. USA* **2004**, *101*, 221-226.
- (35) Rabinovich, B. A.; Ye, Y.; Etto, T.; Chen, J. Q.; Levitsky, H. I.; Overwijk, W. W.; Cooper, L. J.; Gelovani, J.; Hwu, P. Visualizing fewer than 10 mouse T cells with an enhanced firefly luciferase in immunocompetent mouse models of cancer. *Proc. Natl. Acad. Sci. USA* **2008**, *105*, 14342-14346.
- (36) Knorr, D. A.; Bock, A.; Brentjens, R. J.; Kaufman, D. S. Engineered human embryonic stem cell-derived lymphocytes to study *in vivo* trafficking and immunotherapy. *Stem Cells Dev.* **2013**, *22*, 1861-1869
- (37) Leveson-Gower D. B.; Olson, J. A.; Sega, E. I.; Luong, R. H.; Baker, J.; Zeiser, R.; Negrin, R. S. Low doses of natural killer T cells provide protection from acute graft-versus-host disease via an IL-4-dependent mechanism. *Blood* **2011**, *117*, 3220-3229.
- (38) Tsukahara, T.; Ohmine, K.; Yamamoto, C.; Uchibori R.; Ido H.; Teruya, T.; Urabe, M.; Mizukami, H.; Kume, A.; Nakamura, M.; Mineno, J.; Takesako, K.; Riviere, I.; Sadelain, M.; Brentjens, R.; Ozawa, K. CD19 target-engineered T-cells accumulate at tumor

- lesions in human B-cell lymphoma xenograft mouse models. *Biochem. Biophys. Res. Commun.* **2013**, *438*, 84-89.
- (39) Santos, E. B.; Yeh, R.; Lee, J.; Nikhamin, Y.; Punzalan, B.; Punzalan, B.; Perle, K. L.; Larson, S. M.; Sadelain, M.; Brentjens, R. J. Sensitive *in vivo* imaging of T cells using a membrane-bound *Gaussia princeps* luciferase. *Nat. Med.* **2009**, *15*, 338-344.
- (40) Lewandrowski, G. K.; Magee, C. N.; Mounayar, M.; Tannous, B. A.; Azzi, J. (2014) Simultaneous *in vivo* monitoring of regulatory and effector T lymphocytes using secreted *gaussia* luciferase, firefly luciferase, and secreted alkaline phosphatase. In: *Bioluminescent Imaging*. Springer, pp 211-227.
- (41) Charles, J. I. P.; Fuchs, J.; Hefter, M.; Vischedyk, J. B.; Kleint, M.; Vogiatzi, F.; Schafer, J. A.; Nist, A.; Timofeev, O.; Wanzel, M.; Stiewe, T. Monitoring the dynamics of clonal tumour evolution *in vivo* using secreted luciferases. *Nat. Commun.* **2014**, *5*, 1-11.
- (42) Donat, S.; Hasenberg, M.; Schafer, T.; Ohlsen, K.; Gunzer, M.; Einsele, H.; Löffler, J.; Beilhack, A.; Krappmann, S. Surface display of *Gaussia princeps* luciferase allows sensitive fungal pathogen detection during cutaneous aspergillosis. *Virulence* **2012**, *3*, 51-61.
- (43) Vecchiarelli, A.; d'Enfert, C. Shedding natural light on fungal infections. *Virulence* **2012**, *3*, 15-17.
- (44) Vande Velde, G.; Kucharkov, S.; Schrevels, S.; Himmelreich, U.; Van Dijck, P. Towards non-invasive monitoring of pathogen, host interactions during *Candida albicans* biofilm formation using *in vivo* bioluminescence. *Cell. Microbiol.* **2014**, *16*, 115-130.
- (45) Maguire, C. A.; Bovenberg, M. S.; Crommentuijn, M. H.; Niers, J. M.; Kerami, M.; Teng, J.; Sena-Esteves, M.; Badr, C. E.; Tannous, B. A. Triple bioluminescence imaging for *in vivo* monitoring of cellular processes. *Mol. Ther. Nucleic Acids* **2013**, *2*, e99.
- (46) Chen, Z. H.; Zhao, R. J.; Li, R. H.; Guo, C. P.; Zhang, G. J. Bioluminescence imaging of DNA synthetic phase of cell cycle in living animals. *PLoS One* **2013**, *8*, e53291.
- (47) Patel, M. R.; Chang, Y. F.; Chen, I. Y.; Bachmann, M. H.; Yan, X.; Contag, C. H.; Gambhir, S. S. Longitudinal, noninvasive imaging of T-cell effector function and proliferation in living subjects. *Cancer Res.* **2010**, *70*, 10141-10149.
- (48) Bhang, H. E.; Gabrielson, K. L.; Lathera, J.; Fisher, P. B.; Pomper, M. G. (2011) Tumor-specific imaging through progression elevated gene-3 promoter-driven gene expression. *Nat. Med.* **2011**, *17*, 123-129.
- (49) Watts, J. C.; Giles, K.; Oehler, A.; Middleton, L.; Dexter, D. T.; Gentleman, S. M.; DeArmond, S. J.; Prusiner, S. B. Transmission of multiple system atrophy prions to transgenic mice. *Proc. Natl. Acad. Sci. USA* **2013**, *110*, 19555-19560.

- (50) Moroz, E.; Carlins S.; Dyominas K.; Burkes S.; Thalers H. T.; Blasberg, R.; Serganova, I. Real-time imaging of HIF-1alpha stabilization and degradation. *PloS One* **2009**, *4*, e5077.
- (51) Klaus, A.; Birchmeier, W. Wnt signalling and its impact on development and cancer. *Nat. Rev. Cancer* **2008**, *8*, 387-398
- (52) Naik, S.; Piwnica-Worms, D. Real-time imaging of beta-catenin dynamics in cells and living mice. *Proc. Natl. Acad. Sci. USA* **2007**, *104*, 17465-17470.
- (53) Compan, V.; Baroja-Mazo, A.; Bragg, L.; Verkhratsky, A.; Perroy, J.; Pelegrin, P. (2012) A genetically encoded IL-1beta bioluminescence resonance energy transfer sensor to monitor inflammasome activity. *J. Immunol.* **2012**, *189*, 2131-2137.
- (54) Shaner, N. C.; Lambert, G. G.; Chamma, A.; Ni, Y.; Cranfill, P. J.; Baird, M. A.; Sell, B. R.; Allen, J. R.; Day, R. N.; Israelsson, M.; Davidson, M. W.; Wang, J. A bright monomeric green fluorescent protein derived from *Branchiostoma lanceolatum*. *Nat. Methods* **2013**, *10*, 407-409
- (55) Park, J. G.; Palmer, A. E. Quantitative measurement of Ca²⁺ and Zn²⁺ in mammalian cells using genetically encoded fluorescent biosensors. *Methods Mol. Biol.* **2014**, *1071*, 29-47.
- (56) Zhong, S.; Navaratnam, D.; Santos-Sacchi, J. A genetically-encoded YFP sensor with enhanced chloride sensitivity, photostability and reduced pH interference demonstrates augmented transmembrane chloride movement by gerbil prestin (SLC26a5). *PLoS One* **2014**, *9*, e99095.
- (57) Uttamapinant, C.; White, K. A.; Baruah, H.; Thompson, S.; Fernandez-Surez, M.; Puthenveetil, S.; Ting, A. Y. A fluorophore ligase for site-specific protein labeling inside living cells. *Proc. Natl. Acad. Sci. USA.* **2010**, *107*, 10914-10919.
- (58) Liu, D. S.; Loh, K. H.; Lam, S. S.; White, K. A.; Ting, A. Y. Imaging trans-cellular neurexin-neurologin interactions by enzymatic probe ligation. *PLoS One* **2013**, *8*, e52823.
- (59) Feinberg, E. H.; VanHoven, M. K.; Bendesky, A.; Wang, G.; Fetter, R. D.; Shen, K.; Bargmann, C. I. GFP reconstitution across synaptic partners (GRASP) defines cell contacts and synapses in living nervous systems. *Neuron* **2008**, *57*, 353-363.
- (60) Branchini, B. R.; Magyar, R. A.; Murtiashaw, M. H.; Anderson, S. M.; Helgersson, L. C.; Zimmer, M. Site-directed mutagenesis of firefly luciferase active site amino acids: a proposed model for bioluminescence color. *Biochemistry* **1999**, *38*, 13223-13230.

- (61) Viviani, V. R.; Amaral, D. T.; Neves, D. R.; Simoes, A.; Arnoldi, F. G. The luciferin binding site residues C/T311 (S314) influence the bioluminescence color of beetle luciferases through main-chain interaction with oxyluciferin phenolate. *Biochemistry* **2013**, *52*, 19-27.
- (62) Degeling, M. H.; Bovenberg, M. S.; Lewandrowski, G. K.; de Gooijer, M. C.; Vleggeert-Lankamp, C. L.; Tannous, M.; Maguire, C. A.; Tannous, B. A. Directed molecular evolution reveals *Gaussia* luciferase variants with enhanced light output stability. *Anal. Chem.* **2013**, *85*, 3006-3012.
- (63) Kojima, R.; Takakura, H.; Ozawa, T.; Tada, Y.; Nagano, T.; Urano, Y. Rational design and development of near-infrared-emitting firefly luciferins available *in vivo*. *Angew. Chem. Int. Ed.* **2013**, *52*, 1175-1179.
- (64) Reddy, G. R.; Thompson, W. C.; Miller, S. C. Robust light emission from cyclic alkylaminoluciferin substrates for firefly luciferase. *J. Am. Chem. Soc.* **2010**, *132*, 13586-13587.
- (65) McCutcheon, D. C.; Paley, M. A.; Steinhardt, R. C.; Prescher, J. A. Expedient synthesis of electronically modified luciferins for bioluminescence imaging. *J. Am. Chem. Soc.* **2012**, *134*, 7604-7607.
- (66) Conley, N. R.; Dragulescu-Andrasi, A.; Rao, J.; Moerner, W. E. A selenium analogue of firefly D-luciferin with red-shifted bioluminescence emission. *Angew. Chem. Int. Ed.* **2012**, *51*, 3350-3353.
- (67) McCutcheon, D. C.; Porterfield, W. B.; Prescher, J. A. Rapid and scalable assembly of firefly luciferase substrates. *Org. Biomol. Chem.* **2015**, *13*, 2117-2121.
- (68) Jones, K. A.; Li, D. J.; Hui, E.; Sellmyer, M. A.; Prescher, J. A. Visualizing cell proximity with genetically encoded bioluminescent reporters *ACS Chem. Biol.* **2015**, *10*, 933-938.
- (69) Li, J.; Chen, L.; Du, L.; Li, M. Cage the firefly luciferin! – A strategy for developing bioluminescent probes. *Chem. Soc. Rev.* **2013**, *42*, 662-676.
- (70) Sellmyer, M. A.; Bronsart, L.; Imoto, H.; Contag, C. H.; Wandless, T. J.; Prescher, J. A. Visualizing cellular interactions with a generalized proximity reporter. *Proc. Natl. Acad. Sci. USA* **2013**, *110*, 8567-8572.

CHAPTER 2: Rapid and scalable assembly of firefly luciferase scaffolds

2.1 Introduction

Bioluminescence imaging is among the most powerful techniques for visualizing cells and other biological features [1,2]. At the heart of this technology are enzymes (luciferases) that catalyze the oxidation of small molecule substrates (luciferins), releasing visible light in the process (Figure 2-1) [2]. Bioluminescent photons can penetrate tissues—even in intact rodents—making this technique well suited for imaging *in vivo* and other complex environments. Indeed, bioluminescence has been widely used to monitor cell proliferation and migration, gene expression patterns, and enzyme activities in a variety of preclinical models [1,2].

The most prevalent luciferase–luciferin pair in biological imaging originates from the firefly. Firefly luciferase (Fluc) catalyzes the oxidation of D-luciferin (**2.1**), producing yellow-green light at room temperature (Figure 2-1) [3]. Fluc can be expressed in many cell and tissue types, and when D-luciferin is administered, photons are produced. Fluc can also catalyze light emission with a variety of D-luciferin analogs [4], including the 6'-amino variant (**2.2**) [5–7] and related cyclic amino analogs [8,9], heterocyclic derivatives [4,10–12], and luciferins with extended pi systems [13]. Some of these molecules emit different colors of light and are thus useful for multi-spectral imaging. Other analogs are more cell permeant than D-luciferin [14], making them attractive for sensitive imaging applications. “Caged” forms of luciferin can also be used in conjunction with Fluc to measure enzyme activities [15] and monitor cell–cell interactions *in vivo* [16].

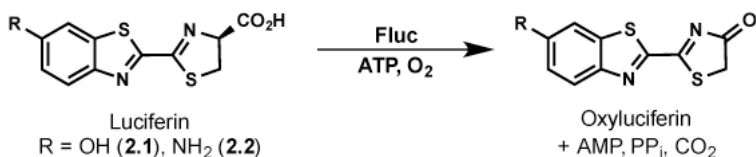


Figure 2-1: Firefly luciferase (Fluc) catalyzes the oxidation of D-luciferin (**2.1**), its native substrate, and various analogs, including the 6'-amino compound (**2.2**). Light is produced during the enzymatic reactions. This figure is reproduced with permission from McCutcheon, *et al. Org. Biomol. Chem.* **2015**, *13*, 2117-2121.

2.2 Evolution of the D-luciferin synthesis

Given their broad utility and critical roles in biological imaging, it is surprising that luciferins remain difficult to access in an expedient and cost-effective manner [17,18]. The first synthesis of D-luciferin reported by White in 1961 was seven steps and provided the compound in only 6% overall yield [19–21]. Iterative improvements to this route have been reported over the past several decades, although the basic strategy remains the same: generate a 2-carboxy-substituted benzothiazole, replace the carboxylate with a cyano group, and condense the resulting cyanobenzothiazole with D-cysteine [17,22–24]. While reliable, these routes remain low yielding and unnecessarily long. Functionalized cyanobenzothiazoles can be purchased directly from commercial suppliers and condensed with cysteine to prepare luciferins in a single step. However, these reagents are expensive and not practical for studies requiring multi-gram quantities of a light-emitting substrate.

We aim to develop an alternative method to synthesize D-luciferin. Our approach focused on benzothiazole formation from aniline starting materials and the dithiazolium chloride salt **2.3** (also known as Appel's salt). Appel's salt condenses readily with arylamines, and the

resulting iminodithiazoles can be fragmented with a variety of nucleophiles, generating cyanothioformamides; these moieties can then be cyclized to afford benzothiazole products (Figure 2-2) [25–27]. Appel's salt can also be prepared in bulk quantities (>500 g from simple addition of sulfur monochloride to chloroacetonitrile) and stored indefinitely, making it attractive for large-scale work.

To investigate the utility of Appel's salt for luciferin synthesis, we first used the reagent to prepare the cyanobenzothiazole **2.7** (en route to D-luciferin, Scheme 2-1). *p*-Anisidine (**2.4**) was treated with **2.3** to provide the expected dithiazole adduct **2.5**. This intermediate was isolable using standard chromatographic techniques and found to be remarkably shelf stable. Treatment of **2.5** with excess DBU produced cyanothioformamide **2.6** in excellent yield. Palladium- and copper-mediated cyclization of this compound generated the key cyanobenzothiazole **2.7**. Notably, this route to **2.7** is four steps shorter than the sequence employed by White and provides the compound in markedly better yield (84% versus 10% overall). Subsequent protecting group removal and cysteine condensation ultimately provided the desired luciferin **2.1**. Altogether, this route provided D-luciferin in just 5 steps and 42% overall yield.

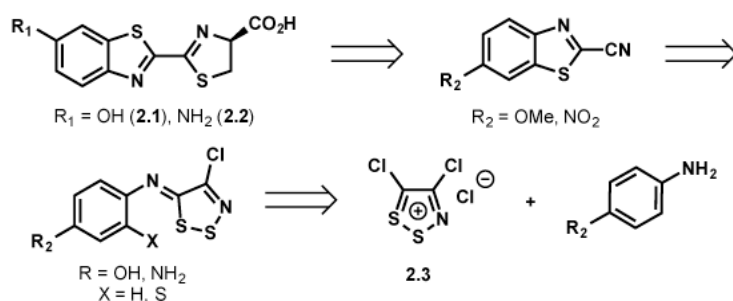
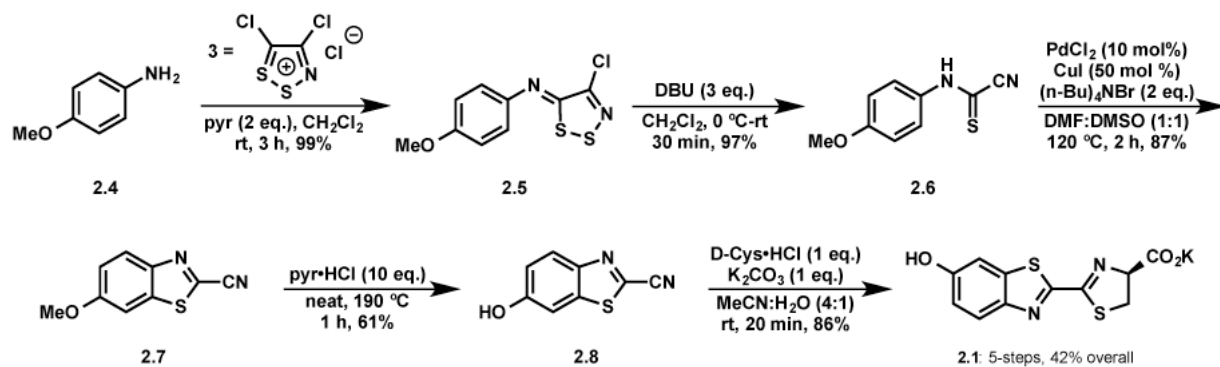


Figure 2-2: Retrosynthetic analysis of D-luciferin (**2.1**) and its 6'-amino analog (**2.2**). Both molecules can be accessed from aniline starting materials and Appel's salt (**2.3**). This figure is reproduced with permission from McCutcheon, *et al. Org. Biomol. Chem.* **2015**, *13*, 2117-2121.

Despite the initial successes and notable advances of the previous route, limitations remained. The synthesis employed expensive metal reagents and large volumes of solvent. Several time-intensive purification steps were also required. These features precluded the easy preparation of large quantities (>10 g) of **2.1**. We thus sought an improved, streamlined synthesis of D-luciferin (**2.1**) from inexpensive starting materials. We also envisioned that the route could be applied to other analogs, including aminoluciferin (**2.2**).

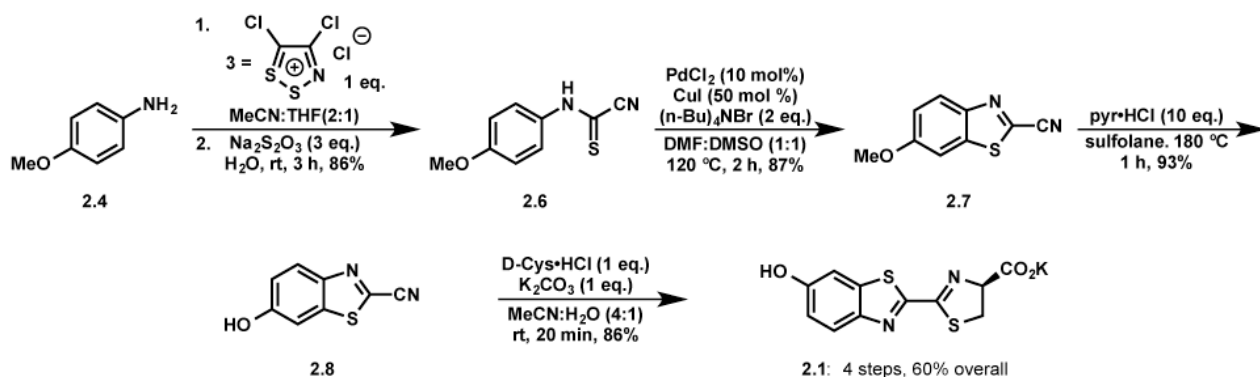
Scheme 2-1: Initial synthetic route to D-luciferin. This scheme is modified with permission from McCutcheon, *et al. Org. Biomol. Chem.* **2015**, *13*, 2117-2121.



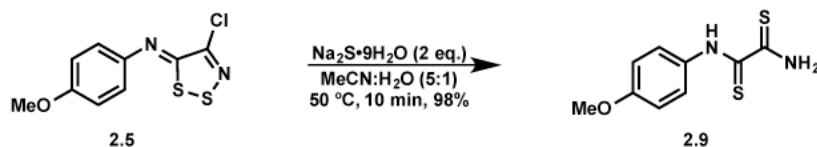
In early attempts to optimize our previous synthesis, we focused on the dithiazole fragmentation procedure (step 2, Scheme 2-1). This reaction employed DBU, a reagent that is notoriously difficult to remove from reaction mixtures via extraction or flash column chromatography. Indeed, in our hands, multiple chromatographic separations were required to isolate **2.6** from residual DBU upon scale up; this purification scheme quickly became impractical. Since DBU functions to break apart the dithiazole, we reasoned that other, more

tractable nucleophiles could be used in its place. Initial attempts with triphenyl phosphine and sodium sulfide, though, proved unsuccessful. Triphenyl phosphine (and the corresponding oxide) was similarly difficult to remove from the reaction mixture. Sodium sulfide, by contrast, was easy to remove, but converted **2.5** to an *N*-aryl dithiooxamide (**2.9**, Scheme 2-3) instead of the desired formamide **2.6**. We attributed this result to sulfide being a strong, yet sterically unencumbered nucleophile, capable of additional reactivity with cyanothioformamides. Fortunately, a less nucleophilic anion—thisosulfate ($S_2O_3^{2-}$)—provided **2.6** in excellent yield (Scheme 2-2) with no dithiooxamide observed. Compound **2.6** also precipitated from the reaction mixture and could be collected by filtration, eliminating the need for column chromatography. We further discovered that both the formation and fragmentation of **2.5** (with thiosulfate) could be performed in a single pot, eliminating another onerous purification step. With **2.6** in hand, we completed the synthesis of D-luciferin (**2.1**) using our previous method. Collectively, this route improved the overall yield of D-luciferin (60%) and shortened the time involved by eliminating one synthetic step entirely, along with two chromatographic separations.

Scheme 2-2: Improved synthesis of D-luciferin (**2.1**) using an initial one-pot condensation/fragmentation procedure. This scheme is reproduced with permission from McCutcheon, *et al. Org. Biomol. Chem.* **2015**, *13*, 2117-2121.



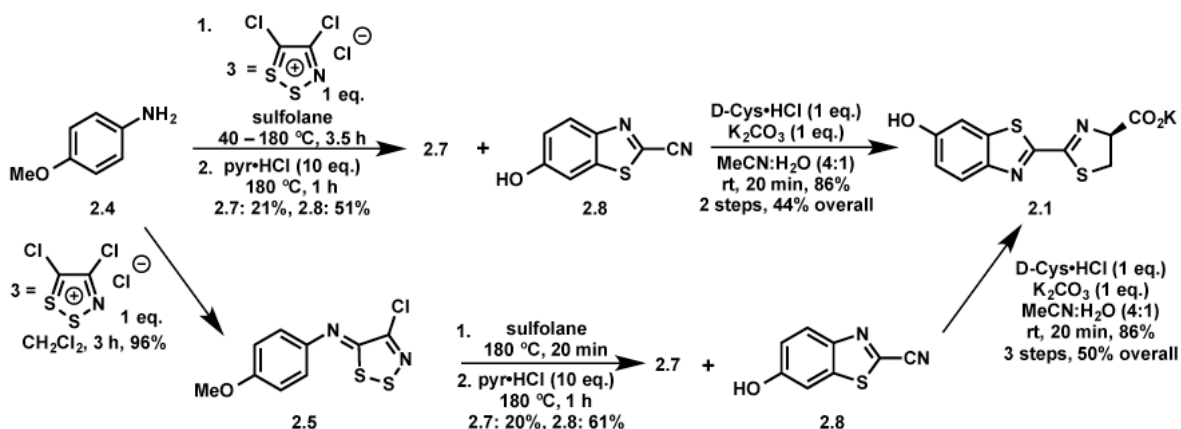
Scheme 2-3: Mild and efficient synthesis of monoaryl - dithiooxamide **2.9**. This scheme is reproduced with permission from McCutcheon, *et al. Org. Biomol. Chem.* **2015**, *13*, 2117-2121.



In addition to the fragmentation step, we recognized that formation of cyanobenzothiazole **7** in the original synthesis (step 3, Scheme 2-1) was not optimal. This step required expensive metal reagents, non-ideal solvents, excess TBAB, and dilute conditions [28]. Based on work from Rees [29–31], we reasoned that **2.7** might be attainable directly from **2.5** via thermolysis. This would eliminate the need for metal-mediated cyclization entirely and shorten the overall synthesis. However, initial attempts to cyclize **2.5** in refluxing DMF resulted in degradation or afforded thioformamide **2.6** as the major product. The cyclization yield improved dramatically at higher temperatures using sulfolane and sealed tubes. Under these conditions, we also observed trace amounts of deprotected phenol **2.8**. This prompted us to explore whether **2.5** could be cyclized and deprotected in a single pot (Scheme 2-4, lower). Indeed, upon heating **2.5** in sulfolane and subsequent treatment with $\text{pyr}\cdot\text{HCl}$, **2.8** was isolated in moderate yield (61%), along with the protected phenol **2.7** (20%). Re-subjecting **2.7** to $\text{pyr}\cdot\text{HCl}$ increased the total yield of **2.8**. Excitingly, the cyclization/deprotection sequence could also be coupled with the first synthetic step: formation of imine **2.5**. When **2.4** was treated with Appel's salt, followed by rigorous heating and subsequent addition of $\text{pyr}\cdot\text{HCl}$, **2.8** and **2.7** were isolated in 51 and 21 percent yields, respectively (Scheme 2-4, upper). Further condensation of **2.8** with D-cysteine provided luciferin **2.1**. Thus, D-luciferin (**2.1**) can be prepared from inexpensive starting materials in only two steps and 44% overall yield. To our knowledge, this represents the shortest

synthesis of D-luciferin from simple anilines to date. Moreover, these conditions are scalable (>10 g of **2.8** can be routinely produced in a single reaction step), and the route is compatible with a variety of phenol protecting groups.

Scheme 2-4: Synthesis of D-luciferin (**2.1**) via Appel's salt condensation and thermolysis. The iminodithiazole adduct **2.5** can be isolated following treatment of *p*-anisidine (**2.4**) with Appel's salt (lower) or carried on directly into the cyclization and deprotection steps (upper). This scheme is reproduced with permission from McCutcheon, *et al. Org. Biomol. Chem.* **2015**, *13*, 2117-2121.



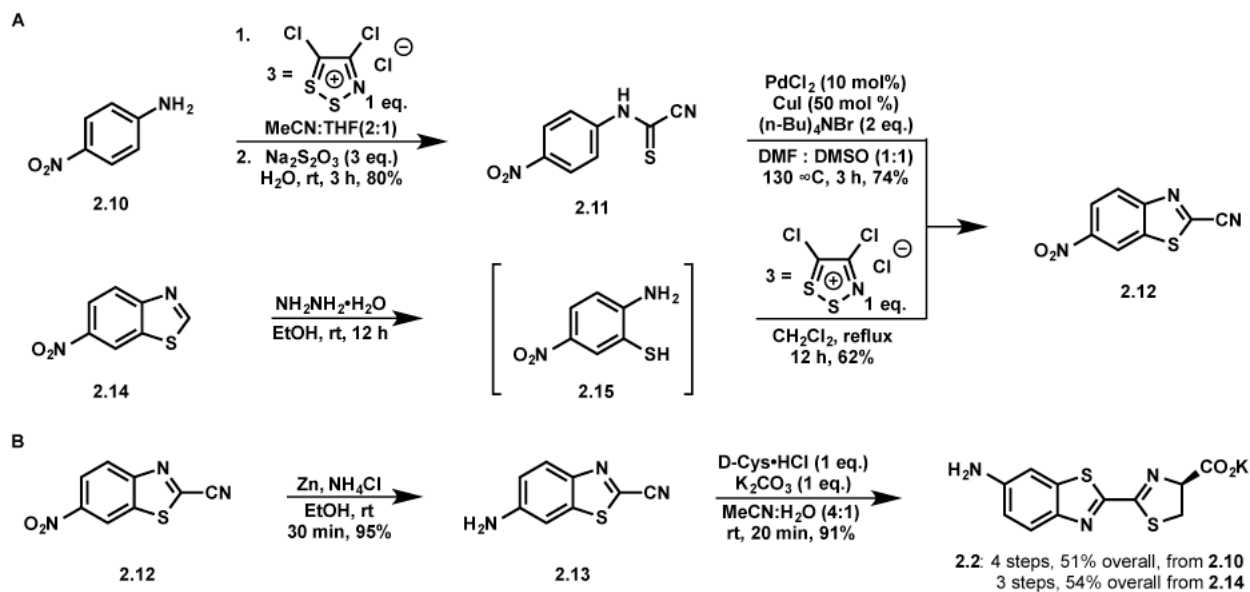
We next attempted to apply the improved route to the synthesis of aminoluciferin **2.2**. This analogue and related variants are attractive for bioluminescence imaging owing to their ease of derivatization and, in some cases, enhanced cell permeability [4,6,14]. Initial attempts to access **2.2** from *p*-phenylenediamine, though, were unsuccessful and afforded a complex mixture of products. We therefore moved forward with nitroaniline **2.10** and condensed this material with Appel's salt **2.3** (Scheme 2-5A). Attempts to generate benzothiazole **2.12** *via* thermal cyclization of the corresponding dithiazole adduct were low yielding, likely due to the electron-deficient

nature of the aromatic ring. Benzothiazole **2.12** was accessible on gram-scale, though, using a route similar to the one shown in Scheme 2.2. Aniline **2.10** was treated with Appel's salt (**2.3**), followed by sodium thiosulfate (to fragment the dithiazole intermediate) to provide **2.11**. Subsequent Pd-mediated cyclization generated **2.12** in 74% yield (Scheme 2-5A). Reduction of the nitro group followed by cysteine condensation ultimately afforded aminoluciferin **2.2**.

We were able to further improve the aminoluciferin synthesis drawing inspiration from our earlier work. We previously demonstrated that ortho-nucleophiles can trap Appel's salt adducts to afford cyclized products. Thus, we reasoned that installing a thiol ortho to the amine in **2.10** would enable more facile access to 6'-aminoluciferin (**2.2**, Scheme 2-5B). Attempts to prepare aminothiols **2.15** from the corresponding ortho-chloro aniline via nucleophilic aromatic substitution were not successful. However, **2.15** could be generated *in situ* by incubating commercially available **2.14** with hydrazine (Scheme 2-5A, lower). Subsequent addition of Appel's salt **2.3** provided **2.12** in 62% yield. Subsequent nitro group reduction and cyclization provided **2.2** in 54% overall yield. Notably, this is the shortest and highest yielding synthesis of 6'-aminoluciferin (**2.2**) to date.

In summary, we developed an improved method to access two key luciferin molecules for bioluminescence imaging. The approach builds off earlier work using anilines and readily accessible Appel's salt to generate luciferin cores. The processes eliminate costly reagents and time-intensive purifications, improving both the speed and efficiency of luciferin construction. The syntheses are also scalable and have been used to produce bulk quantities of the light-emitting substrates. The methods reported here will streamline the production of both known and novel luciferins, and thus drive the continued expansion of the bioluminescent toolkit.

Scheme 2-5: Synthesis of aminoluciferin **2.2**. (A) Cyanobenzothiazole intermediate **2.12** was accessed via palladium-mediated cyclization (top) or metal-free cyclization (bottom). (B) A reduction-condensation sequence was used to prepare **2.2**. This scheme is reproduced with permission from McCutcheon et. al. *Org. Biomol. Chem.* **2015**, *13*, 2117-2121.



Materials and methods

General synthetic methods

All reagents purchased from commercial suppliers were of analytical grade and used without further purification. Reaction progress was monitored by thin-layer chromatography (TLC) using EMD 60 F254 plates and visualization with UV light, ceric ammonium molybdate (CAM), chloranil, or KMnO₄ stain. Compounds were purified via flash-column chromatography using Sorbent Technologies 60 Å, 230-400 mesh silica gel, unless otherwise noted. Anhydrous solvents were dried by passage over neutral alumina with the exception of DMF, which was passed over activated molecular sieves. Reaction vessels were either flame- or oven-dried prior to use. NMR spectra were acquired with Bruker Advanced spectrometers. All spectra were acquired at 298 K, unless otherwise specified. ¹H-NMR spectra were acquired at either 500 or 400 MHz, and ¹³C-NMR spectra were acquired at 125 or 100 MHz. Coupling constants (*J*) are provided in Hz and chemical shifts are reported in ppm relative to either residual non-deuterated NMR solvent or a calculated DSS reference for those ¹³C-spectra acquired in D₂O. Low and high-resolution electrospray ionization (ESI) mass spectra were collected at the University of California-Irvine Mass Spectrometry Facility.

4,5-Dichloro-1,2,3-dithiazolium chloride (Appel's salt, 2.3)

Chloroacetonitrile (69.5 mL, 1.10 mol) was combined with S₂Cl₂ (360 mL, 4.5 mol) and anhydrous CH₂Cl₂ (25 mL) in a flame-dried reaction vessel equipped with a gas outlet. The mixture was thoroughly mixed then left to stand without agitation at rt under N₂. Over 3 h, the yellow solution darkened and vigorously evolved gas. The reaction was allowed to stand under an inert atmosphere at rt for an additional 48 h. The precipitate was filtered and washed with

anhydrous CH₂Cl₂ (3 x 100 mL) under a N₂ atmosphere to provide a dark green solid (207 g, 90%). Appel's salt **3** was found to be shelf stable for >1 year when stored in desiccator at rt. This material is also commercially available from Oakwood Chemicals (CAS #: 75318-43-3).

Synthetic procedures for D-luciferin synthesis [10,32]

Method A (Scheme 2-2) [10]:

4-Chloro-5-([4-methoxyphenyl]imino)-5H-1,2,3-dithiazole (2.5):

4,5-Dichloro-1,2,3-dithiazole (**2.3**) (2.09 g, 10.0 mmol) was added to a 100-mL round-bottom flask, followed by anhydrous CH₂Cl₂ (24 mL) and *p*-anisidine (1.23 g, 10.0 mmol). The green-brown mixture was stirred at room temperature under N₂. After 1 h, anhydrous pyridine (1.6 mL, 20.0 mmol) was slowly added to the suspension, and the resulting red-brown mixture was stirred for an additional 2 h. The mixture was concentrated *in vacuo* and purified by flash column chromatography, eluting with hexanes followed by CH₂Cl₂, to afford (**2.5**) (5.2 g, 99%) as a yellow solid: ¹H NMR (400 MHz, CDCl₃) δ 7.28 (d, *J* = 8.9, 2H), 6.99 (d, *J* = 8.9, 2H), 3.85 (s, 3H); ¹³C NMR (125 MHz, CDCl₃) δ 158.5, 155.8, 148.6, 143.3, 122.0, 114.9, 55.7.

***N*-(*p*-Methoxyphenyl)cyanothioformamide (2.6):**

DBU (8.9 mL, 60.0 mmol) was added at a rate of 0.5 mL/min to a -5 °C solution of (**2.5**) (5.20 g, 20.0 mmol) in anhydrous CH₂Cl₂ (102 mL). The resulting red-brown mixture was stirred at -5 °C for 30 min. The crude reaction mixture was washed with 1 M NaHSO₄ (3 x 20 mL) H₂O (2 x 30 mL), brine (1 x 50 mL), The organic phase was then, dried over Na₂SO₄, filtered, and adsorbed to Celite. The crude material was purified using a plug of silica gel, eluting with 1:1 hexanes:EtOAc, to provide (**2.6**) (3.6 g, 93%) as a dark red-brown solid: ¹H NMR (400

MHz, CDCl₃) δ 9.60 (br s, 1H), 7.72 (d, J = 9.0, 2H), 7.31 (d, J = 8.9, 1H), 6.93-6.97 (m, 2H), 3.84 (s, 3H); ¹³C NMR (125 MHz, CDCl₃) δ 161.5, 159.2, 130.0, 125.1, 124.5, 115.2, 114.6, 113.8, 55.8.

6-Methoxy-1,3-benzothiazole-2-carbonitrile (2.7):

Palladium chloride (314 mg, 1.87 mmol), CuI (1.78 g, 9.36 mmol), TBAB (12.0 g, 37.4 mmol), and **(11)** (3.60 g, 18.7 mmol,) were suspended in anhydrous 1:1 DMF:DMSO (375 mL). The resultant red-brown mixture was placed under N₂ and stirred at 120 °C for 3 h. The reaction was then diluted with ethyl acetate and washed with H₂O (4 x 50 mL). The organics were then dried over Na₂SO₄, filtered, and concentrated in vacuo. The crude product was purified by flash column chromatography (5:1 hexanes:EtOAc) to provide **2.7** (3.09 g, 87%) as a light yellow solid. ¹H NMR (500 MHz, CDCl₃) δ 8.08 (d, J = 9.1, 1H), 7.36 (d, J = 2.4, 1H), 7.24 (dd, J = 2.4, J = 9.1, 1H), 3.93 (s, 3H); ¹³C NMR (125 MHz, CDCl₃) δ 160.7, 147.1, 137.7, 133.6, 126.1, 118.8, 113.4, 103.1, 56.2.

6-Hydroxy-1,3-benzothiazole-2-carbonitrile (2.8):

Pyridine hydrochloride (1.18 g, 10.2 mmol) and **(2.7)** (195 mg, 1.02 mmol) were combined in a rigorously dried sealed tube, placed under N₂, and stirred at 180 °C for 1 h. The resulting red-brown residue was suspended in EtOAc and washed with saturated NaHCO₃ (2 x 20 mL), 1 M NaHSO₄ (2 x 20 mL), H₂O (2 x 40 mL), and brine (1 x 50 mL). The organics were then dried over MgSO₄, filtered, and concentrated *in vacuo*. The crude product was purified via flash column chromatography, eluting with 3:1 hexanes:EtOAc, to yield **12** (111 mg, 61%) as a pale yellow solid. ¹H NMR (500 MHz, CD₃OD) δ 7.89 (d, J = 9.0, 1H), 7.31 (d, J = 2.0, 1H),

7.08 (dd, $J = 2.4$, $J = 9.0$, 1H); ^{13}C NMR (125 MHz, CD_3OD) δ 160.4, 147.4, 139.1, 134.0, 126.7, 119.7, 114.4, 107.1.

D-Luciferin (2.1):

D-Cysteine hydrochloride monohydrate (30.0 mg, 0.171 mmol) and (**12**) (28.7 mg, 0.163 mmol) were suspended in 2:1 MeOH:H₂O (1 mL) in a 20 mL vial. Potassium carbonate (22.7 mg, 0.164 mmol) was then added to the mixture, and the resulting bright yellow-green solution was stirred under N₂ for 20 min. Upon consumption of (**2.8**) the methanol was removed *in vacuo* and the remaining aqueous solution acidified to pH 3 with 3 M HCl. The reaction was then extracted with EtOAc (5 x 20 mL). The combined organics were dried over NaSO₄, filtered, concentrated *in vacuo*, purified with flash column chromatography (3:3:1 CH₂Cl₂:EtOAc:MeOH) to provide pure (**1**) (39.1 mg, 86%) as a pale yellow solid. ^1H NMR (500 MHz, CD_3OD) δ 7.88 (d, $J = 8.9$, 1H), 7.33 (d, $J = 2.3$, 1H), 7.05 (dd, $J = 2.3$, $J = 8.9$, 1H), 5.37 (app t, $J = 9.0$, 1H), 3.73-3.76 (m, 2H); ^{13}C NMR (125 MHz, CD_3OD) δ 172.1, 166.2, 157.6, 157.1, 146.8, 137.7, 124.5, 116.8, 105.9, 78.2, 34.5.

Method B (Scheme 2-3) [32]:

***N*-(*p*-Methoxyphenyl)cyanothioformamide (2.6)**

p-Anisidine (**2.4**, 1.23 g, 10.0 mmol) and **3** (2.19 g, 10.5 mmol) were stirred in 90 mL of anhydrous solvent (2:1 MeCN:THF) under N₂ for ~1 h (until **4** was consumed). A solution of sodium thiosulfate (4.74 g, 30.0 mmol in 20 mL H₂O) was then added, and the mixture was vigorously stirred for an additional 3 h. The reaction mixture was filtered to remove elemental sulfur, and the volatiles were removed *in vacuo*. The remaining aqueous mixture was again filtered to remove residual solids and the filtrate acidified with 1 M NaHSO₄. Cyanothioformamide **2.6** precipitated from solution and was collected by vacuum filtration. The material was washed with additional H₂O, then dried to provide **6** as a vivid orange solid (1.7 g, 86%). Compound **6** was characterized as a mixture of tautomers. ¹H NMR (500 MHz, acetone-*d*₆) δ 12.1 (br s, 1H), 7.92 (d, *J* = 9.1, 1.5H), 7.48 (d, *J* = 8.9, 0.4H), 7.02 (m, 2H), 3.84 (s, 3H); ¹³C NMR (125 MHz, acetone-*d*₆) δ 162.4, 160.0, 132.1, 125.4, 115.2, 114.9, 56.2.

6-Methoxy-1,3-benzothiazole-2-carbonitrile (2.7)

In Method B, compound **2.7** was prepared as in method A [10].

6-Hydroxy-1,3-benzothiazole-2-carbonitrile (2.8)

Pyridine hydrochloride (6.7 g, 53 mmol) and **2.7** (1.0 g, 5.3 mmol) were placed in a rigorously dried sealed tube, along with dry sulfolane (2.5 mL). The reaction mixture was sealed under N₂ and stirred at 180 °C for 1.5 h. The mixture was allowed to cool to rt, and the remaining residue was suspended in MTBE (100 mL), then washed with H₂O (2 x 20 mL) and brine (1 x 50 mL). The organics were then dried over Na₂SO₄, filtered, and concentrated *in*

vacuo. The crude product was purified via flash column chromatography (eluting with 3:1 hexanes:ethyl acetate) to provide **2.8** (810 mg, 93%) as a pale yellow solid. ¹H NMR (500 MHz, acetone-*d*₆) δ 9.43 (br s, 1H) 8.05 (dd, *J* = 3.3, *J* = 9.0, 1H), 7.61 (d, *J* = 2.4, 1H), 7.27 (dd, *J* = 2.4, *J* = 9.0, 1H); ¹³C NMR (125 MHz, acetone-*d*₆) δ 159.8, 147.5, 138.9, 133.9, 126.9, 119.7, 114.5, 107.5.

D-Luciferin (2.1)

In Method B, compound **2.1** was synthesized as in method A [10].

Method C (Scheme 2-4):

4-Chloro-5-([4-methoxyphenyl]imino)-5H-1,2,3-dithiazole (2.5)

4,5-Dichloro-1,2,3-dithiazole (**2.5**) (21.9 g, 105 mmol) was added to a 500-mL round-bottom flask, followed by anhydrous CH₂Cl₂ (300 mL) and *p*-anisidine (12.3 g, 100 mmol). The green mixture was stirred at rt under N₂ for 3 h or until TLC (4:1 hexanes:EtOAc) showed full consumption of *p*-anisidine. The solvent was then removed *in vacuo*, and the crude material was stirred in warm hexanes (50 °C, 10 min) to solubilize residual sulfur. The suspension was quickly filtered and washed with additional warm hexanes. The precipitate (containing the hydrochloride salt) was then suspended in H₂O (500 mL) and extracted with MTBE (5 x 200 mL). The combined organics were washed with H₂O (200 mL) and brine (100 mL) and concentrated *in vacuo* to afford **5** (25 g, 96%) as a yellow solid. In some cases, this material was taken on directly to the next step. ¹H NMR (500 MHz, acetone-*d*₆) δ 7.31 (d, *J* = 8.9, 2H) 7.07 (d, *J* = 8.9, 2H), 3.85 (s, 3H); ¹³C NMR (125 MHz, acetone-*d*₆) δ 159.8, 156.7, 149.6, 144.4, 123.2, 116.1, 56.4.

6-Methoxy-1,3-benzothiazole-2-carbonitrile (2.7) and 6-hydroxy-1,3-benzothiazole-2-carbonitrile (2.8)

p-Anisidine (2.46 g, 20.0 mmol) and 4,5-dichloro-1,2,3-dithiazolium chloride **2.3** (4.37 g, 21.0 mmol) were added to a rigorously dried sealed tube, suspended in dry sulfolane (10 mL), and placed under N₂. The sealed reaction was stirred for 3 h at 40 °C, then directly transferred to a pre-heated silicon oil bath (180 °C) and stirred for an additional 20 min. Upon cooling to rt, pyridine hydrochloride (23.0 g, 0.200 mol) was added to the reaction mixture. The reaction vessel was re-sealed under N₂ and stirred at 180 °C for 1 h. The mixture was allowed to cool to

rt, and the resulting crude residue was suspended in MTBE (400 mL), then washed with H₂O (3 x 200 mL) and brine (100 mL). The organics were dried over Na₂SO₄, filtered, and concentrated *in vacuo*. The material was then purified via flash column chromatography (eluting with 10:1 – 1:1 hexanes:ethyl acetate). The desired phenol **2.8** was isolated as a pale yellow solid (1.81 g, 51%) along with the methyl ether precursor **2.7** (796 mg, 21%). In some cases, the imino adduct **2.5** was isolated and purified prior to thermolysis and deprotection at 180 °C. In these cases, a mixture of **2.7** and **2.8** (20% and 61%, respectively) was obtained. Additional **2.8** was obtained by re-subjecting isolated **2.7** to pyr•HCl deprotection (outlined in method A above). The NMR spectra of **2.8** were in agreement with the values tabulated in method B above. Compound **2.7**: ¹H NMR (500 MHz, acetone-*d*₆) δ 8.08 (d, *J* = 9.1, 1H), 7.76 (d, *J* = 2.5, 1H), 7.30 (dd, *J* = 2.5, *J* = 9.1, 1H), 3.95 (s, 3H); ¹³C NMR (125 MHz, acetone-*d*₆) δ 162.0, 148.2, 139.1, 134.8, 126.8, 120.0, 114.6, 105.1, 57.0.

D-Luciferin (2.1)

In Method C, compound **2.1** was synthesized as previously reported [10].

Synthetic procedures for 6'-aminoluciferin [32]

Method A (from **2.10**, Scheme 2-5):

(4-Nitrophenyl)cyanothioformamide (2.11)

4,5-Dichloro-1,2,3-dithiazole (**2.3**, 0.302 g, 1.45 mmol) and 4-nitroaniline (**2.10**, 0.200 g, 1.45 mmol) were added to a round-bottom flask and placed under N₂. THF (6 mL) and MeCN (6 mL) were then added and the resulting solution was stirred for 5 min at rt. Pyridine (0.23 mL, 2.9 mmol) was added dropwise to the flask. The mixture was stirred for 60 min (when TLC with 7:3 hexanes:ethyl acetate indicated full consumption of **2.10**). A solution of sodium thiosulfate (0.686 g in 3 mL H₂O) was then added, and the mixture was stirred for 50 min at rt. The reaction was then diluted with 1 M sodium bisulfate (30 mL) and extracted with EtOAc (3 x 30 mL). The organic layer was washed with 1 M sodium bisulfate (3 x 25 mL) and brine (3 x 25 mL), dried over MgSO₄, filtered, and concentrated *in vacuo*. The crude material was purified via flash column chromatography (eluting with 9:1 to 7:3 hexanes:ethyl acetate) to provide **2.11** as a red-orange solid (0.24 g, 80%). ¹H NMR (400 MHz, acetone-*d*₆, mixture of tautomers) δ 8.42 (app d, *J* = 8.3, 0.26H), 8.38 (app d, *J* = 9.2, 1.74H), 8.30 (app d, *J* = 9.2, 1.74H), 7.91 (app d, *J* = 8.4, 0.26H). ¹³C NMR (125 MHz, acetone-*d*₆, mixture of tautomers) δ 167.0, 164.6, 146.6, 143.8, 126.0, 125.5, 124.1, 123.8, 114.3, 113.3; HRMS (ESI⁺) calcd for C₈H₄N₃O₂S [M – H]⁺ 206.0024, found 206.0017.

6-Nitro-1,3-benzothiazole-2-carbonitrile (2.12)

Palladium chloride (0.112 g, 0.634 mmol), CuI (0.458 g, 3.17 mmol), TBAB (4.08 g, 12.7 mmol) and **2.11** (1.30 g, 6.34 mmol) were placed in a flame-dried flask, flushed with N₂ and suspended in 190 mL of anhydrous DMF:DMSO (1:1). The resulting mixture was stirred at 130

°C under N₂ for 4 h. The reaction was then diluted with EtOAc (150 mL) and water (100 mL). The organic layer was isolated and the aqueous layer was extracted with additional ethyl acetate (4 x 100 mL). The organic layers were combined and washed with water (5 x 100 mL) and brine (2 x 100 mL), then dried over MgSO₄, filtered and concentrated *in vacuo*. The crude material was purified via flash column chromatography (eluting with 7:3 hexanes:ethyl acetate) to provide **2.12** as a fluffy, light yellow solid (0.96 g, 74%). The NMR spectra were consistent with previous reports. ¹H NMR (500 MHz, CDCl₃) δ 8.97 (d, *J* = 2.2, 1H), 8.53 (dd, *J* = 2.2, *J* = 9.1, 1H), 8.39 (d, *J* = 9.1, 1H); ¹³C NMR (125 MHz, CDCl₃) δ 155.4, 147.4, 141.9, 135.7, 126.2, 123.2, 118.7, 112.1.

6-Amino-1,3-benzothiazole-2-carbonitrile (2.13)

Ammonium chloride (6.01 g, 113 mmol) was added to a solution of **2.12** (2.33 g, 11.3 mmol) in reagent grade EtOH (400 mL). The mixture was stirred at rt for 5 min. Zinc powder (14.8 g, 227 mmol) was then added, and the reaction was stirred vigorously at rt for 30 min. The heterogeneous mixture was filtered through Celite using copious amounts of MeOH. The filtrate was collected and concentrated *in vacuo*. The isolated crude material was purified by flash column chromatography (eluting with 2:1 hexanes:ethyl acetate) to provide amine **2.13** (1.9 g, 94%) as a pale yellow solid. The NMR spectra were in agreement with previously published values. ¹H NMR (500 MHz, acetone-*d*₆) δ 7.87 (d, *J* = 8.9, 1H), 7.26 (d, *J* = 2.1, 1H), 7.09 (dd, *J* = 2.1, *J* = 8.9, 1H), 5.64 (br s, 2H); ¹³C NMR (125 MHz, acetone-*d*₆) δ 151.4, 145.3, 139.5, 129.8, 126.3, 118.5, 114.8, 103.7.

6'-Aminoluciferin (2.2)

D-Cysteine hydrochloride monohydrate (81.2 mg, 0.462 mmol) and **2.13** (71.0 mg, 0.405 mmol) were suspended in MeCN (5 mL) in a 20 mL vial. A solution of K₂CO₃ (56.5 mg, 0.409 mmol) in 400 μ L of H₂O was added to the mixture, and the resulting solution stirred vigorously at rt under N₂. A bright yellow precipitate formed as the reaction proceeded. After 20 min of stirring this precipitate was vacuum filtered and dried. The crude material was triturated with MeCN and vacuum filtered once more to provide the analytically pure potassium salt **2.2** in excellent yield (117 mg, 91%) as a bright yellow powder. ¹H NMR (500 MHz, D₂O) δ 7.53 (d, *J* = 8.8, 1H), 7.07 (s, 1H), 6.88 (d, *J* = 8.5, 1H), 5.09 (app t, *J* = 8.9, 1H), 3.72 (app t, *J* = 10.5, 1H) 3.54 (dd, *J* = 8.3, *J* = 10.5, 1H); ¹³C NMR (125 MHz, D₂O) δ 180.4, 168.2, 159.1, 149.4, 147.9, 139.9, 126.4, 120.2, 108.9, 82.7, 38.9.

Method B (from **2.14**, Scheme 2-5):

6-Nitro-1,3-benzothiazole-2-carbonitrile (2.12)

Benzothiazole **2.14** (901 mg, 5.00 mmol) and hydrazine monohydrate (2.5 ml, 50 mmol) were suspended in reagent grade ethanol (50 mL), and the mixture was stirred at rt for 12 h. The deep red solution was then cooled in an ice bath. HCl (5 M solution) was added until a brilliant yellow precipitate formed. The precipitate was filtered and washed with cold H₂O, affording **14** upon drying (under vacuum). Aminothiol **2.15** was then suspended in dry CH₂Cl₂ (10 mL) and dithiazolium chloride **2.3** (619 mg, 3.00 mmol) was added. The resulting solution was stirred at reflux for 12 h. The crude mixture was adsorbed to silica gel, concentrated and purified by flash column chromatography (eluting with 20:1 to 5:1 hexanes:ethyl acetate) to provide nitro benzothiazole **2.12** (380 mg, 62%) as a pale orange solid. The NMR spectra were consistent with

previous reports. ^1H NMR (500 MHz, acetone- d_6) δ 9.35 (d, $J = 2.1$, 1H), 8.57 (dd, $J = 2.1$, $J = 9.1$, 1H), 8.48 (d, $J = 9.1$, 1H); ^{13}C NMR (125 MHz, acetone- d_6) δ 156.8, 148.7, 144.3, 137.6, 127.0, 124.3, 121.2, 113.9.

6-Amino-1,3-benzothiazole-2-carbonitrile (2.13)

In Method B, compound **2.13** was prepared according to the procedure described above in Method A.

6'-Aminoluciferin (2.2)

In Method B, compound **2.2** was prepared according to the procedure described above in Method A.

Synthesis of dithiooxamide byproduct:

***N'*-(4-Methoxyphenyl)ethanedithioamide (2.9)**

Imino adduct **2.5** (262 mg, 1.01 mmol) was suspended in MeCN (10 mL) and a solution of $\text{Na}_2\text{S}\cdot 9\text{H}_2\text{O}$ (482 mg in 2 mL H_2O) was added. The reaction was then vigorously stirred at 50 $^\circ\text{C}$ for 10 min. Upon cooling to rt, the reaction mixture was filtered through filter paper to remove elemental sulfur and the MeCN evaporated *in vacuo*. Upon removal of the organics, a fine red solid precipitated. This material was isolated via vacuum filtration and washed with excess H_2O . The material was further dried under vacuum to provide **2.9** as a bright red solid (224 mg, 98%). The NMR spectra were in agreement with previously published values. ^1H NMR (500 MHz, acetone- d_6) δ 12.1 (br s, 1H), 9.89 (br s, 2H), 8.04 (d, $J = 9.1$, 2H), 7.05 (d, $J = 9.1$,

2H), 3.87 (s, 3H); ¹³C NMR (125 MHz, acetone-*d*₆) δ 191.8, 181.9, 159.9, 133.1, 125.1, 115.3, 56.4.

References

- (1) Paley, M. A.; Prescher, J. A. Bioluminescence: a versatile technique for imaging cellular and molecular features. *MedChemComm* **2014**, *5*, 255.
- (2) Prescher, J. A.; Contag, C. H. Guided by the light: visualizing biomolecular processes in living animals with bioluminescence. *Curr. Op. Chem. Biol.* **2010**, *14*, 80.
- (3) Wood, K. V. The chemical mechanism and evolutionary development of beetle bioluminescence. *Photochem. Photobiol.* **1995**, *62*, 662.
- (4) Adams, S. T., Jr.; Miller, S. C. Beyond D-luciferin: expanding the scope of bioluminescence imaging in vivo. *Curr. Op. Chem. Bio.* **2014**, *21*, 112.
- (5) White, E. H.; Worther, H.; Seliger, H. H.; McElroy, W. D. Amino Analogs of Firefly Luciferin and Biological Activity Thereof. *J. Am. Chem. Soc.* **1966**, *88*, 2015.
- (6) Shinde, R.; Perkins, J.; Contag, C. H. Luciferin derivatives for enhanced in vitro and in vivo bioluminescence assays. *Biochemistry* **2006**, *45*, 11103.
- (7) Viviani, V. R.; Neves, D. R.; Amaral, D. T.; Prado, R. A.; Matsushashi, T.; Hirano, T. Bioluminescence of beetle luciferases with 6'-amino-D-luciferin analogues reveals excited keto-oxyluciferin as the emitter and phenolate/luciferin binding site interactions modulate bioluminescence colors. *Biochemistry* **2014**, *53*, 5208.
- (8) Reddy, G. R.; Thompson, W. C.; Miller, S. C. Robust light emission from cyclic alkylaminoluciferin substrates for firefly luciferase. *J. Am. Chem. Soc.* **2010**, *132*, 13586.
- (9) Mofford, D. M.; Reddy, R. R.; Miller, S. C. Aminoluciferins Extend Firefly Luciferase Bioluminescence into the Near-Infrared and Can Be Preferred Substrates over d-Luciferin. *J. Am. Chem. Soc.* **2014**, *136*, 13277.
- (10) McCutcheon, D. C.; Paley, M. A.; Steinhardt, R. C.; Prescher, J. A. Expedient synthesis of electronically modified luciferins for bioluminescence imaging. *J. Am. Chem. Soc.* **2012**, *134*, 7604.
- (11) Conley, N. R.; Dragulescu-Andrasi, A.; Rao, J.; Moerner, W. E. A selenium analogue of firefly D-luciferin with red-shifted bioluminescence emission. *Angew. Chem. Int. Ed. Engl.* **2012**, *51*, 3350.

- (12) Woodrooffe, C. C.; Meisenheimer, P. L.; Klaubert, D. H.; Kovic, Y.; Rosenberg, J. C.; Behney, C. E.; Southworth, T. L.; Branchini, B. R. Novel heterocyclic analogues of firefly luciferin. *Biochemistry* **2012**, *51*, 9807.
- (13) Jathoul, A. P.; Grounds, H.; Anderson, J. C.; Pule, M. A. A dual-color far-red to near-infrared firefly luciferin analogue designed for multiparametric bioluminescence imaging. *Angew. Chem. Int. Ed. Engl.* **2014**.
- (14) Evans, M. S.; Chaurrette, J. P.; Adams, S. T., Jr.; Reddy, G. R.; Paley, M. A.; Aronin, N.; Prescher, J. A.; Miller, S. C. A synthetic luciferin improves bioluminescence imaging in live mice. *Nat. Methods* **2014**, *11*, 393.
- (15) Li, J.; Chen, L. Z.; Du, L. P.; Li, M. Y. Cage the firefly luciferin! - A strategy for developing bioluminescent probes. *Chem. Soc. Rev.* **2013**, *42*, 662.
- (16) Sellmyer, M. A.; Bronsart, L.; Imoto, H.; Contag, C. H.; Wandless, T. J.; Prescher, J. A. Visualizing cellular interactions with a generalized proximity reporter. *Proc. Natl. Acad. Sci. USA* **2013**, *110*, 8567.
- (17) Meroni, G.; Rajabi, M.; Santaniello, E. D-Luciferin, derivatives and analogues: synthesis and in vitro/in vivo luciferase-catalyzed bioluminescent activity. *ARKIVOC* **2009**, 265.
- (18) Fraga, H. Firefly luminescence: A historical perspective and recent developments. *Photochem. Photobiol. Sci.* **2008**, *7*, 146.
- (19) White, E. H.; McCapra, F.; Field, G. F.; McElroy, W. D. the structure and synthesis of firefly luciferin. *J. Am. Chem. Soc.* **1961**, *83*, 2402.
- (20) White, E. H.; McCapra, F.; Field, G. F. The structure and synthesis of firefly luciferin. *J. Am. Chem. Soc.* **1963**, *85*, 337.
- (21) White, E. H.; Rapaport, E.; Seliger, H., H.; Hopkins, T. A. The chemi- and bioluminescence of firefly luciferin: An efficient chemical production of electronically excited states. *Bioorg. Chem.* **1971**, *1*, 92.
- (22) Seto, S.; Ogura, K.; Nishiyama, Y. A Convenient synthetic method of 2-carbamoyl-6-methoxybenzothiazole, one of intermediates for the synthesis of firefly luciferin. *Bull. Chem. Soc. Jpn.* **1963**, *36*, 331.
- (23) Wurfel, H.; Weiss, D.; Beckert, R.; Guther, A. A new application of the "mild thiolation" concept for an efficient three-step synthesis of 2-cyanobenzothiazoles: a new approach to Firefly-luciferin precursor. *J. Sulfur Chem.* **2012**, *33*, 9.
- (24) Ciuffreda, P.; Casati, S.; Meroni, G.; Santaniello, E. A new synthesis of dehydroluciferin [2-(6'-hydroxy-2'-benzothiazolyl)-thiazole-4-carboxylic acid] from 1,4-benzoquinone. *Tetrahedron* **2013**, *69*, 5893.

- (25) Appel, R.; Janssen, H.; Siray, M.; Knoch, F. Synthese und reaktionen des 4,5-dichloro-1,2,3-dithiazolium-chlorids. *Eur. J. Inorg. Chem.* **1985**, *118*, 1632.
- (26) Kim, K. Synthesis and Reactions of 1,2,3-Dithiazoles. *Sulfur Reports* **1998**, *21*, 147.
- (27) Cuadro, A. M.; Alvarezbuilla, J. 4,5-Dichloro-1,2,3-Dithiazolium chloride (Appels Salt) - reactions with N-nucleophiles. *Tetrahedron* **1994**, *50*, 10037.
- (28) Inamoto, K.; Hasegawa, C.; Hiroya, K.; Doi, T. Palladium-catalyzed synthesis of 2-substituted benzothiazoles via a C-H functionalization/intramolecular C-S bond formation process. *Org. Lett.* **2008**, *10*, 5147.
- (29) Rees, C. W. Polysulfur-nitrogen heterocyclic chemistry. *J. Heterocycl. Chem.* **1992**, *29*, 639.
- (30) Rakitin, O. A.; Rees, C. W.; Vlasova, O. G. Direct synthesis of 2-cyanobenzimidazoles and the generation of S₂. *Tetrahedron Lett.* **1996**, *37*, 4589.
- (31) Besson, T.; Rees, C. W. Some chemistry of 4,5-dichloro-1,2,3-dithiazolium chloride and its derivatives *J. Chem. Soc., Perkin Trans. 1* **1995**, 1659.
- (32) McCutcheon, D. C.; Porterfield, W. B.; Prescher, J. A. Rapid and scalable assembly of firefly luciferase substrates. *Org. Biomol. Chem.* **2015**, *13*, 2117

CHAPTER 3: Expedient synthesis of electronically modified luciferins

3.1 Introduction

Despite its remarkable versatility, bioluminescence has been largely limited to monitoring one cell type or biological feature at a time. This is because only a handful of luciferases are suitable for biological work and, of these, nearly all utilize the same substrate (D-luciferin) [1-5]. The vast majority of efforts to develop new bioluminescent tools have focused on mutating luciferase enzymes from the firefly (Fluc) and related organisms [6,7]. By contrast, only a handful of studies have focused on modifying the structure of D-luciferin (**3.1**), the substrate common to all insect luciferases. This disparity is surprising, given the prominent role of the small molecule in the light-emitting reaction. During the Fluc-catalyzed oxidation of D-luciferin, an excited-state version of the product (oxyluciferin) is generated; relaxation of this molecule to the ground state releases a photon of yellow-green light [8]. Since the chemical makeup of the excited-state emitter influences light production, modifications to the aromatic core can alter the wavelength and intensity of photons released. Miller and others have shown that luciferin variants containing a nitrogen atom in place of the exocyclic oxygen are efficiently processed by Fluc and emit red light [9–11]. In related work, Branchini and others replaced the entire benzothiazole core of d-luciferin with quinoline, naphthalene, and coumarin units. These analogs emitted different colors of light with Fluc, but elevated pH values were required to achieve robust emission in most cases [12–13]. Although these luciferins have somewhat limited utility in biological assays, they remain the only examples of Fluc substrates that do not contain a benzothiazole moiety.

Retooling bioluminescence technology for multicomponent imaging requires access to larger collections of light-emitting luciferins. Such molecules could potentially provide different colors of bioluminescent light or be utilized by novel luciferase variants. Unfortunately, luciferins have been notoriously difficult to produce, owing to a lack of rapid and reliable syntheses for these richly functionalized molecules. We aimed to expand the repertoire of modified heteroaromatic luciferins suitable for biological studies. In particular, we were attracted to luciferins with benzimidazole and imidazoline rings (the nitrogenous counterparts to the benzothiazole and thiazoline units in D-luciferin, **3.2–3.4**). Heterocycles of this sort are capable of absorbing and emitting light, an important criterion for bioluminescent substrates [14–15]. White and McElroy have also shown that benzimidazole and other heterocycles are competitive inhibitors of Fluc, suggesting that **3.2–3.4** would be able to access the substrate binding pocket [16]. Last, since benzimidazole and imidazoline motifs are present in numerous pharmaceutical agents, we felt that the electronically modified analogs would possess reasonable bioavailability and metabolic stability for use in cells and animal models [17,18].

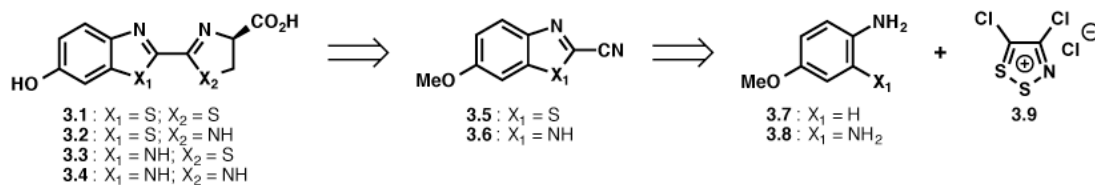
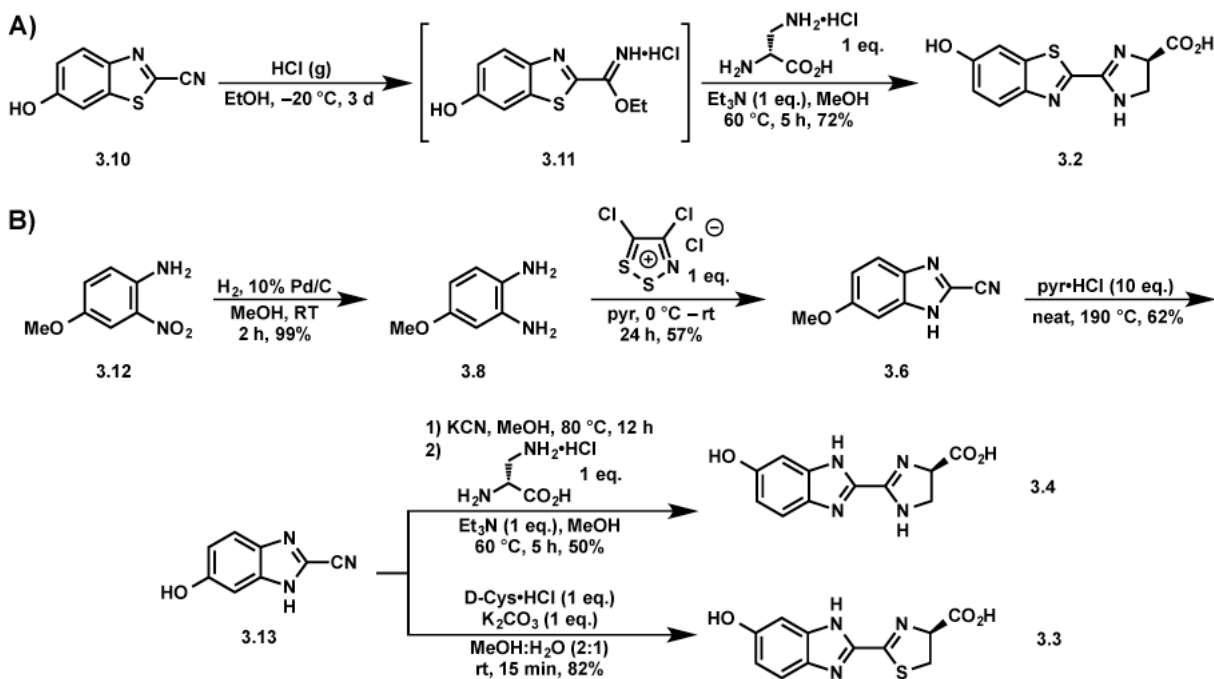


Figure 3-1: Retrosynthetic analysis of nitrogenous luciferin analogs. This figure is reproduced with permission from McCutcheon, *et al. J. Am. Chem. Soc.* **2012**, *134*, 7604–7607.

Analogs **3.2–3.4**, like D-luciferin, contain a unique 2–2' linkage of heteroaromatic rings. This connectivity is scarcely observed in known natural products, and facile methods to prepare such linkages are rare [19]. In fact, the first synthesis of D-luciferin, reported by White in 1963, is basically the same route used to produce nearly all luciferins today [20]. This synthesis proceeds through a cyanobenzothiazole intermediate (**3.5**), which, upon protecting group removal, can be condensed with D-cysteine to provide the native luciferin. This condensation is both mild and high-yielding, making it an appealing method for late-stage introduction of the luciferin stereocenter. Unfortunately, the White synthesis of **3.5** requires seven steps and is not amenable to heteroatom substitutions.

Scheme 3-1: Synthesis of nitrogenous luciferin scaffolds: **A)** imidazoline containing analog **3.2**; **B)** benzimidazole-containing analogs **3.2** and **3.3**. This scheme is modified with permission from McCutcheon, *et al. J. Am. Chem Soc.* **2012**, *134*, 7604–7607.



Recognizing the utility of cyano heterocycles for luciferin production, we aimed to utilize dithiazolium chemistry to access cyanobenzimidazole **3.6**. Condensation of these scaffolds with either D-cysteine or diaminopropionic acid could provide the entire set of luciferin analogs (**3.2**–**3.4**). To access **3.5** and **3.5** in tandem, we were drawn to the dithiazolium chloride **3.9** (Figure 3-1). This reagent, also known as Appel's salt, has previously been used to synthesize both benzothiazole and benzimidazole scaffolds from anilines [21]. Appel's salt condenses readily with arylamines, and the resulting iminodithiazoles can be easily opened with a variety of nucleophiles [22]. If the nucleophile is present on the aniline itself (as in the case of *o*-aminoanilines), cyanobenzimidazole structures can be isolated directly.

To investigate the utility of Appel's salt for luciferin analog synthesis, we first used the reagent to prepare benzimidazole **3.6** (Scheme 3-1B). Gratifyingly, this molecule was isolated in a single step upon incubation of bis-aniline **3.8** with **3.9**. In this reaction, the initial dithiazole adduct is likely trapped by the *o*-amino substituent of **3.8**, providing the cyclized product. Cyanobenzimidazole **3.6** was ultimately demethylated and condensed with D-cysteine as above to isolate luciferin **3.3**. Multigram quantities of **3.3** have been produced using the route outlined in Scheme 3.1, highlighting the scalability of the approach.

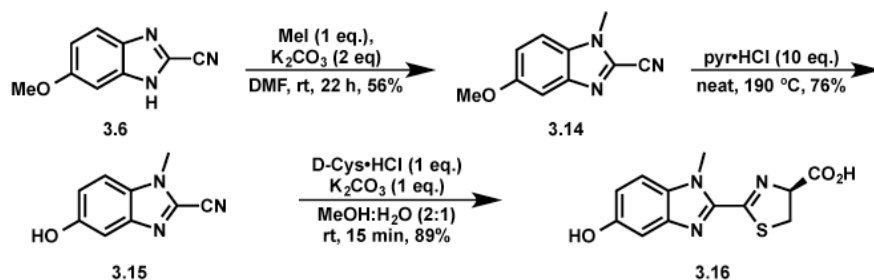
The cyano heterocycles produced with Appel's salt can be condensed with a variety of other 1,2-disubstituted nucleophiles in addition to D-cysteine. We exploited this mode of reactivity to generate the imidazoline rings present in luciferins **3.2** and **3.4**. First, intermediates **3.10** and **3.13** were converted into the corresponding imidates using standard conditions. The imidates were not isolated but treated directly with diaminopropionic acid to afford the desired luciferins in reasonable yield.



Figure 3-2: N-H tautomerization of benzimidazole analog. This figure is reproduced with permission from McCutcheon, *et al. J. Am. Chem. Soc.* **2012**, *134*, 7604–7607.

Our initial efforts to characterize luciferins **3.2–3.4** were complicated by tautomerism. Benzimidazole scaffolds are known to undergo rapid N–H isomerization in solution (Figure 3-2), resulting in significantly broadened ^1H and ^{13}C NMR signals. We were also concerned that such rapid tautomerization would suppress bioluminescent light emission from the analogues. Such quenching behavior has been observed with other electronically excited benzimidazoles [23,24]. To mitigate against potential quenching effects and aid our structural characterization efforts, we prepared a methylated version of **3.3** (Scheme 3-2). Interestingly, only one *N*-methyl regioisomer (**3.14**) was formed in reasonable yield from intermediate **3.6**.

Scheme 3-2: Synthesis of methylated benzimidazole analog **3.16**. This scheme is reproduced with permission from McCutcheon, *et al. J. Am. Chem. Soc.* **2012**, *134*, 7604–7607.



With the nitrogenous analogs in hand, we assayed the compounds for light emission with Fluc. Luciferins **3.2–3.4** and **3.16** were incubated with the enzyme, ATP, and coenzyme A (to reduce product inhibition) at pH 7.4 [25]. Light emission was measured using a cooled CCD camera, and representative images are shown in Figure 3-3. No photons were detected for analogue **3.2**, and only minimal light emission was observed with the related imidazoline **3.4** at low substrate concentrations. These reduced intensities may be attributed to poor binding to Fluc, lower efficiencies of light production, or a combination of factors. By contrast, robust emission was observed with the benzimidazole variants **3.3** and **3.16**, suggesting that these molecules can be converted to light-emitting species in the enzyme active site (Figure 3-3). Both analogs are weaker emitters than the native substrate (~100-fold reduced emission intensities in the low μM range, but on par with other luciferin scaffolds used in biological assays [10]. Additional improvements in light output may also be obtained using the analogs in combination with mutant luciferases [9,26]. Importantly, the bioluminescence emissions from **3.3** and **3.16** are long-lived (Figure 3-4). Prolonged light release is necessary for numerous imaging applications *in vivo* and has been difficult to achieve with other luciferins.

We next analyzed the bioluminescence emission profiles for **3.3**, **3.4**, and **3.16**. The spectra for these analogs, like most luciferins, are quite broad and indicate the presence of tautomers in aqueous solution (Figure 3-3C). Benzimidazole analog **3.3** was found to emit maximally at 578 nm, slightly red-shifted from d-luciferin ($\lambda_{\text{max}} = 557 \text{ nm}$) at room temperature. The bioluminescence spectrum of **3.3** is also substantially different from the analog's fluorescence profile, indicating a potential role for Fluc in modulating the color of light released (Table 3-1). Interestingly, the bioluminescence spectrum for benzimidazole analog **3.16** is substantially blue-shifted from those of luciferins **3.1** and **3.3**.

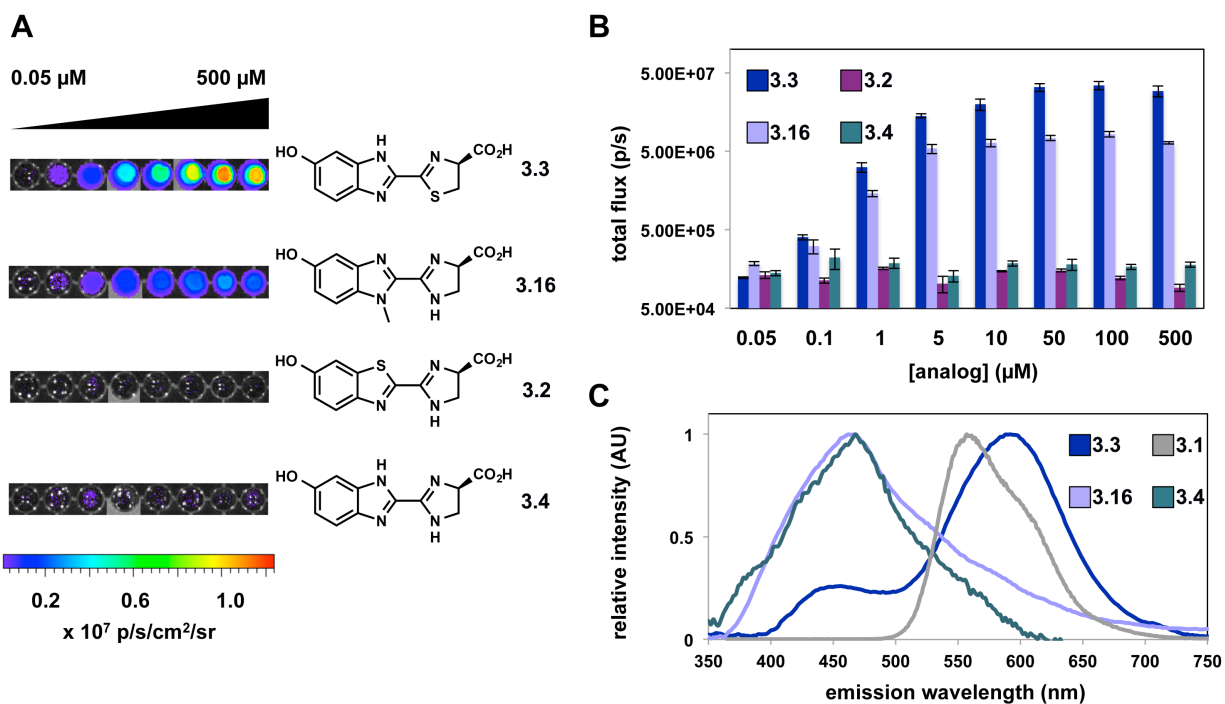


Figure 3-3: Light production from luciferin analogs. (A) Bioluminescence images from analogues **3.2–3.4** and **3.16** (0.05–500 μM) incubated with Fluc or no enzyme. (B) Quantification of the images from (A). (C) Bioluminescence emission spectra for luciferins **3.1**, **3.3**, **3.4**, and **3.16**. This figure is reproduced with permission from McCutcheon, *et al. J. Am. Chem Soc.* **2012**, *134*, 7604–7607

Table 3-2 Fluorescence emission for nitrogenous luciferin analogs in *in vitro* assay buffer and methanol.

Substrate	Maximum fluorescence λ_{max} (nm)	
	<i>in vitro</i> assay buffer	methanol
3.3	441	430
3.6	462	447
3.4	376	355

With peak emission near 460 nm, analog **3.16** emits the largest percentage of blue light among the known Fluc substrates. This result also implies that **3.16** may be useful for multicomponent imaging applications, as its emission can be readily resolved from other luciferins using appropriate filter sets.

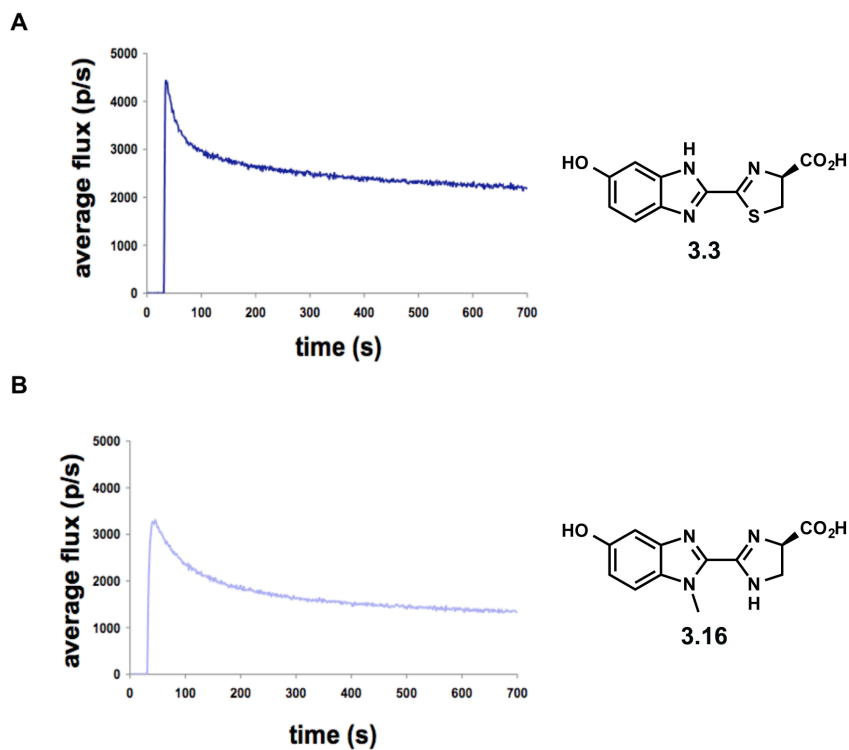


Figure 3-4: Prolonged bioluminescent light emission observed with (A) 250 μM **3.3** or (B) 250 μM **3.16** in the presence of Fluc. This figure is reproduced with permission from McCutcheon, *et al. J. Am. Chem Soc.* **2012**, *134*, 7604–7607.

To probe whether the light-emitting luciferins would also be useful for cell studies, we incubated **3.3**, **3.4**, and **3.16** with Fluc-expressing HEK 293 cells. Photon emission was measured using a cooled CCD camera, and sample images are shown in Figure 3.5. Dose-dependent light emission was observed for both **3.3** and **3.16**, with photon intensities peaking around 10–20 min

after substrate addition (Figure 3-6). No emission was observed from the nitrogenous analog **3.4** in this assay, even at high substrate concentrations. It should also be noted that no light was observed in the absence of the analogs, or when the compounds were incubated with non-luciferase-expressing cells (Figure 3-5). These results are consistent with the light-emitting behavior of D-luciferin in whole cells, and suggest that the benzimidazole scaffolds are sufficiently biocompatible for use in cellular imaging studies [2,10].

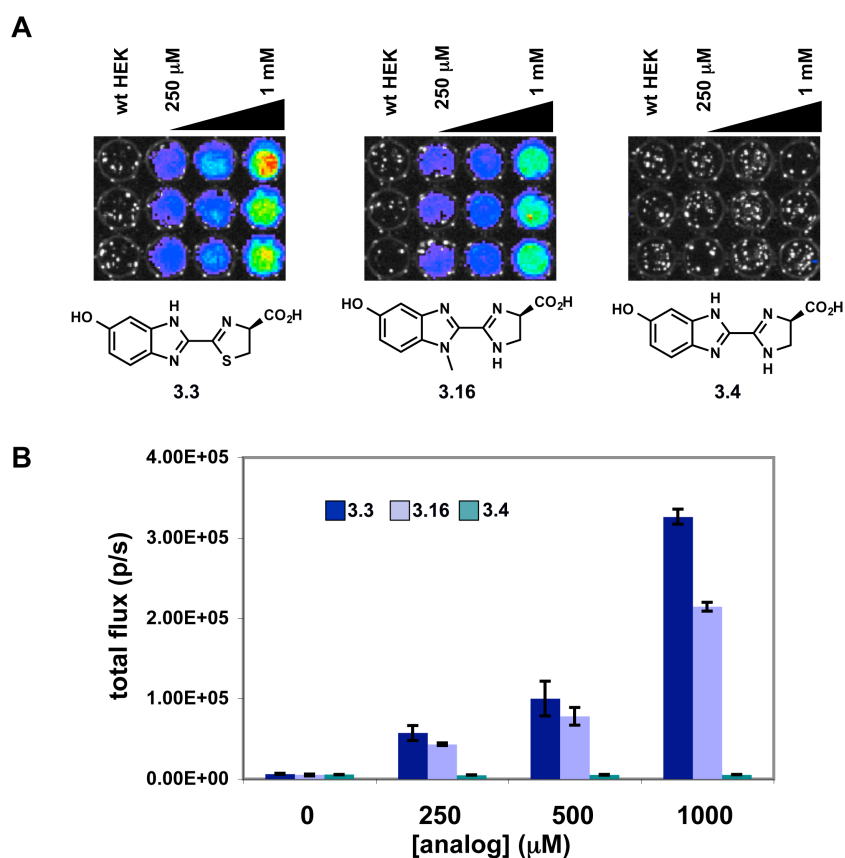


Figure 3-5: Cellular imaging with luciferin analogs. (A) Bioluminescence images from **3.2**, **3.4**, and **3.16** (250 μM –1 mM) incubated with luciferase-expressing HEK 293 cells or wild-type cells (wt HEK). (B) Quantification of the images from (A). This figure is reproduced with permission from McCutcheon, *et al. J. Am. Chem Soc.* **2012**, *134*, 7604–7607.

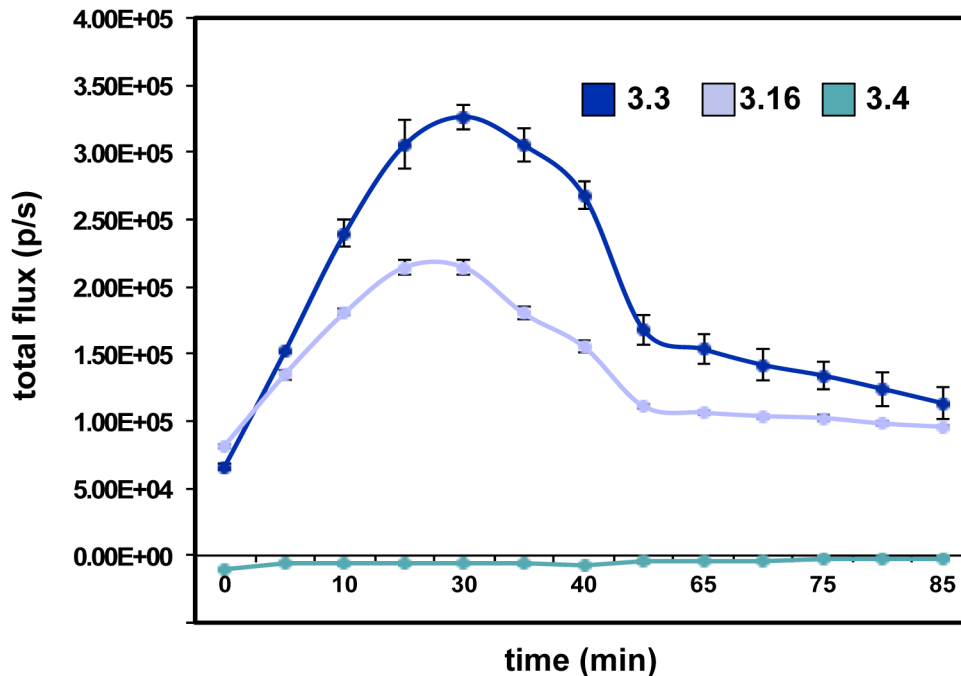


Figure 3-6: Time-dependent light emission measured for analogs **3.3**, **3.4**, and **3.16** (1 mM) incubated with Fluc-expressing HEK 293 cells. This figure is reproduced with permission from McCutcheon, *et al. J. Am. Chem Soc.* **2012**, *134*, 7604–7607.

In summary, we have developed a facile method to prepare luciferins from aniline starting materials and Appel's salt. This procedure was used to synthesize D-luciferin, the native substrate for Fluc, along with a series of nitrogenous analogs. Two of the analogs were found to emit light with purified Fluc and in live cells, and these scaffolds will be generally useful for imaging studies. More broadly, the chemistry reported here provides a gateway to access additional luciferin architectures. For example, the adducts formed upon aniline condensation with Appel's salt can be selectively fragmented to access quinazolines, benzoxazoles, and a variety of other heterocycles in addition to the benzothiazole and benzimidazole scaffolds examined here [22]. This diverse manifold of reactivity will likely be exploited for synthesizing new classes of heteroaromatic luciferins in the near future. The ability to rapidly access novel

luciferin substrates will expand the imaging toolkit and inspire new applications of bioluminescence technology.

Materials and methods

Recombinant luciferase production

The gene encoding Fluc was incorporated into a protein expression vector using standard molecular biology techniques. In brief, Fluc was amplified from a pcDNA3.1(+) plasmid containing an Fluc(pgl4 “luc2”)-IRES-eGFP fusion gene (courtesy of the Contag lab, Stanford). The PCR amplification primers were flanked with NcoI and NotI restriction enzyme sites. The amplified insert and the pET28a(+) expression vector were digested with NcoI and NotI (New England Biolabs). The digested insert was ligated into the pET28a backbone using a 3:1 insert:vector ratio and T4 DNA ligase (New England Biolabs, 400 U). The ligation reaction was performed at 16 °C for 16 h prior to transformation into chemically competent TOP10 cells (Invitrogen). Successful transformants were identified via bioluminescence imaging, and the desired pET28-Fluc-His₆ plasmid was retrieved using a mini-prep kit (Qiagen). Sequencing analysis confirmed the presence of the desired insert within the expression vector. To produce luciferase, pET28-Fluc-His₆ was transformed into BL21-DE3* cells (Novagen). The cells were spread on LB-agar plates containing 40 µg/mL of kanamycin. Following overnight growth, a single colony was used to inoculate a 10 mL culture in LB broth containing 40 µg/mL kanamycin. The culture was grown for 6-8 hours before transfer to 1L of LB broth. This culture was grown to OD₆₀₀=0.8, and protein expression was subsequently induced with 500 µM IPTG (Sigma Aldrich). The expression culture was placed in a 22 °C shaker overnight. The bacteria were then harvested by centrifugation (10 krpm, 15 min) and re-suspended in 40 mL of lysis

buffer (50 mM Tris-HCl, 500 mM NaCl, 1 mM DTT, 0.5% (v/v) Tween-20, 1 mM PMSF, pH 7.4). Cells were further ruptured by sonication (7 rounds, 70% output, 1 min pulsing at 70% frequency with a 3 min rest between pulses). The lysate was clarified by centrifugation (14 krpm, 1 h), and the desired luciferase protein was isolated via Ni²⁺-NTA affinity chromatography (Bio-Rad). Captured protein was eluted from the resin using 150 mM imidazole. Fractions containing purified Fluc were identified using SDS-PAGE and concentrated to 2 mg/mL. Fluc stocks were stored in 10% glycerol at -20 °C.

General bioluminescence imaging protocol

Samples were imaged using an IVIS Lumina (Xenogen) system (equipped with a cooled CCD camera). Exposure times ranged from 5 s – 5 min and were controlled using Living Image software. This software was also used to measure photon flux values from defined regions of interest. Such data were exported to Microsoft Excel for further analyses.

Light emission assays with recombinant luciferase

Bioluminescence assays with all luciferin compounds were carried out in triplicate, using solid black, flat-bottom, 96-well plates (BD Bioscience). Assay wells contained purified Fluc (0 or 2 µg), luciferin substrate (0-1 mM), DMSO (10 µL), ATP (Sigma, 0-1 mM), coenzyme-A (trithium salt, Calbiochem, 0-1 mM), and reaction buffer (20 mM Tris-HCl, 0.5 mg/mL BSA, 0.1 mM EDTA, 1 mM TCEP, 2 mM MgSO₄ pH 7.6), totaling 100 µL. For each assay, the CoA and ATP cofactors were used at equimolar concentrations with respect to the analog. Additionally, all non-enzyme assay components were premixed in the wells prior to Fluc addition. Images for all assays were acquired as described above.

Bioluminescence emission spectra

Emission spectra for all luciferin analogs were recorded on a Horiba Jobin Yvon FluoroMax-4 spectrometer. Each luciferin (2 mM) was incubated in a 10 mm path length cuvette with ATP (2 mM), LiCoA (2 mM) and reaction buffer totaling 900 μ L. Purified Flug (20 μ g) was added immediately prior to data acquisition. The excitation and emission slit widths on the instrument were adjusted to 0 and 29.4 nm, respectively. Emission data were collected at 2 nm intervals from 350-750 nm at ambient temperature. Acquisition time varied between 0.1-60 sec/wavelength depending on the amount of light produced. Light emission was measured in Relative Luminescence Units (RLU), and the intensities were normalized across the panel of luciferin substrates.

Cell-based bioluminescence assays

HEK-293 cells stably expressing Fluc (provided by the Contag lab, Stanford) were grown in DMEM media supplemented with fetal bovine serum (FBS, 10%), penicillin (10 units/mL), and streptomycin (10 mg/mL). The cells were cultured in a CO₂ (5%) humidified incubator at 37 °C. For light emission assays, approximately 10,000 cells were plated in 96-well black well plates. The cells were incubated with luciferin analogs (0-1000 μ M), and bioluminescence images were acquired as above.

General synthetic methods

All reagents purchased from commercial suppliers were of analytical grade and used without further purification. Appel's salt, 4,5-dichloro-1,2,3-dithiazolium chloride was prepared as described in chapter 2. Reaction progress was monitored by thin-layer chromatography on EMD 60 F₂₅₄ plates, visualized with UV light, ceric ammonium molybdate (CAM), chloranil, or KMnO₄ stain. All compounds were purified via flash column chromatography using Sorbent Technologies 60 Å, 230-400 mesh silica gel, unless otherwise stated. All anhydrous solvents were dried by passage over neutral alumina with the exception of DMF, which was passed over activated molecular sieves. Reaction vessels were either flame or oven dried prior to use. Reactions described below were performed under an atmosphere of N₂ and precautions were taken to rigorously exclude water.

NMR spectra were acquired with a Bruker DRX400 with a switchable QNP probe, a Bruker DRX500 spectrometer with a BBO probe, or a Bruker DRX500 spectrometer outfitted with a cryoprobe. All spectra were acquired at 298 K, unless otherwise specified. ¹H-NMR spectra were acquired at either 500 or 400 MHz, and ¹³C-NMR spectra were acquired at 125 or 100 MHz. For ¹³C-NMR data obtained via distortionless enhancement by polarization transfer (DeptQ), signals for tertiary and primary carbons are shown as negative, while the signals for quaternary and secondary carbons, along with solvent signals, are positive. Chemical shifts are reported in ppm relative to tetramethylsilane or residual NMR solvent, and coupling constants (*J*) are provided in Hz. Low and high-resolution electrospray ionization (ESI) mass spectra were collected at the University of California-Irvine Mass Spectrometry Facility.

Synthetic procedures

(R)-2-(6-Hydroxy-2-benzothiazolyl)-2-imidazoline-4-carboxylic acid (3.2):

Hydrogen chloride gas, generated from the combination of anhydrous CaCl₂ (2.0 g) and concentrated HCl (10 mL), was bubbled through a septum-sealed vial, cooled to 0 °C, containing a solution of **3.10** (111 mg, 0.629 mmol) in anhydrous ethanol (2 mL). After 20 min, the HCl generator was removed and the sealed reaction vessel stored at -20 °C for 48 h to afford a pale yellow precipitate. The crude solid was filtered and washed with chilled ether to provide ethyl 6-hydroxybenzothiazole-2-carboximidate (**3.11**) (89.9 mg) as a light yellow solid that was used without further purification. Ethyl carboximidate (**3.11**), (80.0 mg, 0.309 mmol) was added to a solution of D-2,3-diaminopropionic acid hydrochloride (43.9 mg, 0.312 mmol) and triethylamine (48 µL, 0.34 mmol) in MeOH (4.0 mL) at 0 °C. The reaction was then stirred at reflux for 5 h. A precipitate formed during the reaction that was collected via filtration and subsequently washed with chilled ether. In addition, the mother liquor was concentrated *in vacuo* and purified via flash column chromatography, using 4:1 EtOAc:MeOH, to give (**3**) (73.6 mg, 91%) as a pale yellow solid. ¹H NMR (500 MHz, DMSO-*d*₆, 393 K) δ 7.84 (d, *J* = 9.0, 1H), 7.37 (d, *J* = 2.5, 1H), 7.03 (dd, *J* = 2.5, *J* = 9.0, 1H), 4.51 (dd, *J* = 7.9, *J* = 11.0 1H), 3.99 (app t, *J* = 12.1, 1H), 3.87 (dd, *J* = 7.7, *J* = 12.8, 1H); ¹³C NMR (125 MHz, DMSO-*d*₆, 393 K) δ 173.8, 159.4, 157.4, 155.7, 147.0, 137.6, 124.6, 117.3, 107.2, 63.0, 55.3; HRMS (ESI+): Calcd. for C₁₁H₉N₃O₃SNa [M + Na]⁺ 286.0262, found 286.0259.

2-Cyano-6-methoxybenzimidazole (3.6):

A suspension of 4-methoxy-2-nitroaniline (6.81 g, 40.5 mmol) and 10% Pd/C (688 mg) in MeOH (120 mL) was purged with excess H₂. The reaction was then stirred under a hydrogen-

saturated atmosphere at ambient temperature for 2 h. The mixture was then filtered through Celite, and concentrated *in vacuo* to provide 4-methoxy-*o*-phenylenediamine (**3.8**) as a violet oil, this material was used without further purification. Crude **3.8** (5.24 g, 38.0 mmol) was dissolved in anhydrous pyridine (230 mL) and cooled to 0 °C under N₂. Appel's salt (**3.9**, 7.19 g, 34.5 mmol) was added and the mixture stirred under an inert atmosphere. The resulting red-brown mixture was stirred under N₂ and allowed to warm to room temperature over 24 h. The volatiles were removed *in vacuo*, and the crude residue filtered through a pad of silica gel, eluting with a gradient of 2:1 hexanes:EtOAc to 100% EtOAc, to provide **3.6** (3.34 g, 56%) as a red-brown powder. ¹H NMR (500 MHz, DMSO-*d*₆, 393 K) δ 7.57 (d, *J* = 8.9, 1H), 7.10 (s, 1H), 7.02 (d, *J* = 8.9, 1H), 3.83 (s, 3H); ¹³C NMR (125 MHz, DMSO-*d*₆, 393 K) δ 157.7, 122.7, 117.6, 115.0, 111.7, 96.8, 55.3. HRMS (ESI+): Calcd. for C₉H₈N₃O [M + H]⁺ 174.0667, found 174.0661.

2-Cyano-6-hydroxybenzimidazole (3.13):

Pyridine hydrochloride (1.58 g, 13.7 mmol) and benzothiazole **3.6** (237 mg, 1.37 mmol) were combined in a dried sealed tube, placed under N₂, and stirred at 180 °C for 1 h. The resulting residue was diluted with EtOAc and washed with saturated NaHCO₃ (2 x 20 mL), 1 M NaHSO₄ (2 x 20 mL), H₂O (2 x 40 mL), and brine (1 x 50 mL). The organics were then dried over MgSO₄, filtered, and concentrated *in vacuo*. The crude material was purified via flash column chromatography, using 3:1 hexanes:EtOAc to provide **3.13** (138 mg, 62%) as a pale yellow solid. ¹H NMR (500 MHz, DMSO-*d*₆) δ 7.51 (d, *J* = 8.8, 1H), 6.96 (dd, *J* = 2.3, *J* = 8.8, 1H), 6.93 (d, *J* = 1.8, 1H); ¹³C NMR (125 MHz, DMSO-*d*₆) δ 158.2, 138.3, 135.2, 124.4, 120.0, 117.4, 113.0, 99.1. HRMS (ESI-): Calcd. for C₈H₄N₃O [M - H]⁻ 158.0354, found 158.0355.

(S)-2-(6-Hydroxy-2-benzimidazolyl)-2-thiazoline-4-carboxylic acid (3.3):

D-Cysteine hydrochloride monohydrate (230 mg, 1.29 mmol) and benzimidazole **3.13** (195 mg, 1.22 mmol) were suspended in 2:1 MeOH:H₂O (7.5 mL). Potassium carbonate (171 mg, 1.24 mmol) was then added to the reaction and the resulting dark yellow solution was stirred under N₂ for 20 min. Upon consumption of **3.13** the methanol was removed *in vacuo* and the remaining aqueous solution acidified to pH 3 with 3 M HCl. The reaction was then extracted with EtOAc (5 x 20 mL). The combined organics were dried over Na₂SO₄, filtered, concentrated *in vacuo*. The crude material was purified with flash column chromatography, eluting with 2:1:1 CH₂Cl₂:EtOAc:MeOH, to provide pure (**2**) (263 mg, 82%) as a yellow solid. ¹H NMR (500 MHz, CD₃OD) δ 7.48 (d, *J* = 8.7, 1H), 6.94 (s, 1H), 6.87 (d, *J* = 8.2, 1H), 5.39 (app t, *J* = 8.9, 1H), 3.75 (app t, *J* = 9.7, 2H); ¹³C NMR (125 MHz, CD₃OD) δ 173.9, 163.7, 157.1, 145.4, 139.1, 135.8, 119.2, 115.7, 99.5, 79.8, 36.1; HRMS (ESI⁻): C₁₁H₉N₃O₃S [M - H]⁻ 262.0286, found 262.0277.

(R)-2-(6-Hydroxy-2-benzimidazolyl)-2-imidazoline-4-carboxylic acid (3.4):

Potassium cyanide (88.0 mg, 1.35 mmol) was added to a solution of benzimidazole **3.13** (281 mg, 1.15 mmol) in anhydrous methanol (39 mL), and the reaction was stirred at reflux for 24 h. The volatiles were then removed *in vacuo*, and the crude residue was passed through a pad of silica gel to provide crude methyl 6-hydroxybenzimidazole-2-carboximidate (219 mg) as a yellow solid. This material was used without further purification. Methyl carboximidate (219 mg, 1.15 mmol) was added to a solution of D-2,3-diaminopropionic acid hydrochloride (132.6 mg, 0.943 mmol) and triethylamine (168 μL, 1.21 mmol) in MeOH (14 mL) at 0 °C. The reaction was then stirred at reflux for 5 h. A precipitate formed during the reaction that was collected via filtration and subsequently washed with chilled ether. In addition, the mother

liquor was concentrated *in vacuo* and purified via flash column chromatography, using 2:1:1 EtOAc:MeOH:H₂O, to give (**3.4**) (117 mg, 50%) as a pale yellow solid. ¹H NMR (500 MHz, DMSO-*d*₆, 393 K) δ 7.42 (bd, *J* = 7.8, 1H), 6.95 (s, 1H), 6.78 (bd, *J* = 7.3, 1H), 4.53 (bs, 1H), 3.73-4.98 (m, 2H); HRMS (ESI⁻): Calcd. for C₁₁H₉N₄O₃N [M - H]⁻ 245.0675, found 245.0672.

2-Cyano-5-methoxy-1-methylbenzimidazole (3.14):

Iodomethane (339 μ L, 5.42 mmol) was added to a solution of benzimidazole **3.6** (853 mg, 4.93 mmol) in anhydrous DMF (34 mL). The resulting solution was stirred at room temperature for 22 h. Residual iodomethane was quenched by the slow addition of H₂O (30 mL), followed by stirring for 10 min. The solution was then extracted with EtOAc (3 x 30 mL). The organics were combined, washed with brine (1 x 30 mL), dried over MgSO₄, filtered, and concentrated *in vacuo*. The isolated residue was purified by flash column chromatography, using a gradient elution from 5:1 hexanes:EtOAc to 3:1 hexanes:EtOAc. The desired methylated benzimidazole product was isolated as a yellow solid (mixture of regio-isomers, 837 mg, 91%). ¹H NMR (400 MHz, CD₃Cl) δ 7.31 (d, *J* = 9.0, 1H), 7.23 (d, *J* = 2.3, 1H), 7.15 (dd, *J* = 2.4, *J* = 9.0, 1H), 3.99 (s, 3H), 3.87 (s, 3H); (125 MHz, CDCl₃) δ 157.9, 143.7, 129.7, 126.8, 118.4, 111.4, 110.9, 102.0, 55.9, 31.6; HRMS (ESI⁺): Calcd. for C₁₀H₁₀N₃O [M + H]⁺ 188.0824, found 188.0828.

2-Cyano-5-hydroxy-1-methylbenzimidazole (3.15):

Pyridine hydrochloride (1.48 g, 12.7 mmol) and benzothiazole **3.6** (237 mg, 1.27 mmol) were combined in a dried sealed tube, placed under N₂, and stirred at 180 °C for 1 h. The resulting residue was diluted with EtOAc and washed with saturated NaHCO₃ (2 x 20 mL), 1 M NaHSO₄ (2 x 20 mL), H₂O (2 x 40 mL), and brine (1 x 50 mL). The organics were then dried over MgSO₄, filtered, and concentrated *in vacuo*. The crude material was purified via flash column chromatography, using 5:1 hexanes:EtOAc to provide **3.15** (138 mg, 62%) as a pale yellow solid. ¹H NMR (400 MHz, CD₃OD) δ 7.47 (dd, *J* = 3.5, *J* = 8.8, 1H), 7.23 (d, *J* = 8.9, 1H), 7.15 (s, 1H), 3.99 (s, 3H); (125 MHz, DMSO-*d*₆) δ 157.0, 144.4, 130.6, 127.9, 118.9, 112.8, 112.1, 104.5, 32.0; HRMS (ESI⁻): Calcd. for C₉H₆N₃O [M – H] 172.0511, found 172.0503.

(S)-2-(5-Hydroxy-1-methylbenzimidazol-2-yl)-2-thiazoline-4-carboxylic acid (3.16):

D-Cysteine hydrochloride monohydrate (179 mg, 1.02 mmol) and nitrile **3.15** (168 mg, 0.969 mmol) were suspended in 2:1 MeOH:H₂O (7 mL). Potassium carbonate (135 mg, 0.979 mmol) was then added to the reaction and the resulting dark yellow solution was stirred under N₂ for 20 min. Upon consumption of **3.15** the methanol was removed *in vacuo* and the remaining aqueous solution acidified to pH 3 with 3 M HCl. The reaction was then extracted with EtOAc (5 x 20 mL). The combined organics were dried over Na₂SO₄, filtered, concentrated *in vacuo*, and purified with flash column chromatography, eluting with 3:2:2 CH₂Cl₂:EtOAc:MeOH, to provide pure **3.16** (239 mg, 89%) as a yellow solid. ¹H NMR (500 MHz, acetone-*d*₆) δ 7.44 (d, *J* = 8.8, 1H), 7.11 (s, 1H), 7.01 (d, *J* = 8.8, 1H), 5.56 (app t, *J* = 8.9, 1H), 3.63-3.72 (m, 2H); ¹³C NMR (125 MHz, CDCl₃) δ 172.3, 165.0, 155.5, 145.3, 144.7, 132.9, 116.7, 112.4, 105.4, 80.9, 34.6, 33.0; HRMS (ESI⁺): Calcd. for C₁₂H₁₂N₃O₃S [M + H]⁺ 278.0599, found 278.0595.

References

- (1) Contag, C. H. *In vivo* pathology: Seeing with molecular specificity and cellular resolution in the living body. *Annual Review of Pathology: Mechanisms of Disease* **2007**, *2*, 277.
- (2) Prescher, J. A.; Contag, C. H. Guided by the light: Visualizing biomolecular processes in living animals with bioluminescence. *Curr. Opin. Chem. Biol.* **2010**, *14*, 80.
- (3) Dothager, R. S.; Flentie, K.; Moss, B.; Pan, M.-H.; Kesarwala, A.; Piwnica-Worms, D. Advances in bioluminescence imaging of live animal models. *Curr. Opin. Biotech.* **2009**, *20*, 45.
- (4) Thorne, N.; Inglese, J.; Auld, D. S. Illuminating insights into firefly luciferase and other bioluminescent reporters used in chemical biology. *Chem. Biol.* **2010**, *17*, 646.
- (5) McMillin, D. W.; Delmore, J.; Weisberg, E.; Negri, J. M.; Geer, D. C.; Klippel, S.; Mitsiades, N.; Schlossman, R. L.; Munshi, N. C.; Kung, A. L.; Griffin, J. D.; Richardson, P. G.; Anderson, K. C.; Mitsiades, C. S. Tumor cell-specific bioluminescence platform to identify stroma-induced changes to anticancer drug activity. *Nat. Med.* **2010**, *16*, 483.
- (6) Branchini, B. R.; Ablamsky, D. M.; Davis, A. L.; Southworth, T. L.; Butler, B.; Fan, F.; Jathoul, A. P.; Pule, M. A. Red-emitting luciferases for bioluminescence reporter and imaging applications. *Anal. Biochem.* **2010**, *396*, 290.
- (7) Nakatsu, T.; Ichiyama, S.; Hiratake, J.; Saldanha, A.; Kobashi, N.; Sakata, K.; Kato, H. Structural basis for the spectral difference in luciferase bioluminescence. *Nature* **2006**, *440*, 372.
- (8) Fraga, H. Firefly luminescence: A historical perspective and recent developments. *Photochem. Photobiol. Sci.* **2008**, *7*, 146.
- (9) Reddy, G. R.; Thompson, W. C.; Miller, S. C. Robust light emission from cyclic alkylaminoluciferin substrates for firefly luciferase. *J. Am. Chem. Soc.* **2010**, *132*, 13586.
- (10) Shinde, R.; Perkins, J.; Contag, C. H. Luciferin derivatives for enhanced in vitro and in vivo bioluminescence assays. *Biochemistry* **2006**, *45*, 11103.
- (11) White, E. H.; Wurther, H. Analogs of firefly luciferin. III. *J. Org. Chem.* **1966**, *31*, 1484.
- (12) Branchini, B. R.; Hayward, M. M.; Bamford, S.; Brennan, P. M.; Lajiness, E. J. Naphthyl- and quinolyl-luciferin: green and red light emitting firefly luciferin analogues. *Photochem. Photobiol. Sci.* **1989**, *49*, 689.
- (13) Henary, M. M.; Wu; Cody, J.; Sumalekshmy, S.; Li, J.; Mandal, S.; Fahrni, C. J. Excited-state intramolecular proton transfer in 2-(2-arylsulfonamidophenyl)benzimidazole derivatives: The effect of donor and acceptor substituents. *J. Org. Chem.* **2007**, *72*, 4784.

- (14) Rios Vazquez, S.; Rios Rodriguez, M. C.; Mosquera, M.; Rodriguez-Prieto, F. Rotamerism, tautomerism, and excited-state intramolecular proton transfer in 2-(4-N,N-diethylamino-2-hydroxyphenyl)benzimidazoles: novel benzimidazoles undergoing excited-state intramolecular coupled proton and charge transfer. *J. Phys. Chem. A* **2008**, *112*, 376.
- (15) Baumann, M.; Baxendale, I. R.; Ley, S. V.; Nikbin, N. An overview of the key routes to the best selling 5-membered ring heterocyclic pharmaceuticals. *Beilstein J. Org. Chem.* **2011**, *7*, 442.
- (16) Daniel-Mwambete, K.; Torrado, S.; Cuesta-Bandera, C.; Ponce-Gordo, F.; Torrado, J. J. The effect of solubilization on the oral bioavailability of three benzimidazole carbamate drugs. *Int. J. Pharm.* **2004**, *272*, 29.
- (17) Meroni, G.; Rajabi, M.; Santaniello, E. D-Luciferin, derivatives and analogues: synthesis and in vitro/in vivo luciferase-catalyzed bioluminescent activity. *ARKIVOC: Online J. Org. Chem.* **2009**.
- (18) White, E. H.; McCapra, F.; Field, G. F. The structure and synthesis of firefly luciferin. *J. Am. Chem. Soc.* **1963**, *85*, 337.
- (19) Cuadro, A. M.; Alvarez-Buila, J. 4,5-Dichloro-1,2,3-dithiazolium chloride (Appel's salt): Reactions with N-nucleophiles. *Tetrahedron* **1994**, *50*, 10037.
- (20) Ingram, A. J.; Dunlap, A. G.; DiPietro, R.; Muller, G. Speciation, luminescence, and alkaline fluorescence quenching of 4-(2-methylbutyl)aminodipicolinic acid (H2MEBADPA). *J. Phys. Chem. A* **2011**, *115*, 7912.
- (21) Mukherjee, T. K.; Panda, D.; Datta, A. Excited-state proton transfer of 2-(2-Pyridyl)benzimidazole in microemulsions: selective enhancement and slow dynamics in aerosol OT reverse micelles with an aqueous core. *J. Phys. Chem. B* **2005**, *109*, 18895.
- (22) da Silva, L. P.; Esteves da Silva, J. C. G. Kinetics of inhibition of firefly luciferase by dehydroluciferyl-coenzyme A, dehydroluciferin and l-luciferin. *Photochem. Photobiol. Sci.* **2011**, *10*, 1039.
- (23) Harwood, K. R.; Mofford, D. M.; Reddy, G. R.; Miller, S. C. Identification of mutant firefly luciferases that efficiently utilize aminoluciferins. *Chem. Biol.* **2011**, *18*, 1649.

CHAPTER 4: Expedient synthesis of sterically modified luciferins

4.1 Introduction

As noted in chapter 1, the exquisite sensitivity of bioluminescence has been exploited to visualize numerous biological parameters in preclinical models, including cell homing, proliferation, and communication. While broadly applicable, bioluminescence to date has been largely limited to monitoring one cell type or biological feature at a time. This is due, in part, to a lack of distinguishable luciferase-luciferin pairs for *in vivo* use. Many optimal luciferases for cell and organismal imaging use the same substrate. Thus, the probes cannot be used to distinguish multiple cell types in a single subject and, unlike fluorescent protein technology, a diverse suite of bioluminescent proteins does not yet exist [1].

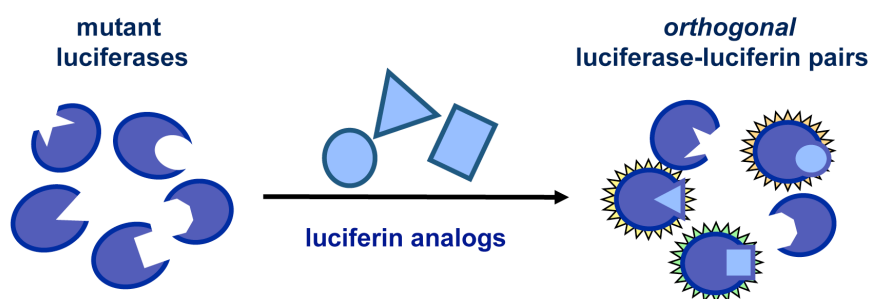


Figure 4-1: Bump-hole approach to develop orthogonal luciferase-luciferin pairs. Luciferase enzymes (dark blue shapes) can be genetically engineered to accept chemically distinct luciferin analogs (light blue shapes). Only complementary enzyme-substrate pairs will interact to produce light.

To expand the bioluminescence toolkit, we aimed to identify new luciferases that are responsive to unique luciferins. Such orthogonal luciferase-luciferin pairs would enable multicomponent imaging in a variety of settings. Our approach involves modifying the enzyme and luciferin concurrently (Figure 4-1). When the mutants and analogs are combined, light will be produced only when complementary enzyme-substrate partners interact. Sequential administration of substrates will enable unique luciferases to be illuminated (and thus resolved) within a complex mixture, even living animals [2]. This approach is distinct from related attempts to generate luciferins that emit different colors of light with a single luciferase [3-5]. To date, the emission spectra observed with these probes are not easily spectrally resolved in complex tissues or animals. Discriminating among different wavelengths (i.e., colors) of light in bioluminescence (and whole body optical imaging, in general) is exceedingly difficult [6]. Thus, instead of achieving spectral resolution with bioluminescent probes, we focused on achieving *substrate orthogonality*. This approach has precedence in nature as a variety of unique luciferase-luciferin pairs exist in nature [7]. Some of these pairs, including those from the firefly and *Renilla reniformis* are routinely used *in vivo* [2,8]. Despite the suboptimal bioavailability and emission wavelength of the Renilla luciferase/substrate (coelenterazine) pair, these orthogonal pairs are routinely used in tandem in two-component imaging studies [9]. Alternative luciferase-luciferin pairs have been identified in other organisms and could be similarly used for multi-component imaging. However, most remain poorly characterized or ill-suited for routine use *in vivo*.

Generating mutant enzymes that utilize chemically modified substrates is a well-known strategy for deciphering the roles of individual members within a large family of related proteins. Among the best examples of this approach is work from the Shokat lab aimed at discriminating

among protein kinases [10]. These researchers demonstrated that ATP analogs with appended functional groups (or “bumps”) are preferentially utilized by kinases possessing complementary mutations (or “holes”) to accommodate the additional steric bulk. Thus, altering the firefly luciferase enzyme-substrate interface by creating luciferase mutants (with “holes”) to accept distinct chemically modified versions of luciferin (with “bumps”) (Figure 4-1). Simultaneous manipulation of firefly luciferase and D-luciferin (**4.1**) is also supported by key literature precedent. Miller and coworkers recently prepared a class of unnatural aminoluciferin analogs that were found to be robust light emitters with luciferase, but the products inhibited the enzymatic reaction [11-13]. Product inhibition was partially relieved using mutated versions of the enzyme (including a Phe 247 deletion to create additional “space” in the binding pocket). These results imply that altered bioluminescent activities can be achieved by simultaneous modification of the enzyme and substrate. Similar strategies have been attempted with aequorin (a marine photoprotein) and a luciferase isolated from a deep-sea shrimp [14,15]. However, these systems are not optimal for *in vivo* imaging based on their wavelengths of emission [6].

To more expediently identify orthogonal luciferase luciferin-pairs, we aimed to screen libraries of mutant firefly luciferases with chemically modified luciferins. Our molecules are sterically modified analogs of D-luciferin, the substrate for firefly luciferase (Fluc). We focused our efforts on the Fluc/D-luciferin pair for a variety of reasons: 1. this bioluminescent pair is the most widely used in biomedical imaging applications [1]. D-luciferin-type scaffolds possess adequate bioavailability in rodent models [16]. the Fluc-catalyzed oxidation of D-luciferin analogs releases the highest percentage of tissue-penetrating light of all the bioluminescent families [6,7,17]. A wealth of structural and biochemical information on Fluc could guide our engineering efforts [18].

4.2 Construction of luciferin scaffolds for rapid diversification

Our approach to building orthogonal bioluminescent tools required access to diverse luciferin scaffolds. The synthetic route described in chapters 2 and 3 was suitable for this purpose. The previously synthesized nitrogenous analogs proved too similar in structure, which led us to develop new compounds. Thus, we turned our attention to sterically modified luciferin analogs. It was important to preserve structural elements required for productive light emission, but sterically modify (the 4' and 7'-position) to disrupt their utilization by WT-Fluc. The 4' and 7'-position were ideal targets for several reasons. Examination of the Fluc crystal structure revealed that carbon-4' and -7' lie in close proximity to the enzymes backbone (Figure 4-2), suggesting that substrates with additional steric modifications at these sites would likely be poorly tolerated [18]. Indeed, docking studies showed that only the analogs with small 7' substitutions were able to attain the presumed light emitting conformation (M. Paley, *pers. commun.*). Larger steric perturbations were blocked from adopting beneficial conformations within the luciferase active site. This is in contrast to other positions on the luciferin core. Recent crystallographic data and molecular dynamics simulations have indicated flexibility within the luciferase active site and “space” to accommodate luciferins with appendages at the 5' and 6'-positions [18]. These results have been corroborated with experimental evidence – a variety of bulky 5'- and 6'-substituted luciferins are viable light-emitting substrates with Fluc [13,19,20].

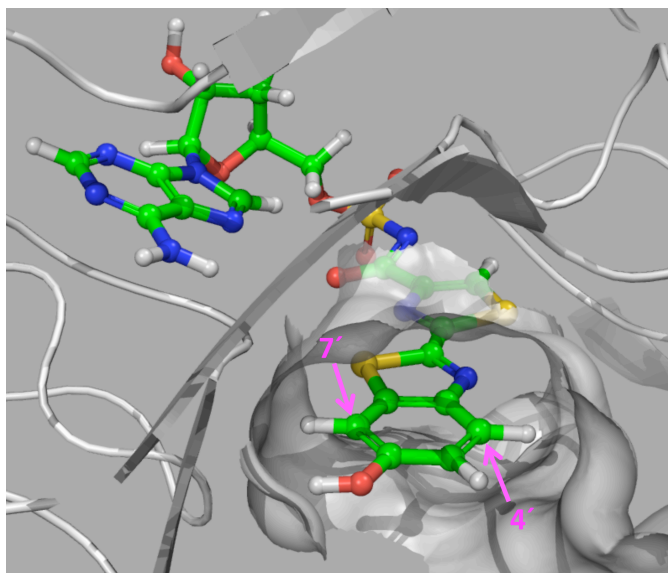


Figure 4-2: Slide chains within the Fluc active site are closest in proximity to the 4' and 7'-positions.

We envisioned installing a functional handle at the 7'-position that could be used to rapidly assemble a variety of structurally modified scaffolds at a late stage in the synthesis. Initially, the aldehyde was an attractive choice, owing to the ease of diversification of this functional group under mild conditions (e.g., reductive amination, Scheme 4-1) and the reaction's compatibility with a broad range of functional groups. We also reasoned that the aldehyde could be regioselectively installed at the 7-position of benzothiazole **4.2**, owing to its increased nucleophilicity. Installation of an aldehyde on the luciferin core, though, presented some interesting challenges. In aqueous environments, aldehydes are in equilibrium with their hydrated hemiacetal form. This equilibrium hindered efforts to characterize reaction products upon isolation. An intractable mixture of two products was isolated from the formylation of phenol **4.2**, attributed to the desired 7-formyl benzathiazole **4.3** and anhydro-byproduct **4.4**. Similar issues have been observed when working with *o*-hydroxybenzaldehydes (salicylaldehydes), wherein the compounds can dimerize to form 2,6,9-

trioxabicyclo[3.3.1]nonanes (Figure 4-3) [21]. Anhydro dimer **4.4** proved to be unexpectedly stable. Efforts recover *o*-hydroxybenzaldehyde **4.3** through hydrolysis of the bis-acetal byproduct were unsuccessful, as the nitrile rapidly hydrolyzed.

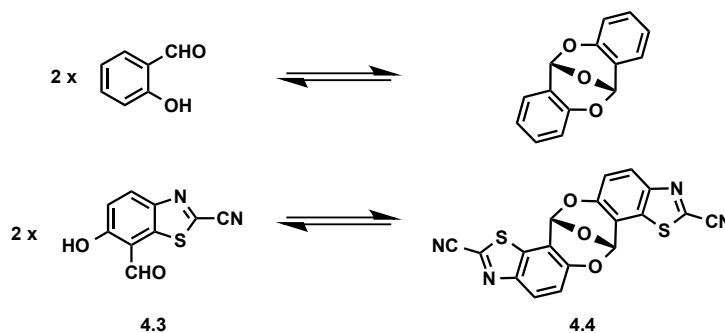
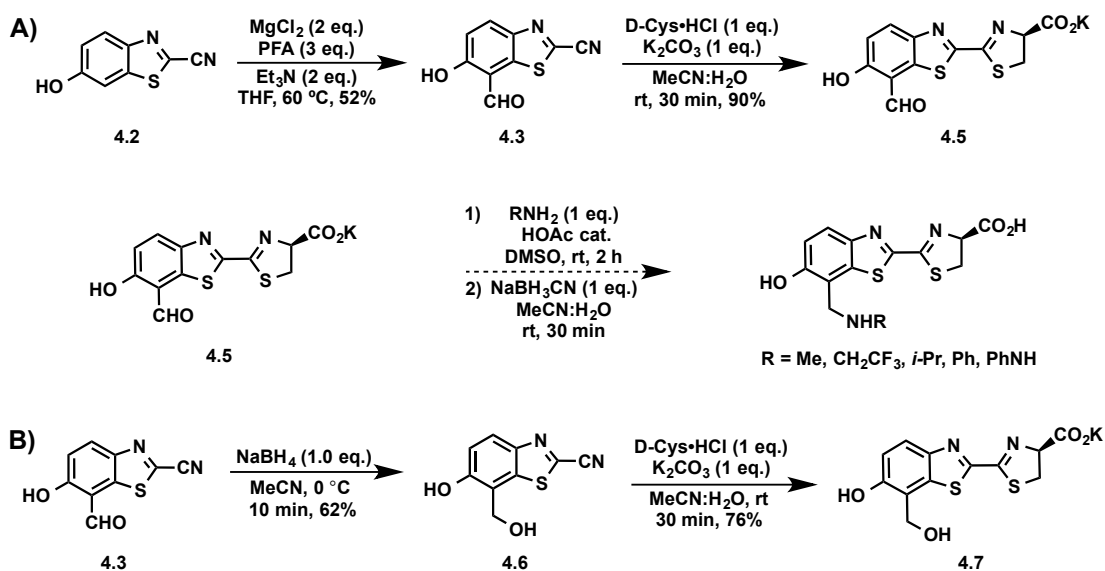


Figure 4-3: Side reactivity of *o*-hydroxybenzaldehyde derivatives to form trioxa[3.3.1]nonanes

The previously developed high-yielding synthesis of phenol **4.2** allowed us to carry out the formylation on large enough scale that **4.3** could be isolated in reasonable quantities after iterative recrystallization. Aldehyde **4.3** was a precursor to several sterically perturbed luciferin analogs including, 7'-formyl (**4.5**), 7'-hydroxymethyl (**4.7**) and several 7'-benzylic amino luciferins (Scheme 4-1). Initially, aldehyde **4.3** was condensed with cysteine to yield luciferin analog **4.5** directly, or reduced to the benzylic alcohol (**4.6**) then reacted with cysteine to give 7'-hydroxymethyl luciferin (**4.7**). The aldehyde of **4.5** was to be further elaborated through reductive amination to achieve larger steric modifications. Unfortunately, the desired luciferins were difficult to purify and prone to rapid degradation. The difficulties encountered during isolation, combined with the previous modest yield of **4.3**, caused us to reevaluate our approach. Efficient syntheses of luciferin scaffolds are essential for orthogonal probe development, as large

amounts of material are required for light emission assays and subsequent screening of mutant luciferase libraries.

Scheme 4-1: A) Synthesis of 7'-formyl luciferin and preliminary attempts to utilize reductive amination to append steric bulk to the 7'-position. B) Synthesis of 7'-hydroxymethyl luciferin.



To circumvent the issues observed upon aldehyde installation and purification, we generated more reactive iminium ion electrophiles that would readily substitute at the 7'-position (Figure 4-4). In this variation of the Mannich reaction a nucleophilic phenol is used to trap an iminium electrophile to yield *o*-hydroxybenzylamines, known generally as Betti bases [22]. Along these lines, a series of sterically encumbered tertiary benzyl amines were synthesized from phenol **4.2** and coupled to iminium ions generated *in situ* (Scheme 4-2). Importantly, this approach proved both modular and amenable to large scale (1–10 g), high-throughput syntheses.

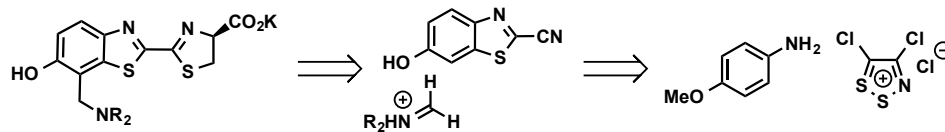
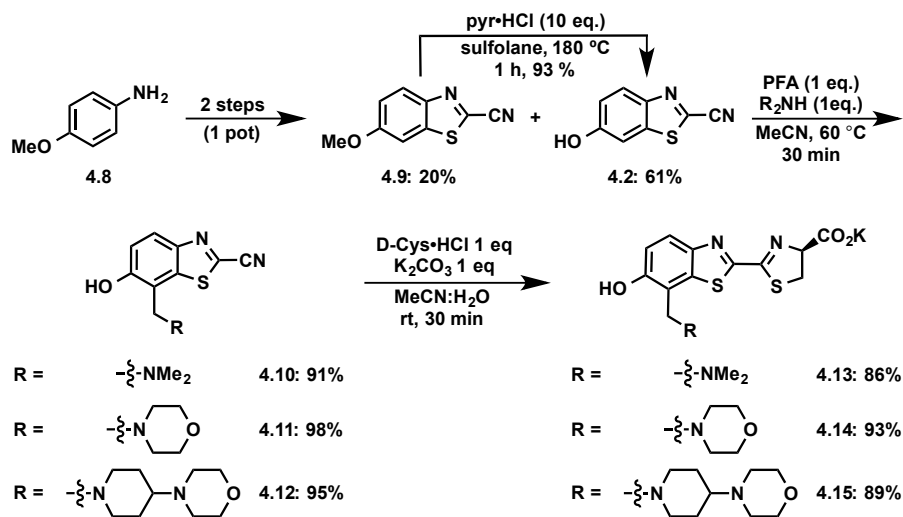


Figure 4-4: Retrosynthetic approach to sterically modify the 7'-position of luciferin using a modified Mannich reaction.

Scheme 4-2: Synthetic route to sterically encumbered 7'-benzylamino luciferin analogs (4.13–4.15)



Having synthesized several 7'-substituted analogs (4.13–4.15), I developed a route to access 4'-substituted luciferin derivatives. As mentioned previously, the 4'-position of luciferin is in close proximity to side chains within the luciferase active site (Figure 4-1). We sought to

bias enzyme-substrate specificity through the addition of steric bulk at the 4'-position without perturbing the electronic structure of the luciferin core. This increased steric clash would likely exclude bulkier analogs from the luciferase active site in the absence of reciprocal enzymatic modifications to create more "space". Accessing the 4'-position required different chemistry than that used with the 7'-substituted derivatives. Unlike the 7-series, electrophilic aromatic substitution was limited as a result of the benzothiazoles decreased nucleophilicity at the 4-position. Preliminary attempts to modify this position involved nucleophilic aromatic substitution of halogen-substituted 2-cyanobenzothiazole derivatives (Figure 4-5A). The halogenated benzothiazoles were available via our previously developed synthesis. This S_NAr route was quickly abandoned due to concerns of functional group incompatibility. Deleterious nitrile degradation was observed under the harsh conditions required to promote S_NAr reactivity. As a result, I attempted to append bulky groups off the amine of a 4-aminobenzothiazole derivative (Figure 4-5B). Once installed the amine could be reacted with aldehydes via reductive amination, alkylated, or be transformed into an azide for further derivatization via "click" chemistry. While dithiazolium chemistry easily provided the requisite 4-nitrobenzothiazole, reduction and subsequent manipulation of the amine proved challenging. In addition to the acyclic oxygen, amine installation increased the molecule's propensity to oxidize.

To avoid these issues, I sought another chemical handle that would tolerate dithiazolium chemistry and also be modified under mild conditions. I settled on a benzylic methyl group, as this moiety is relatively inert the benzylic, but easily modified using single electron chemistries. Installation of a methyl group at the 4-position was achieved using our previous described chemistry (Figure 4-6). In brief, aminotoluene **4.16** was reacted with Appel's salt. The intermediate dithiazole was fragmented *in situ* to provide thioamide **4.17** (Scheme 4-3A). The

thioamide was then oxidatively cyclized to afford the acetyl-protected methylbenzothiazole **4.18**. The differential phenol-protecting strategy (acetyl replacement of the methyl group) is noteworthy and highlights the mild conditions of our synthesis. This chemistry was used to obtain moderate quantities of **4.18**; however, scale up was limited by the dilute concentration required for the cyclization. Moving forward, the synthesis would need to be optimized in order to sustain a screen of mutant luciferases.

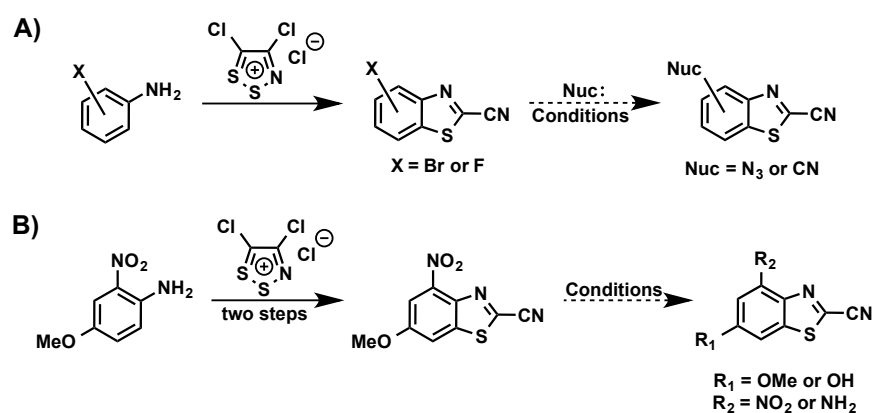


Figure 4-5: Preliminary attempts to access 4'-sterically perturbed luciferin analogs post-benzothiazole formation. (A) S_NAr displacement of a halogen. (B) Reduction of an aryl nitro group.

To address this issue and increase throughput, we relied on the versatility of the Appel salt. As described in chapter 2, dithiazole-adducts may be cyclized to their corresponding 2-cyanobenzothiazoles under thermal conditions. With this in mind, I condensed aniline **4.19** with Appel's salt and heated the solution to 180 °C to cyclize the dithiazole intermediate (Scheme 4-3B). Once cyclized, the methyl ether of **4.20** was cleaved using excess pyridine hydrochloride to

give phenol **4.21**. This one-pot transformation proved scalable and provided large amounts of **4.21**, which was subsequently protected as the acetate (**4.18**). The benzylic methyl group of **4.18** was then brominated under mild conditions using NBS and benzoyl peroxide to provide intermediate **4.22**. Benzyl bromide **4.22** could be employed to access a multitude of 4'-derivatives *via* S_N2 displacement. Initially, simultaneous bromide displacement and acetyl deprotection were facilitated by the addition of two equivalents morpholine as a model amine. Finally, D-cysteine was added to the reaction to give the desired 4'-benzylamino luciferin (**4.23**) in one-pot (Scheme 4-3C).

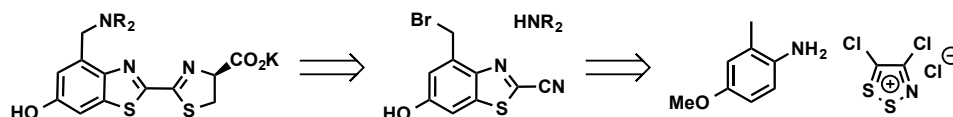
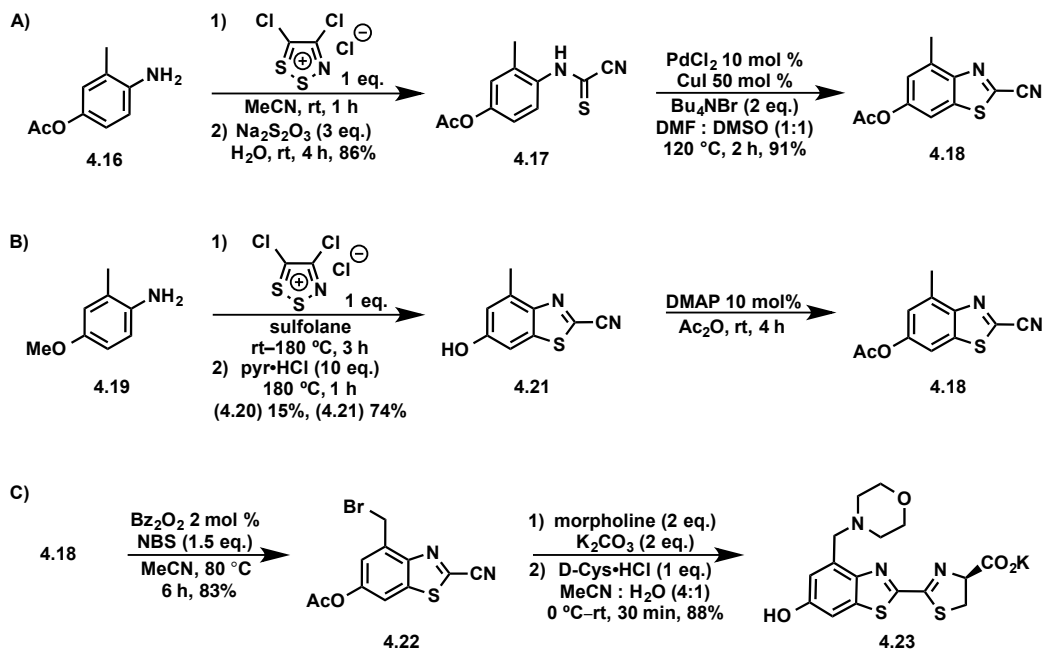


Figure 4-6: Retrosynthetic S_N2 approach to sterically modify the 4'-position of luciferin.

Scheme 4-3: Synthetic route to sterically encumbered 4'-benzylamino luciferins (A) oxidative cyclization route to intermediate **4.18**. (B) Thermal cyclization route to intermediate **4.18**. (C) Three-transformation, one-pot synthesis of 4'-benzylamino luciferin analog **4.23**.



4.3 Luciferin derivatives are weak light emitters

With the steric analogs in hand, we first evaluated their light emitting properties with Fluc. As expected, all of the analogs were weaker emitters than D-luciferin (**4.1**), the native substrate (Figure 4-7). When comparing light emission among the analogs themselves a clear trend emerged. Those with larger steric perturbations, the benzyl amines, emitted less light with Fluc.

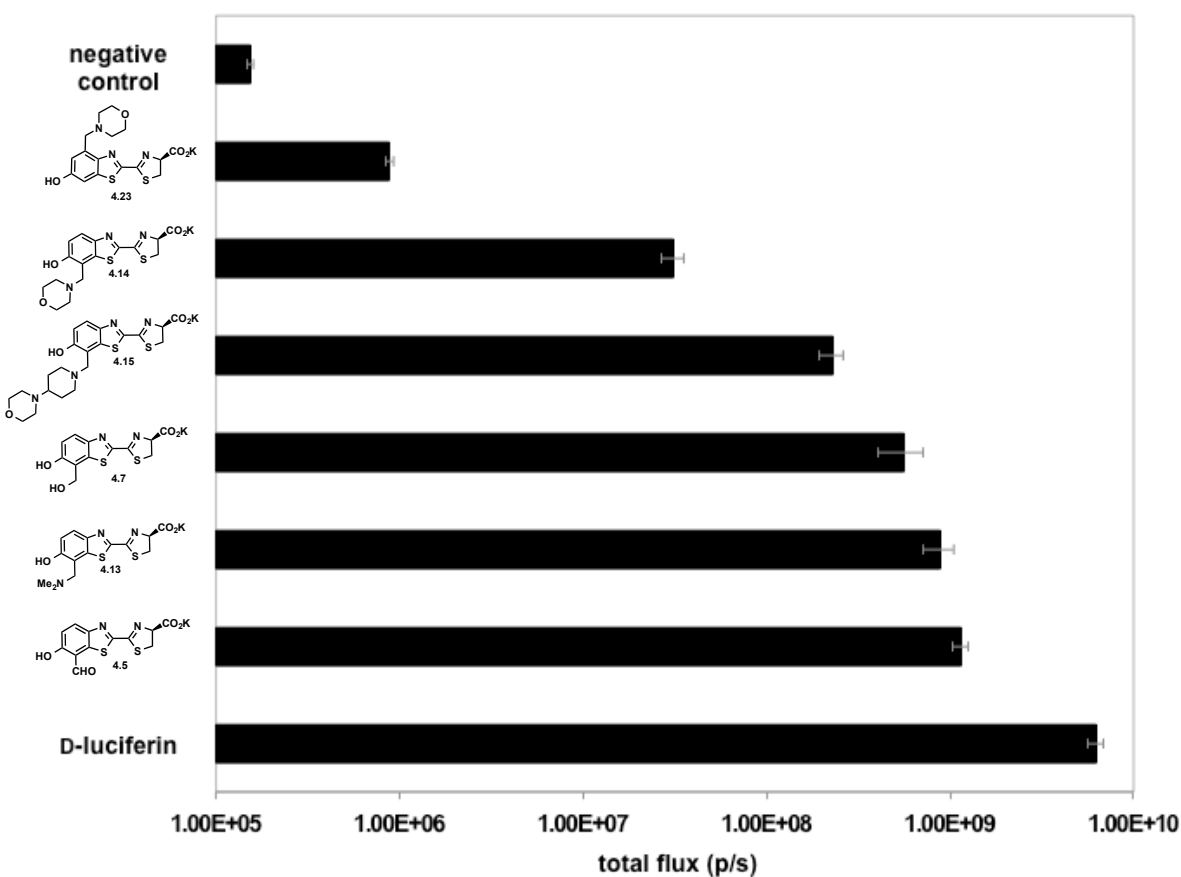


Figure 4-7: Bioluminescence of a series of sterically perturbed luciferin analogs with wild-type luciferase. All compounds were assayed at 100 μ M.

Surprisingly, the largest analog (**4.15**) was not the weakest emitter. We initially thought that the intramolecular hydrogen bond between the phenolic proton and the benzylic amine may be the source of the discrepancy. However, no such effect was observed when the bioluminescence reaction was run over a pH range of 6–10 (Figure 4-8). These findings suggest that the intramolecular hydrogen bond between the phenolic proton and benzylic amine is not responsible for the increased bioluminescent emission of **4.15** over **4.14**.

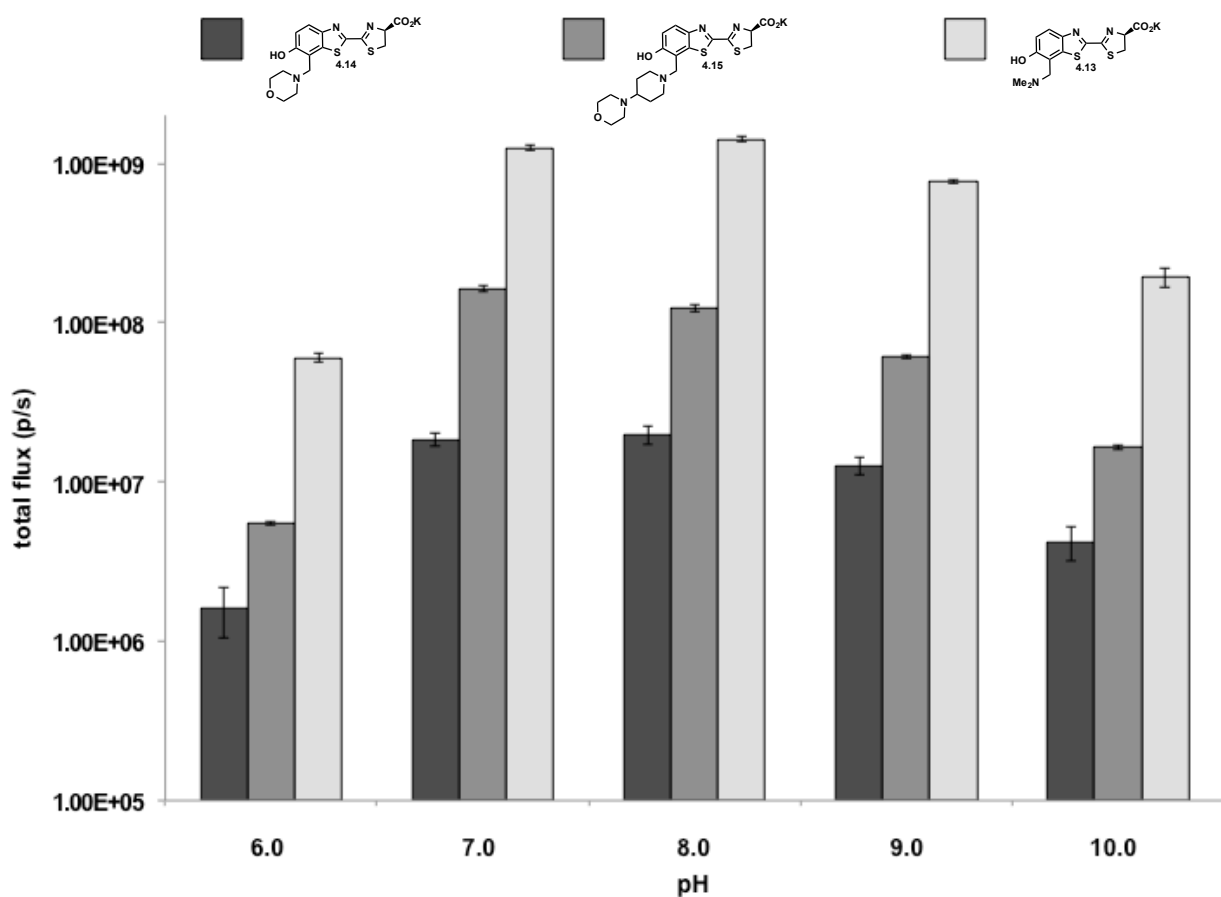


Figure 4-8: Effect of pH on the bioluminescence of a series of 7'-benzylamino luciferin derivatives.

4.4 Poor bioluminescent substrates are still capable of robust light emission.

We attributed the poor bioluminescence emission of analogs **4.13–4.15**, **4.23** to their poor utilization by Fluc. It is possible, though, that the luciferins themselves are not capable of photon production upon activation/oxidation. If the analogs are incapable of reaching the excited state/photon production, reduced light emission with Fluc would be expected. These molecules would also be poor candidates for orthogonal probe development. For productive bioluminescence, an analog must also be able to reach an electronic state (S_1) and relax back to its ground state with concomitant photon release. To ensure that the analogs were intrinsically capable of robust light emission, we turned to a non-enzymatic assay that mimics the bioluminescence reaction: formation of an activated ester intermediate, followed by H-atom/proton abstraction and subsequent reaction with molecular oxygen (Figure 4-9). When D-luciferin is subjected to this assay, a red glow was produced. When analogs **4.13–4.15** and **4.23** were subjected to the assay, robust light emission was also observed, with the photon output on par with the native substrate, D-luciferin (Figure 4-10). A control compound lacking an electron-dense residue on the aromatic ring (a key feature of luciferins) did not produce this level of emission. These results provided assurance that while luciferin scaffolds **4.13–4.15**, **4.23** may be poor substrates for Fluc, they are still capable of emission from an electronic excited state.

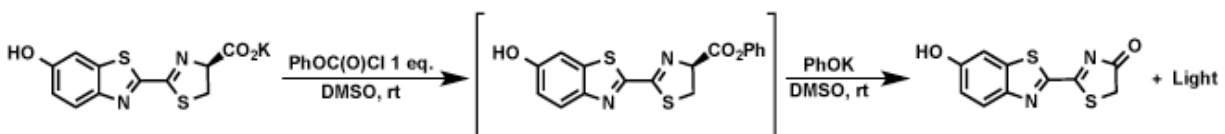


Figure 4-9: Chemiluminescence reaction used to gauge luciferin light emitting ability.

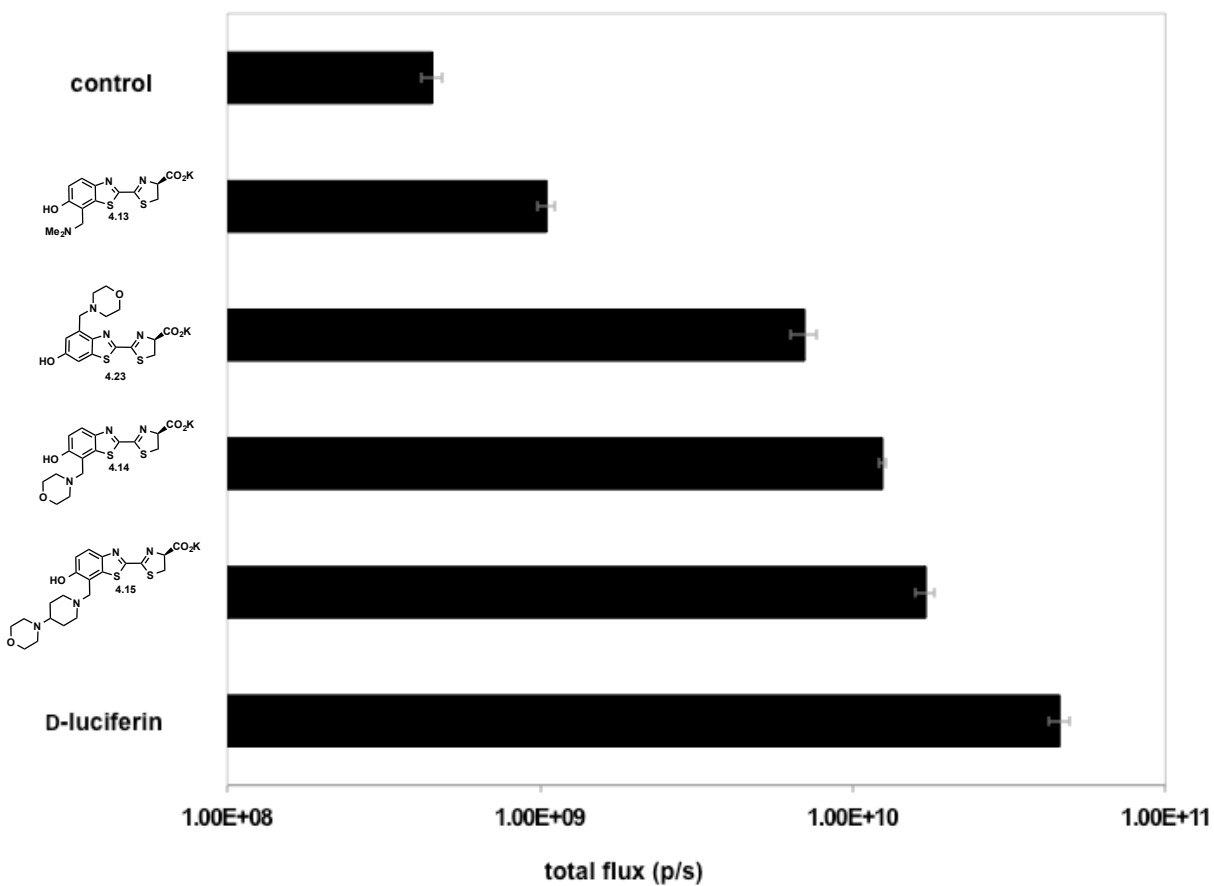


Figure 4-10: Chemiluminescence of a series of sterically perturbed luciferin analogs.

4.5 Conclusion

In this dissertation I described a novel synthetic approach to luciferin scaffolds. Using dithiazole chemistry, a series of electronic and steric luciferin derivatives were synthesized. Bioluminescent light was observed with several of these compounds in conjunction with the wild-type luciferase. The bioluminescence assays allowed us to probe how light emission was affected by structural alteration of the luciferin substrate. As the most salient example, imidazoline replacement of the native thiazoline ring greatly reduced light emission of nitrogenous analogs **3.2** and **3.4** with native luciferase. In contrast, benzimidazole-containing analogs (**3.3** and **3.16**) displayed robust light emission and reasonable cell-permeability. Despite validating the general applicability of our synthesis, the nitrogenous derivatives (**3.2–3.4** and **3.16**) were abandoned during initial luciferase screening. We believed the structural similarities between these electronic derivatives would cause difficulty achieving substrate resolution and, in turn, orthogonality.

In order to address these concerns, we synthesized an array of sterically perturbed derivatives. These sterically modified benzyl amines (**4.13–4.15,4.23**) were all capable of emitting light with native luciferase. In addition, those analogs that were weak bioluminescent emitters (**4.15**, **4.16** and **4.23**) were found to emit light chemically on par with the chemiluminescence of D-luciferin. This observation suggested that these analogs should be capable of bioluminescent light emission comparable to the native substrate with an appropriately modified mutant enzyme. Pools of mutant luciferases are currently being screened with these steric analogs. Variants that optimize the bioluminescence intensity of our analogs will be identified and characterized.

4.5 Materials and methods

General bioluminescence imaging protocol

Samples were imaged using an IVIS Lumina (Xenogen) system (equipped with a cooled CCD camera) interfaced with Living Image software. Exposure times ranged from 1 s - 5 min and photon flux values from defined regions of interest were measured using the Living Image software. Further analysis was performed using Microsoft Excel.

Light emission assays with recombinant luciferase

Bioluminescence assays with all luciferin compounds were carried out in triplicate, using solid black, flat-bottom, 96-well plates (Grenier). Assay wells contained purified Fluc (0 or 2 µg), luciferin substrate (0-1 mM), ATP (Sigma, 1 mM), coenzyme-A (trithium salt, Calbiochem, 1 mM), and reaction buffer (20 mM Tris-HCl, 0.5 mg/mL BSA, 0.1 mM EDTA, 1 mM TCEP, 2 mM MgSO₄ pH 7.6), totaling 100 µL. Additionally, all non-enzyme assay components were premixed in the wells prior to Fluc addition. Images for all assays were acquired as described above.

General chemiluminescence imaging protocol

Chemiluminescence assays were carried out in collaboration with Colin Rathbun (C. Rathbun, *pers. commun.*).

General synthetic methods

All reagents purchased from commercial suppliers were of analytical grade and used without further purification. 4,5-Dichloro-1,2,3-dithiazolium chloride, was prepared according to literature precedent with slight modifications. Reaction progress was monitored by thin-layer chromatography on EMD 60 F254 plates, visualized with UV light, ceric ammonium molybdate (CAM), chloranil, or KMnO₄ stain. Compounds were purified via flash column chromatography using Sorbent Technologies 60 Å, 230-400 mesh silica gel, unless otherwise stated. Anhydrous solvents were dried by passage over neutral alumina with the exception of DMF, which was passed over activated molecular sieves. Reaction vessels were either flame or oven dried prior to use. NMR spectra were acquired with Bruker Advanced spectrometers. All spectra were acquired at 298 K, unless otherwise specified. ¹H-NMR spectra were acquired at either 500 or 400 MHz, and ¹³C-NMR spectra were acquired at 125 or 100 MHz. Coupling constants (*J*) are provided in Hz and chemical shifts are reported in ppm relative to either residual non-deuterated NMR solvent, calculated reference, or to a methanol external reference. Low and high-resolution electrospray ionization (ESI) mass spectra were collected at the University of California-Irvine Mass Spectrometry Facility.

Synthetic Procedures

7-Formyl-6-hydroxy-1,3-benzothiazole-2-carbonitrile (4.3):

Anhydrous MgCl₂ (1.52 g, 15.9 mmol) and paraformaldehyde (646 mg, 21.3 mmol) were added to a rigorously dried 1 L flask. The reagents were then suspended in anhydrous THF (426 mL), and the vessel was purged with N₂. Triethylamine (1.57 mL, 11.2 mmol) was added, and the reaction stirred at 60 °C until most solids dissolved. Heterocyclic phenol **4.2** (939 mg, 5.33

mmol) was added, and the resulting mixture was stirred at 60 °C for an additional 24 h. The reaction progress, having seemingly stalled, was cooled to rt and was THF removed *in vacuo*. The residue was dissolved in Et₂O (200 mL) then washed with 1 M Na₂SO₄ (2 x 50 mL), H₂O (2 x 100 mL), and brine (50 mL). The organics were then dried over Na₂SO₄, filtered, and concentrated *in vacuo*. The crude material was then purified by flash column chromatography (eluting with 3:1 hexanes:EtOAc) to yield formylated phenol **4.3** as an off-white solid (566 mg, 52%). ¹H NMR (400 MHz, acetone-*d*₆) δ 10.6 (s, 1H), 8.34 (d, *J* = 9.0, 1H), 7.49 (d, *J* = 9.0, 1H); ¹³C NMR (125 MHz, acetone-*d*₆) δ 188.1, 164.0, 148.4, 138.7, 135.2, 133.6, 120.8, 117.7, 114.7. HRMS (ESI⁻) calcd for C₉H₃N₂O₂S [M – H]⁻ 202.9915, found 202.9921.

6-Hydroxy-7-(hydroxymethyl)-1,3-benzothiazole-2-carbonitrile (4.6):

Aldehyde **4.3** (87 mg, 0.42 mmol) was dissolved in MeCN (20 mL) and cooled to 0 °C in an ice bath. Sodium borohydride (19 mg, 0.51 mmol) was added in portions over 10 min while stirring the reaction at 0 °C. When NaBH₄ addition was complete, the reaction was stirred, at 0 °C maintaining for an additional 10 min. Upon consumption of starting material, the reaction was quenched with 1M Na₂SO₄ (10 mL) then extracted with EtOAc (3 x 50 mL). The organic phase was concentrated and purified via reversed-phase HPLC to provide benzyl alcohol **4.6** (55 mg, 62%) as an off-white solid. ¹H NMR (400 MHz, acetone-*d*₆) δ 7.92 (d, *J* = 8.8, 1H), 7.27 (d, *J* = 8.8, 1H), 5.00 (s, 2H); ¹³C NMR (125 MHz, acetone-*d*₆) δ 154.8, 148.3, 136.3, 135.3, 124.8, 122.0, 118.8, 114.9, 59.1. HRMS (ESI⁻) calcd for C₉H₅N₂O₂S [M – H]⁻ 205.0072, found 205.0063.

General procedure for synthesis of Betti bases (4.10–4.12)

Paraformaldehyde (64 mg, 2.1 mmol) and various amine (2.1 mmol) were suspended in anhydrous MeCN (10 mL) and stirred at 80 °C for 1 h. Heterocyclic phenol X (350 mg, 2.0 mmol) was dissolved in anhydrous MeCN (6 mL) and flowed into the reaction. The reaction was stirred vigorously at 80 °C until TLC showed complete consumption of starting material (1–2 h). For products that precipitated from solution, purification consisted of filtration followed by recrystallization from warm MeCN. The other reactions were purified by flash column chromatography (eluting with hexanes:EtOAc).

7-[(Dimethylamino)methyl]-6-hydroxy-1,3-benzothiazole-2-carbonitrile (4.10):

Following the general procedure, benzyl amine **4.10** was obtained as an off-white solid (365 mg, 91%) after recrystallization with warm MeCN. ¹H NMR (400 MHz, D₂O) δ 8.02 (d, *J* = 9.1, 1H), 7.32 (d, *J* = 9.1, 1H), 4.53 (s, 2H), 2.94 (s, 6H); ¹³C NMR (125 MHz, D₂O) δ 160.0, 147.9, 142.4, 136.2, 130.0, 120.9, 115.4, 110.9, 59.1, 45.5. HRMS (ESI+) calcd for C₁₁H₁₁N₃OSH [M + H]⁺ 234.0701, found 234.0699.

6-Hydroxy-7-[(morpholin-4-yl)methyl]-1,3-benzothiazole-2-carbonitrile (4.11):

Following the general procedure, benzyl amine **4.11** was obtained as a pale tan solid (538 mg, 98%) after recrystallization with warm MeCN. ¹H NMR (500 MHz, CDCl₃) δ 7.99 (d, *J* = 8.8, 1H), 7.16 (d, *J* = 8.8, 1H), 3.91 (s, 2H), 3.81 (bs, 4H), 2.68 (bs, 4H); HRMS (ESI-) calcd for C₁₃H₁₂N₃O₂S [M – H][–] 274.0650, found 274.0659.

6-Hydroxy-7-[[4-(morpholin-4-yl)piperidin-1-yl]methyl]-1,3-benzothiazole-2-carbonitrile

(4.12):

Following the general procedure, benzyl amine **4.12** was obtained as a yellow solid in 95% yield. ^1H NMR (500 MHz, CDCl_3) δ 7.89 (d, $J = 9.0$, 1H), 7.08 (d, $J = 9.0$, 1H), 3.83 (s, 2H), 3.67-3.69 (m, 4H), 3.06 (app d, $J = 11.6$, 2H), 2.52 (bs, 4H), 2.21-2.28 (m, 3H), 1.90 (app d, $J = 12.8$, 2H), 1.61 (q, $J = 11.2$, 2H); HRMS (ESI $^-$) calcd for $\text{C}_{13}\text{H}_{12}\text{N}_3\text{O}_2\text{S}$ [$\text{M} - \text{H}$] $^-$ 274.0650, found 274.0659.

General procedure for synthesis of luciferin analogs (4.13–4.15)

D-Cysteine hydrochloride monohydrate (0.171 mmol) and 2-cyano benzothiazole (0.163 mmol) were suspended in 4:1 MeCN:H₂O (1 mL) in a 20 mL vial. Potassium carbonate (0.164 mmol) was then added to the mixture, and the resulting bright yellow-green solution was stirred under N₂ for 20 min. Products were isolated by filtration as the potassium salt or purified via reversed-phase HPLC.

7-Formyl luciferin (4.5):

Following the general procedure, the potassium salt of **4.5** was obtained as a dark green solid (90%) after reversed-phase HPLC. ^1H NMR (500 MHz, D₂O) δ 10.0 (s, 1H), 7.63 (d, $J = 9.2$, 1H), 6.71 (d, $J = 9.2$, 1H), 5.17 (app t, $J = 9.0$, 1H), 3.77 (app t, $J = 10.4$, 1H), 3.55 (dd, $J = 8.5$, $J = 10.7$ 1H); ^{13}C NMR (125 MHz, D₂O/MeOH) δ 189.5, 178.6, 176.1, 166.2, 156.5, 143.3, 135.2, 132.1, 125.4, 117.3, 80.7, 36.8. HRMS (ESI $^-$) calcd for $\text{C}_{12}\text{H}_7\text{O}_4\text{N}_2\text{S}_2$ [$\text{M} - \text{H}$] $^-$ 306.9847, found 306.9843.

7-(Hydroxymethyl) luciferin (4.7):

Following the general procedure, the free acid of **4.7** was obtained as a pale yellow solid (76%) after reversed-phase HPLC. ^1H NMR (500 MHz, D_2O) δ 10.0 (s, 1H), 7.63 (d, $J = 9.2$, 1H), 6.71 (d, $J = 9.2$, 1H), 5.17 (app t, $J = 9.0$, 1H), 3.77 (app t, $J = 10.4$, 1H), 3.55 (dd, $J = 8.5$, $J = 10.7$ 1H); ^{13}C NMR (125 MHz, CD_3OD) δ 173.5, 168.0, 160.0, 155.2, 148.8, 137.3, 124.6, 121.3, 117.7, 79.7, 59.5, 35.9. HRMS (ESI $^-$) calcd for $\text{C}_{11}\text{H}_9\text{O}_2\text{N}_2\text{S}_2$ $[\text{M} - \text{CO}_2\text{H}]^-$, calcd 265.0106, found 265.0116.

7-[(Dimethylamino)methyl] luciferin (4.13):

Following the general procedure, the potassium salt of **4.13** was obtained as a tan solid (86%) after filtration and recrystallization with MeCN. ^1H NMR (400 MHz, $\text{DMSO-}d_6$) δ 7.85 (d, $J = 8.8$, 1H), 7.14 (d, $J = 8.8$, 1H), 5.37 (app t, $J = 9.0$, 1H), 3.75-3.65 (m, 4H), 2.27 (s, 6H); ^{13}C NMR (125 MHz, $\text{DMSO-}d_6$) δ 171.4, 164.4, 158.6, 155.0, 146.6, 135.7, 123.3, 116.8, 116.6, 78.6, 56.1, 44.7, 34.6. HRMS (ESI $^-$) calcd for $\text{C}_{13}\text{H}_{14}\text{N}_3\text{OS}_2$ $[\text{M} - \text{H}]^-$, calcd 292.0578, found 292.0588.

7-[(Morpholin-4-yl)methyl] luciferin (4.14):

Following the general procedure, the potassium salt of **4.14** was obtained as a tan solid (93%) after filtration and recrystallization with MeCN. ^1H NMR (400 MHz, D_2O) δ 7.54 (d, $J = 8.9$, 1H), 6.94 (d, $J = 8.9$, 1H), 5.17 (app t, $J = 9.2$, 1H), 3.89-3.59 (m, 7H), (app t, $J = 9.9$, 1H), 2.81 (s, 4H); ^{13}C NMR (125 MHz, D_2O) δ 180.2, 167.9, 160.1, 158.6, 148.1, 139.6, 126.4, 120.3, 115.0, 83.0, 68.4, 60.1, 55.0, 39.0. HRMS (ESI $^-$) calcd for $\text{C}_{15}\text{H}_{16}\text{N}_3\text{O}_2\text{S}_2$ $[\text{M} - \text{CO}_2\text{H}]^-$, calcd 334.0684, found 334.0674.

7-[[4-(morpholin-4-yl)piperidin-1-yl]methyl] luciferin (**4.15**):

Following the general procedure, the potassium salt of **4.15** was obtained as a tan solid (89%) after filtration and recrystallization with MeCN. ^1H NMR (400 MHz, D_2O) δ 7.53 (d, $J = 8.8$, 1H), 6.89 (d, $J = 8.8$, 1H), 5.13 (app t, $J = 9.3$, 1H), 3.95 (dd, $J = 34.0$, $J = 14.1$, 2H), 3.81-3.76 (m, 5H), (app t, $J = 9.9$, 1H), (app t, $J = 12.9$, 2H), 2.78-2.65 (m, 7H), 2.10 (br s, 2H), 1.65 (app d, $J = 11.6$, 2H); ^{13}C NMR (125 MHz, D_2O) δ 180.1, 167.6, 161.9, 159.0, 147.2, 140.6, 127.3, 121.4, 112.8, 83.0, 68.4, 62.6, 59.2, 54.2, 54.1, 51.6, 39.0, 28.3. HRMS (ESI $^-$) calcd for $\text{C}_{20}\text{H}_{25}\text{N}_4\text{O}_2\text{S}_2$ [$\text{M} - \text{CO}_2\text{H}$] $^-$, calcd 417.1419, found 417.1412.

N-(4-Acetoxy-2-methylphenyl)cyanothioformamide (**4.17**)

Aniline **4.16** (8.26 g, 50.0 mmol) and Appel's salt (10.8 g, 52.5 mmol) were stirred in 250 mL of anhydrous CH_2Cl_2 under N_2 for ~ 1 h (until **4.16** was consumed). The CH_2Cl_2 was then reduced to half *in vacuo* and the solids isolated by vacuum filtration. The dry solids were then resuspended in (2:1 MeCN:THF). A solution of sodium thiosulfate (23.0 g, 145.5 mmol in 80 mL H_2O) was then added, and the mixture was vigorously stirred for an additional 3 h. The reaction mixture was filtered to remove elemental sulfur, and the volatiles were removed from the mother liquor *in vacuo*. The remaining aqueous mixture was filtered to remove residual solids and the filtrate acidified with 1 M NaHSO_4 . Cyanothioformamide **4.17** precipitated from solution and was collected by vacuum filtration. The material was washed with additional H_2O , then dried to provide **4.17** as a vivid orange solid (10.7 g, 92%). Compound **4.17** was characterized as a mixture of tautomers. ^1H NMR (500 MHz, CDCl_3) δ 7.49-7.37 (m, 1H), 7.06-6.96 (m, 2H), 2.35-2.20 (m, 6H). ^{13}C NMR (125 MHz, CDCl_3) δ 170.4, 169.7, 167.6, 164.7,

151.0, 150.3, 135.6, 134.9, 133.6, 132.2, 127.1, 127.0, 124.7, 124.5, 120.8, 120.1, 113.5, 112.0, 21.3, 18.2, 18.0. HRMS (ESI⁻) calcd for C₁₁H₉N₂O₂S [M - H]⁻, calcd 233.0385, found 233.0388.

6-Acetoxy-4-methyl-1,3-benzothiazole-2-carbonitrile (4.18):

Palladium chloride (117 mg, 0.639 mmol), CuI (611 mg, 3.20 mmol), TBAB (4.12 g, 12.8 mmol), and (4.17) (1.50 g, 6.39 mmol,) were suspended in anhydrous 1:1 DMF:DMSO (100 mL). The resultant red-brown mixture was placed under N₂ and stirred at 120 °C for 3 h. The reaction was then diluted with ethyl acetate and washed with H₂O (4 x 50 mL). The organics were then dried over Na₂SO₄, filtered, and concentrated *in vacuo*. The crude product was purified by flash column chromatography (eluting with 5:1 hexanes:EtOAc) to provide, (4.18) (1.35 g, 91%) as a light beige solid. ¹H NMR (400 MHz, acetone-*d*₆) δ 7.88 (dd, *J* = 2.2, *J* = 0.6, 1H), 7.32 (dd, *J* = 2.2, *J* = 0.9, 1H), 2.75 (s, 3H), 2.05 (s, 3H); ¹³C NMR (125 MHz, acetone-*d*₆) δ 170.1, 152.5, 150.9, 137.6, 137.5, 137.2, 124.6, 114.4, 114.1, 21.5, 18.7.

6-Methoxy-4-methyl-1,3-benzothiazole-2-carbonitrile (4.20) and 6-hydroxy-4-methyl-1,3-benzothiazole-2-carbonitrile (4.21)

Aniline 4.19 (2.45 mL, 19.0 mmol) and 4,5-dichloro-1,2,3-dithiazolium chloride 2.3 (4.16 g, 20.0 mmol) were added to a rigorously dried sealed tube, suspended in dry sulfolane (10 mL), and placed under N₂. The sealed reaction was stirred for 3 h at 40 °C, then directly transferred to a pre-heated silicon oil bath (180 °C) and stirred for an additional 20 min. Upon cooling to rt, pyridine hydrochloride (23.0 g, 0.200 mol) was added to the reaction mixture. The reaction vessel was re-sealed under N₂ and stirred at 180 °C for 1 h. The mixture was allowed to

cool to rt, and the resulting crude residue was suspended in MTBE (400 mL), then washed with H₂O (3 x 200 mL) and brine (100 mL). The organics were dried over Na₂SO₄, filtered, and concentrated *in vacuo*. The material was then purified via flash column chromatography (eluting with 10:1 – 1:1 hexanes:ethyl acetate). The desired phenol **4.21** was isolated as a pale yellow solid (2.68 g, 74%) along with the methyl ether precursor **4.20** (596 mg, 15%). Additional **4.21** was obtained by re-subjecting isolated **4.21** to pyr•HCl deprotection as previously published. Compound **4.21**: ¹H NMR (400 MHz, acetone-*d*₆) δ 7.41 (d, *J* = 2.0, 1H), 7.07 (s, 1H), 2.67 (s, 3H); ¹³C NMR (125 MHz, acetone-*d*₆) δ 159.9, 147.3, 139.0, 137.6, 132.7, 119.8, 114.8, 105.2, 18.6.

6-Acetoxy-4-methyl-1,3-benzothiazole-2-carbonitrile (4.18):

Phenol **4.21** (4.00 g, 21.0 mmol) and DMAP (13.1mg, 0.105 mmol) were suspended in acetic anhydride (10 ml) and stirred at rt overnight. The reaction was then filtered and the solids washed with chilled H₂O to yield pure **4.18** (4.79 g, 98%) as a light beige solid. NMR matched those reported above.

6-Acetoxy-4-[bromomethyl]-1,3-benzothiazole-2-carbonitrile (4.22):

Compound **4.18** (1.1 g, 4.9 mmol) was placed in a rigorously-dried vessel and dissolved in freshly degassed dry MeCN. To the stirred solution was added NBS (1.73 g, 9.75 mmol) and benzoyl peroxide (118 mg, 0.487 mmol). The system was purged with N₂ and permitted to stir overnight at 80 °C, in the dark under N₂. The reaction was then diluted with ethyl acetate and washed with H₂O (4 x 50 mL). The organics were then dried over Na₂SO₄, filtered, and concentrated *in vacuo*. The crude product was purified by flash column chromatography (eluting

with 10:1 hexanes:EtOAc) to provide **4.22** (1.5 g, 83%) as a light beige solid. ^1H NMR (400 MHz, acetone- d_6) δ 8.07 (d, $J = 2.2$, 1H), 7.65 (s, $J = 2.2$, 1H), 5.12, (s, 2H), 2.35 (s, 3H); ^{13}C NMR (125 MHz, acetone- d_6) δ 170.0, 152.4, 149.5, 138.6, 138.3, 136.7, 125.2, 117.1, 114.3, 29.0, 21.5.

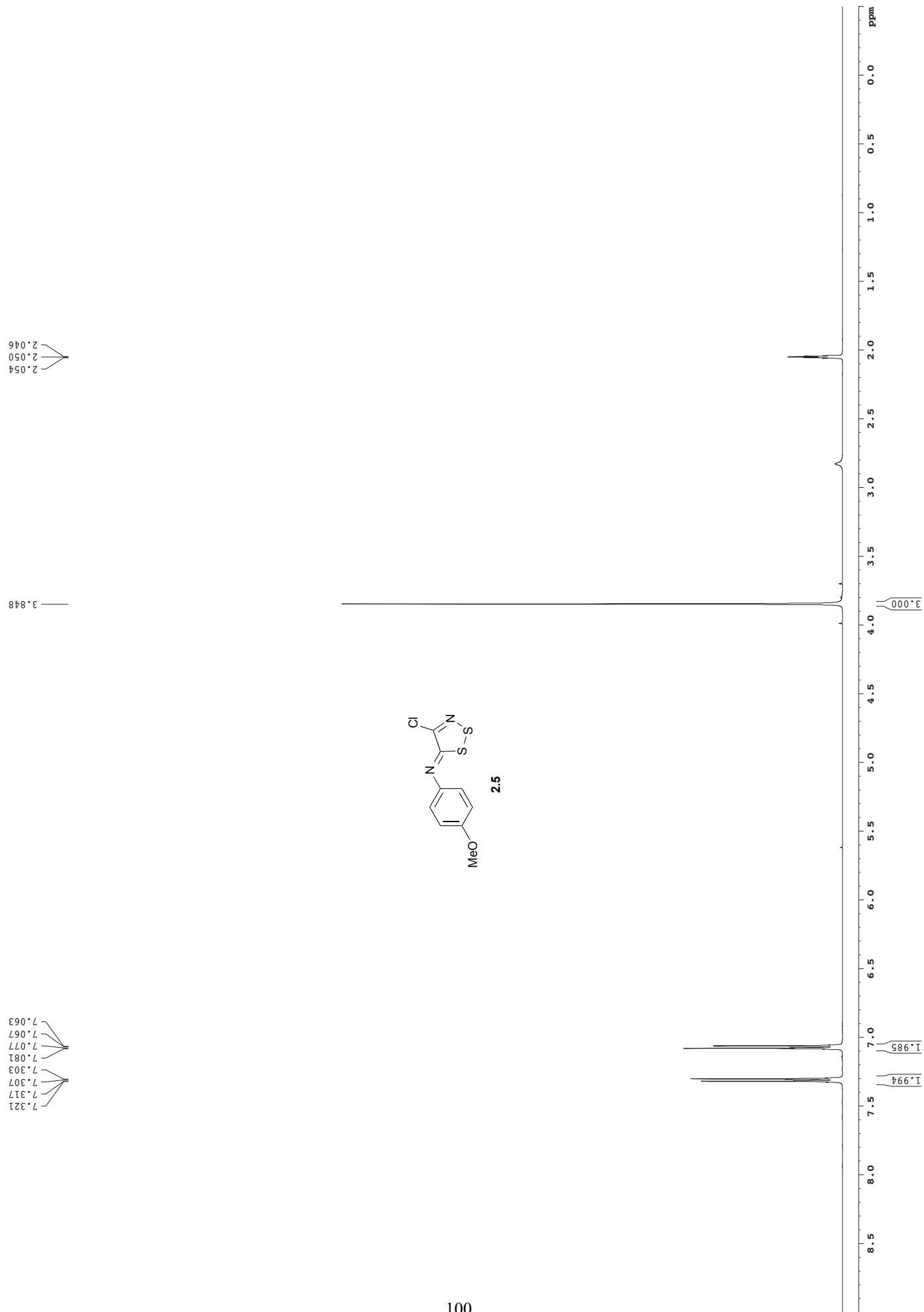
4-[(Morpholin-4-yl)methyl] luciferin (4.23):

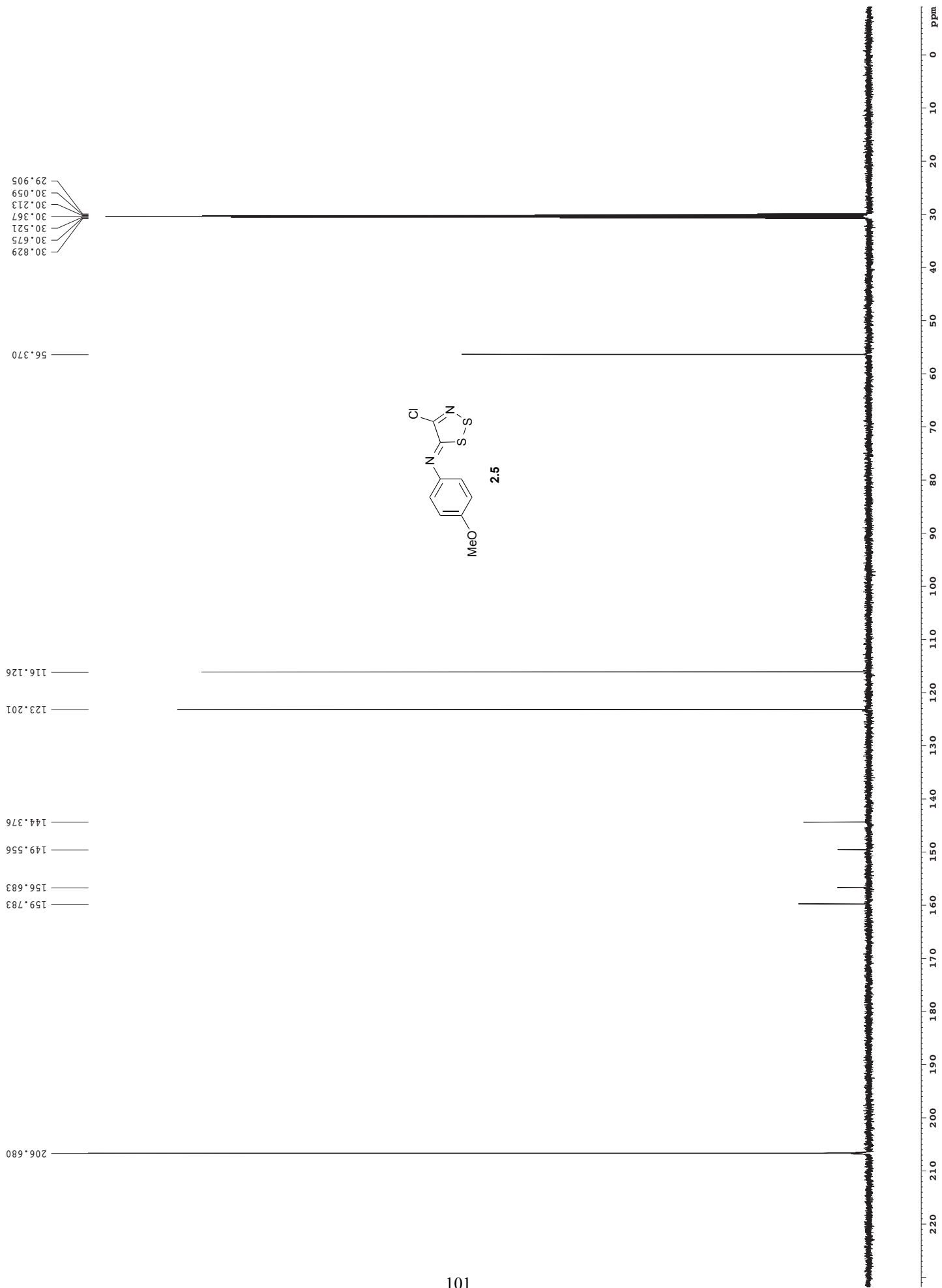
Cyano benzothiazole **4.22** (564 mg, 1.81 mmol) was dissolved in MeCN (11 mL) and stirred at rt. Morpholine (330 μL , 3.64 mmol) and K_2CO_3 (505 mg, 3.64 mmol) were added to the stirred solution. Upon conversion of **4.22** (~2 h) a solution of D-cysteine (354 mg, 2.00 mmol) in H_2O (2 mL) was added and the reaction stirred at rt under N_2 for another 1 h. Precipitate was isolated by vacuum filtration and washed with chilled MeOH. The residual washes and mother liquor was concentrated in vacuo and the residue purified by reversed-phase HPLC ($\text{H}_2\text{O}/\text{MeCN}$). The potassium salt of luciferin **4.23** (666 mg, 88%) was isolated as a greenish solid and stored at $-80\text{ }^\circ\text{C}$. ^1H NMR (500 MHz, D_2O) δ 7.10 (s, 1H), 6.88 (s, 1H), 5.19 (app t, $J = 9.1$, 1H), (dd, $J = 37.6$, $J = 13.0$, 2H), 3.78-3.74 (m, 5H), (app t, $J = 9.6$, 1H), 2.63 (s, 4H); ^{13}C NMR (125 MHz, D_2O) δ 180.5, 168.7, 161.0, 158.8, 148.1, 140.5, 133.8, 122.2, 109.5, 82.8, 68.6, 60.3, 55.2, 38.9. HRMS (ESI $^-$) calcd for $\text{C}_{16}\text{H}_{16}\text{N}_3\text{O}_4\text{S}_2$ $[\text{M} - \text{H}]^-$, calcd 378.0582, found 378.0578.

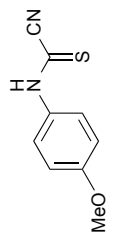
4.6 Reference

- (1) Prescher, J. A.; Contag, C. H. Guided by the light: visualizing biomolecular processes in living animals with bioluminescence. *Curr. Opin. Chem. Biol.* **2010**, *14*, 80.
- (2) Santos, E. B.; Yeh, R.; Lee, J.; Nikhamin, Y.; Punzalan, B.; Punzalan, B.; La Perle, K.; Larson, S. M.; Sadelain, M.; Brentjens, R. J. Sensitive in vivo imaging of T cells using a membrane-bound *Gaussia princeps* luciferase. *Nat. Med.* **2009**, *15*, 338.
- (3) Branchini, B. R.; Magyar, R. A.; Murtiashaw, M. H.; Anderson, S. M.; Helgerson, L. C.; Zimmer, M. Site-directed mutagenesis of firefly luciferase active site amino acids: A proposed model for bioluminescence color. *Biochemistry* **1999**, *38*, 13223.
- (4) Viviani, V. R.; Amaral, D. T.; Neves, D. R.; Simoes, A.; Arnoldi, F. G. C. The Luciferin Binding Site Residues C/T311 (S314) Influence the bioluminescence color of beetle luciferases through main-chain interaction with oxyluciferin phenolate. *Biochemistry* **2013**, *52*, 19.
- (5) Degeling, M. H.; Bovenberg, M. S. S.; Lewandrowski, G. K.; de Gooijer, M. C.; Vleggeert-Lankamp, C. L. A.; Tannous, M.; Maguire, C. A.; Tannous, B. A. Directed molecular evolution reveals *gaussia* luciferase variants with enhanced light output stability. *Anal. Chem.* **2013**, *85*, 3006.
- (6) Jacques, S. L. Optical properties of biological tissues: A review. *Phys. Med. Biol.* **2013**, *58*, R37.
- (7) Paley, M. A.; Prescher, J. A. Bioluminescence: A versatile technique for imaging cellular and molecular features. *MedChemComm* **2014**, *5*, 255.
- (8) Tannous, B. A. *Gaussia* luciferase reporter assay for monitoring biological processes in culture and in vivo. *Nat. Protocols* **2009**, *4*, 582.
- (9) Lewandrowski, G.; Magee, C.; Mounayar, M.; Tannous, B.; Azzi, J. In *Bioluminescent Imaging*; Badr, C. E., Ed.; Humana Press: 2014; Vol. 1098, p 211.
- (10) Shah, K.; Liu, Y.; Deirmengian, C.; Shokat, K. M. Engineering unnatural nucleotide specificity for Rous sarcoma virus tyrosine kinase to uniquely label its direct substrates. *Proc Natl Acad Sci U S A* **1997**, *94*, 3565.
- (11) Mofford, D. M.; Reddy, G. R.; Miller, S. C. Aminoluciferins extend firefly luciferase bioluminescence into the near-infrared and can be preferred substrates over D-luciferin. *J. Am. Chem. Soc.* **2014**, *136*, 13277.
- (12) Adams, S. T., Jr.; Miller, S. C. Beyond D-luciferin: Expanding the scope of bioluminescence imaging in vivo. *Curr. Opin. Chem. Biol.* **2014**, *21*, 112.

- (13) Reddy, G. R.; Thompson, W. C.; Miller, S. C. Robust light emission from cyclic alkylaminoluciferin substrates for firefly luciferase. *J. Am. Chem. Soc.* **2010**, *132*, 13586.
- (14) Hall, M. P.; Unch, J.; Binkowski, B. F.; Valley, M. P.; Butler, B. L.; Wood, M. G.; Otto, P.; Zimmerman, K.; Vidugiris, G.; Machleidt, T.; Robers, M. B.; Benink, H. I. n. A.; Eggers, C. T.; Slater, M. R.; Meisenheimer, P. L.; Klaubert, D. H.; Fan, F.; Encell, L. P.; Wood, K. V. Engineered Luciferase Reporter from a Deep Sea Shrimp Utilizing a Novel Imidazopyrazinone Substrate. *ACS Chemical Biology* **2012**, *7*, 1848.
- (15) Rodriguez-Garcia, A.; Rojo-Ruiz, J.; Navas-Navarro, P.; Aulestia, F. J.; Gallego-Sandin, S.; Garcia-Sancho, J.; Alonso, M. T. GAP, an aequorin-based fluorescent indicator for imaging Ca²⁺ in organelles. *Proc. Natl. Acad. Sci. USA* **2014**, *111*, 2584.
- (16) Evans, M. S.; Chaurette, J. P.; Adams Jr, S. T.; Reddy, G. R.; Paley, M. A.; Aronin, N.; Prescher, J. A.; Miller, S. C. A synthetic luciferin improves bioluminescence imaging in live mice. *Nat. Methods* **2014**, *11*, 393.
- (17) Caysa, H.; Jacob, R.; Muther, N.; Branchini, B.; Messerle, M.; Soling, A. A redshifted codon-optimized firefly luciferase is a sensitive reporter for bioluminescence imaging. *Photochem. Photobiol. Sci.* **2009**, *8*, 52.
- (18) Sundlov, J. A.; Fontaine, D. M.; Southworth, T. L.; Branchini, B. R.; Gulick, A. M. Crystal structure of firefly luciferase in a second catalytic conformation supports a domain alternation mechanism. *Biochemistry* **2012**, *51*, 6493.
- (19) Kojima, R.; Takakura, H.; Ozawa, T.; Tada, Y.; Nagano, T.; Urano, Y. Rational design and development of near-infrared-emitting firefly luciferins available *in vivo*. *Angew. Chem. Int. Ed.* **2013**, *52*, 1175.
- (20) Woodrooffe, C. C.; Shultz, J. W.; Wood, M. G.; Osterman, J.; Cali, J. J.; Daily, W. J.; Meisenheimer, P. L.; Klaubert, D. H. N-Alkylated 6-aminoluciferins are bioluminescent substrates for ultra-glo and quantillum luciferase: New potential scaffolds for bioluminescent assays. *Biochemistry* **2008**, *47*, 10383.
- (21) Jones, P. R.; Gelinas, R. M. The first spectral confirmation for the structures of anhydro dimers of o-hydroxybenzaldehydes. *J. Org. Chem.* **1981**, *46*, 194.
- (22) Phillips, J. P.; Barrall, E. M. Notes - Betti reactions of some phenols. *J. Org. Chem.* **1956**, *21*, 692.







2.6

2.050

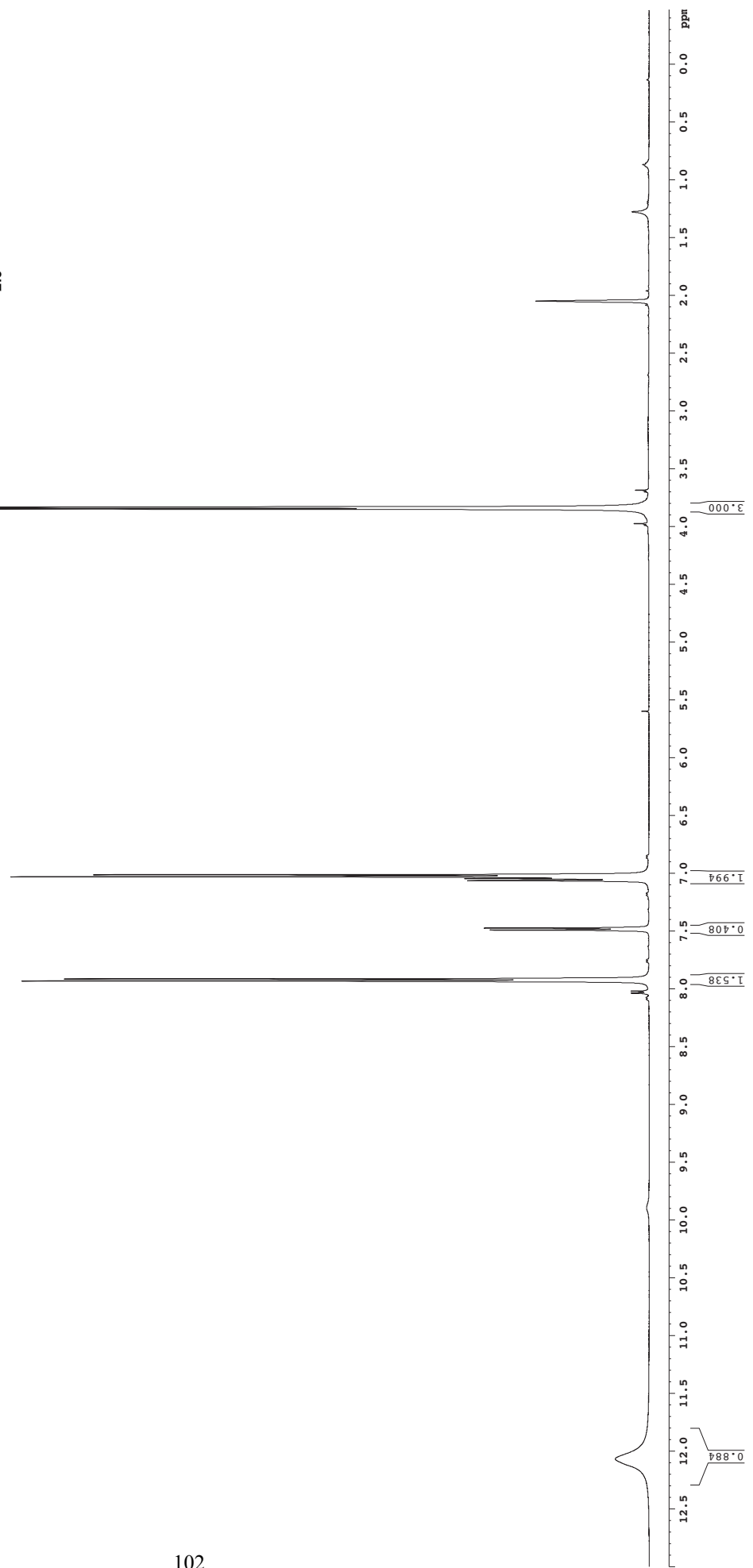
3.849
3.835

7.014
7.032
7.047
7.065

7.475
7.493

7.915
7.934

12.066



30.627
30.474
30.320
30.166
30.012
29.858
29.704

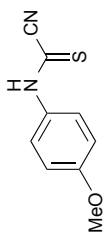
56.243
56.173

114.937
115.188
115.781

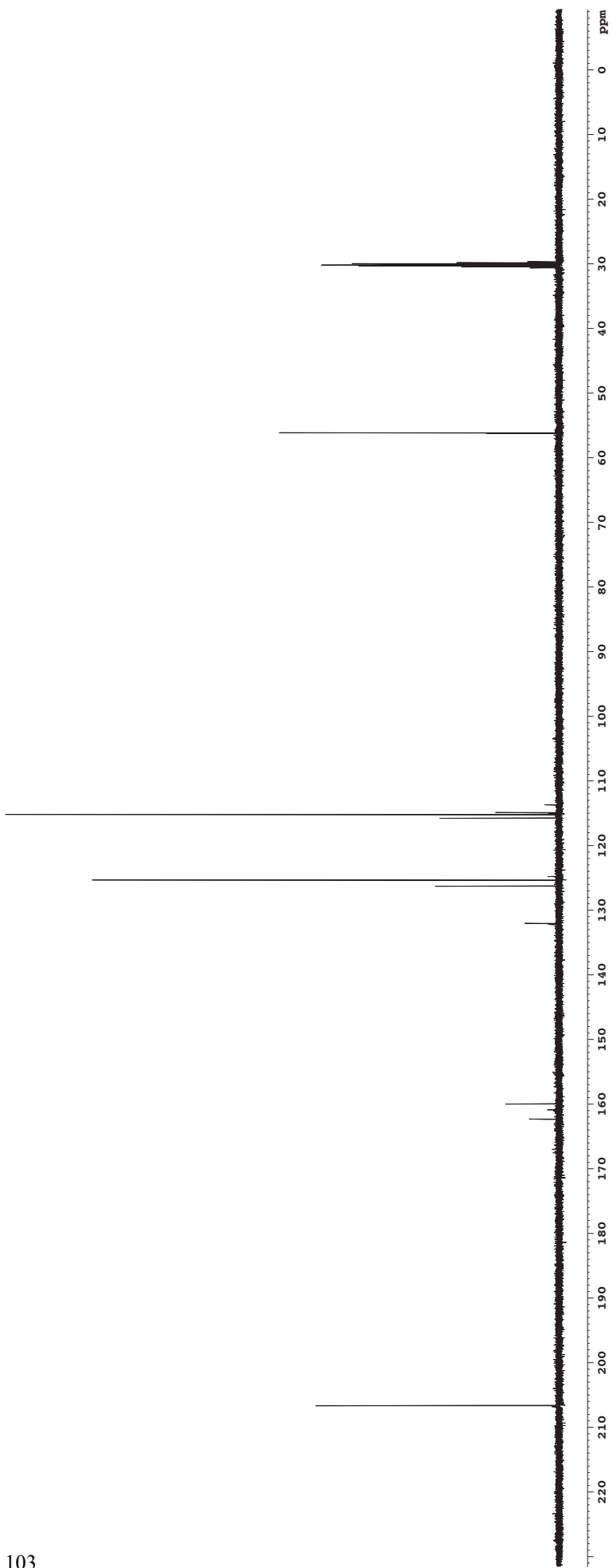
125.366
126.291
132.074

159.992
162.364

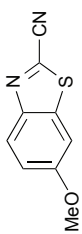
206.680



2.6



2.054
2.050
2.046



2.7

3.947

PPM

3.000

0.984

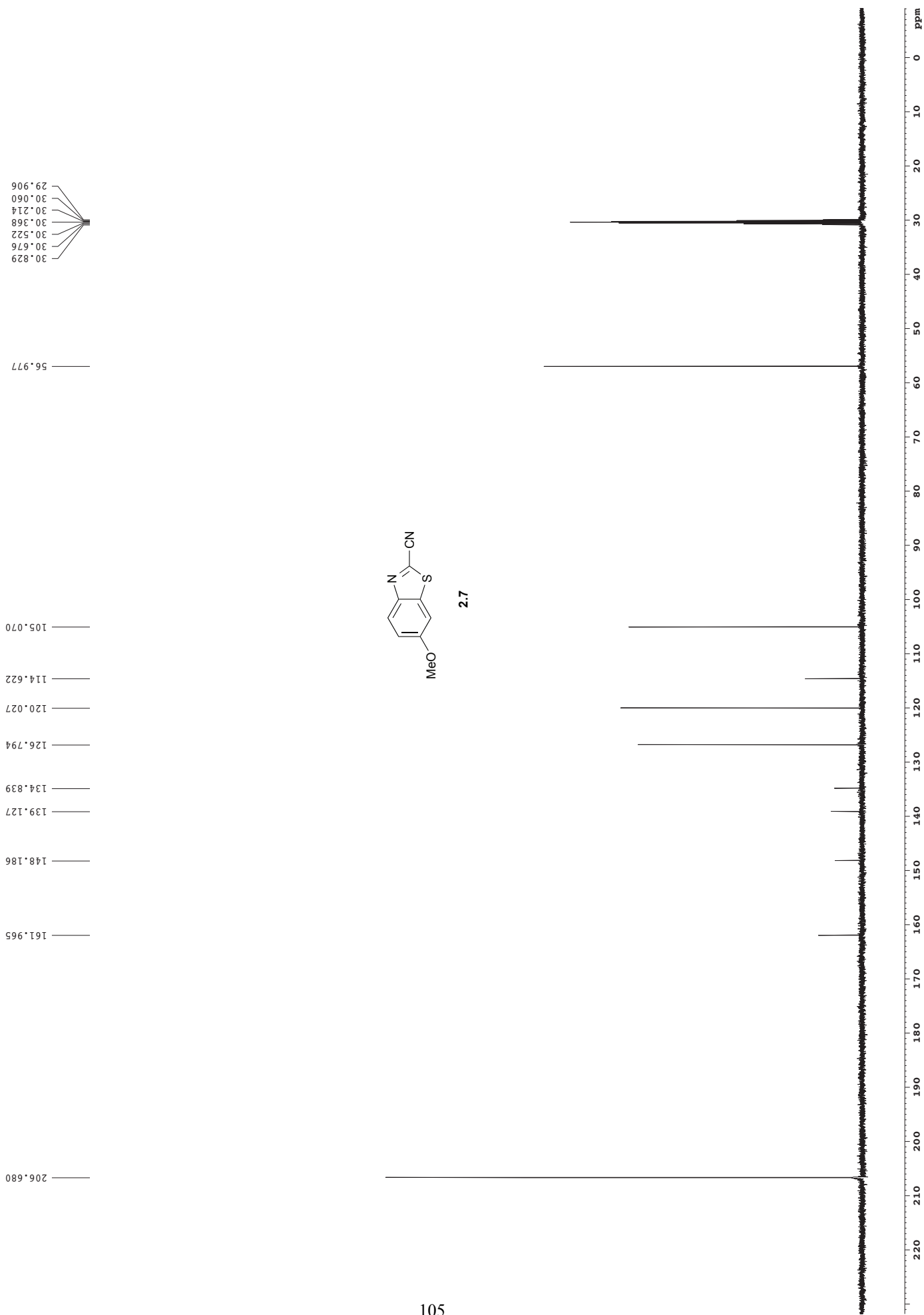
0.966

0.982

7.312
7.307
7.294
7.289

7.760
7.755

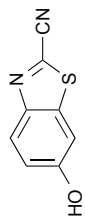
8.071
8.089



2.059
2.054
2.050
2.046
2.041

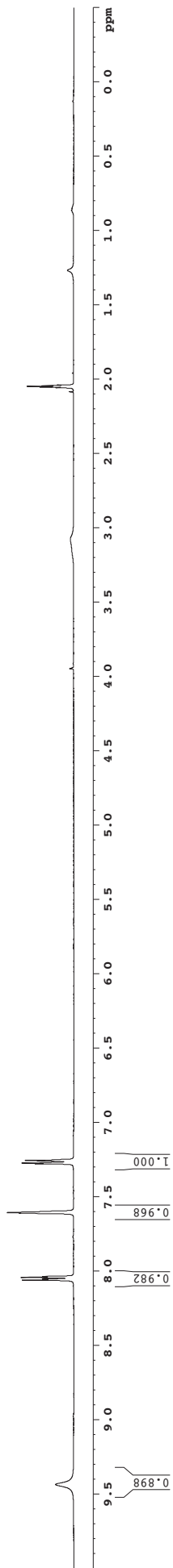
8.063
8.045
8.039
7.613
7.609
7.280
7.275
7.262
7.257

9.435

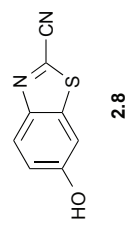


2.8

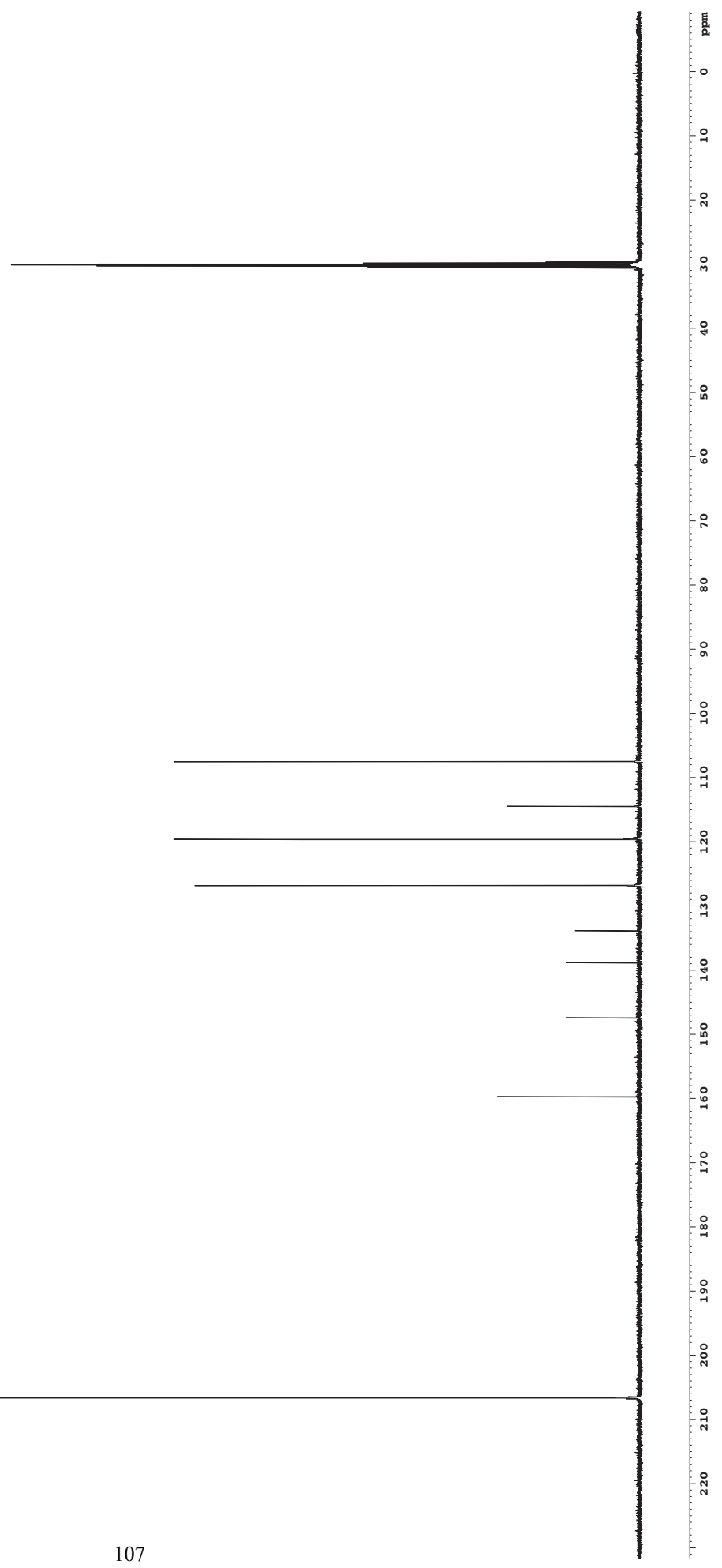
901



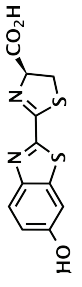
30.622
30.468
30.314
30.160
30.006
29.852
29.698



206.681
159.765
147.458
138.881
133.892
126.870
119.668
114.490
107.549



2.1



3.762
3.751
3.743
3.733
3.338
3.303
3.300
3.296

5.388
5.370
5.352

7.328
7.324
7.062
7.057
7.044
7.040

7.877
7.894

ppm

2.060

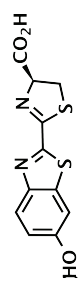
1.121

1.065

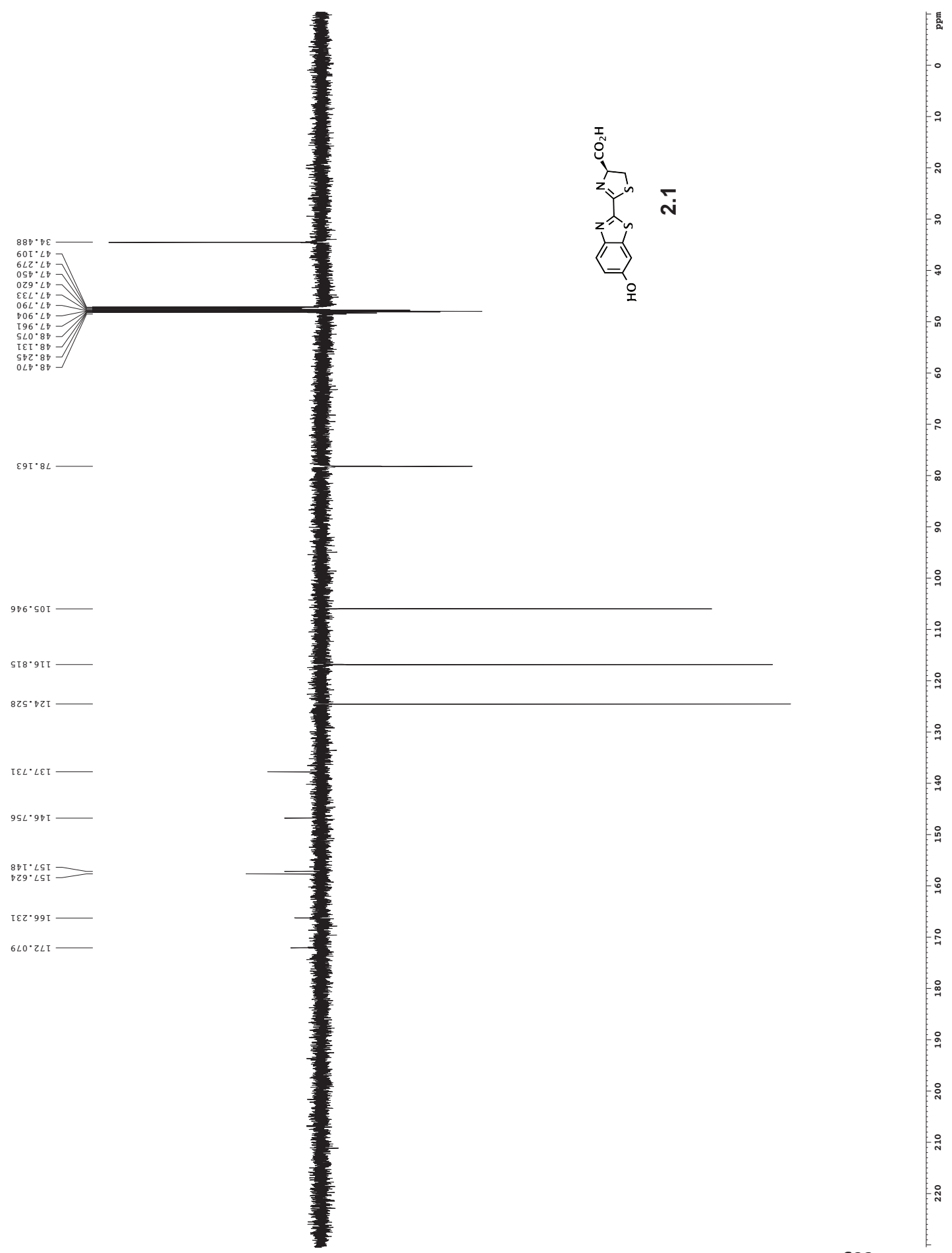
1.016

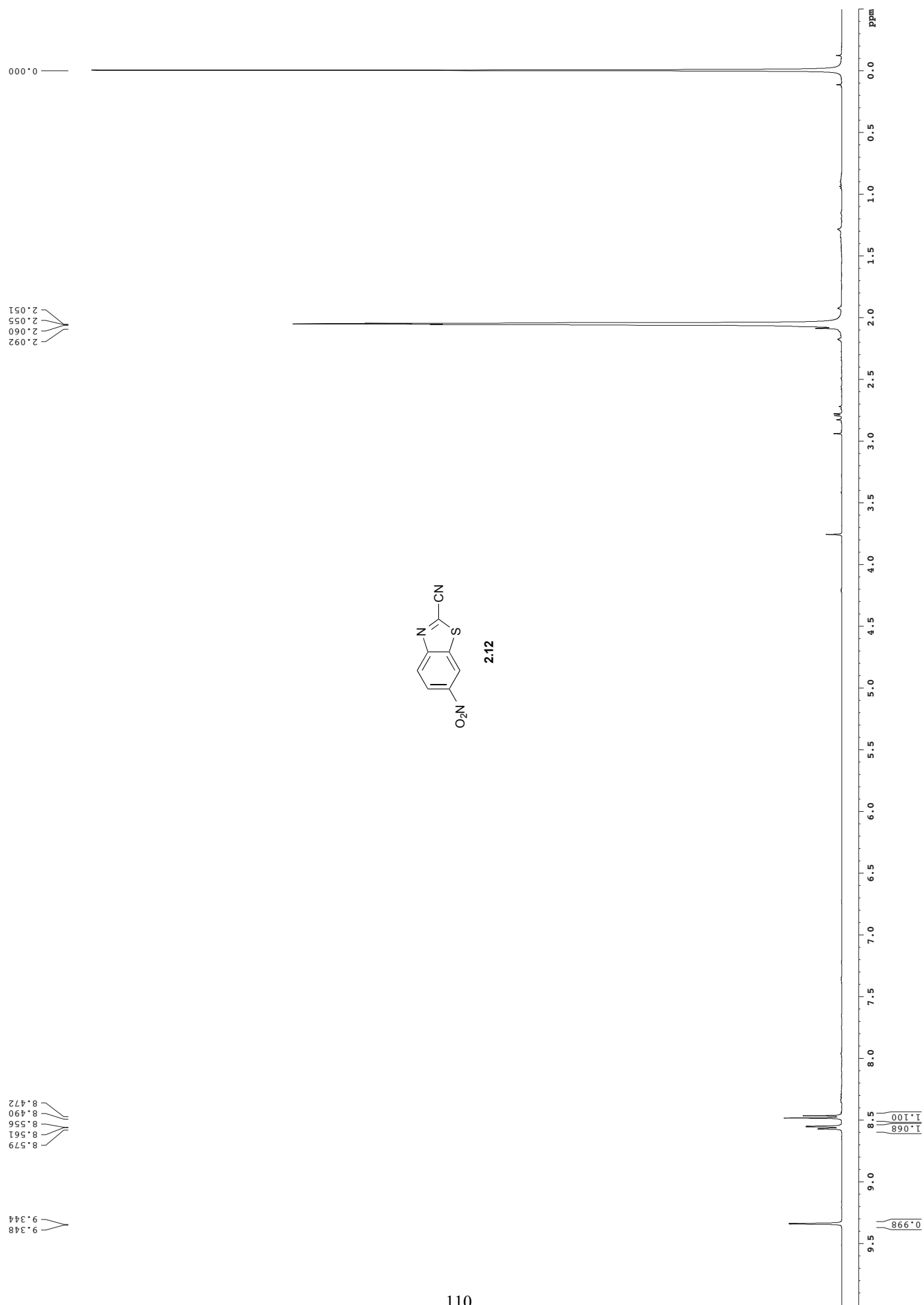
1.000

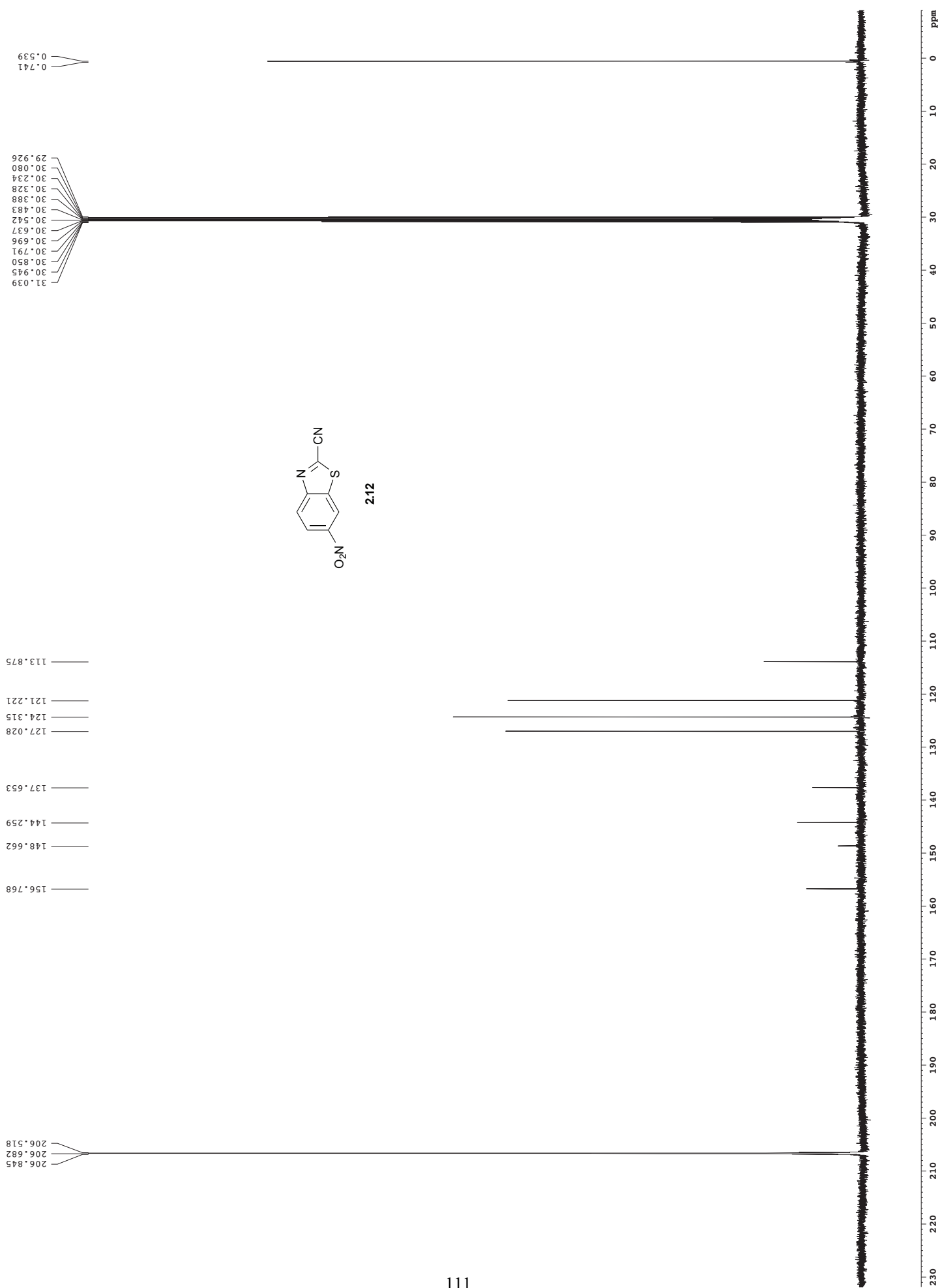
S22

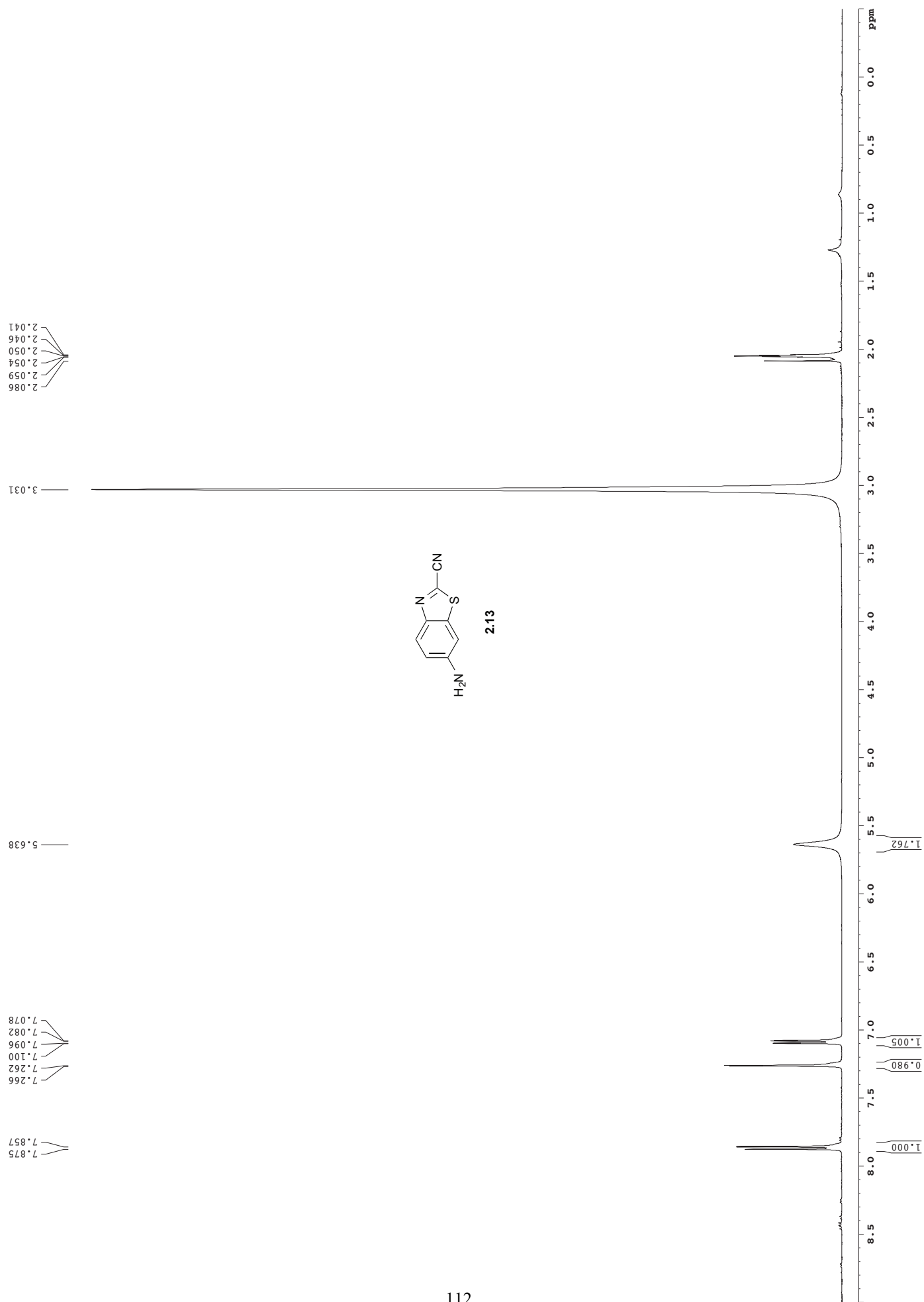


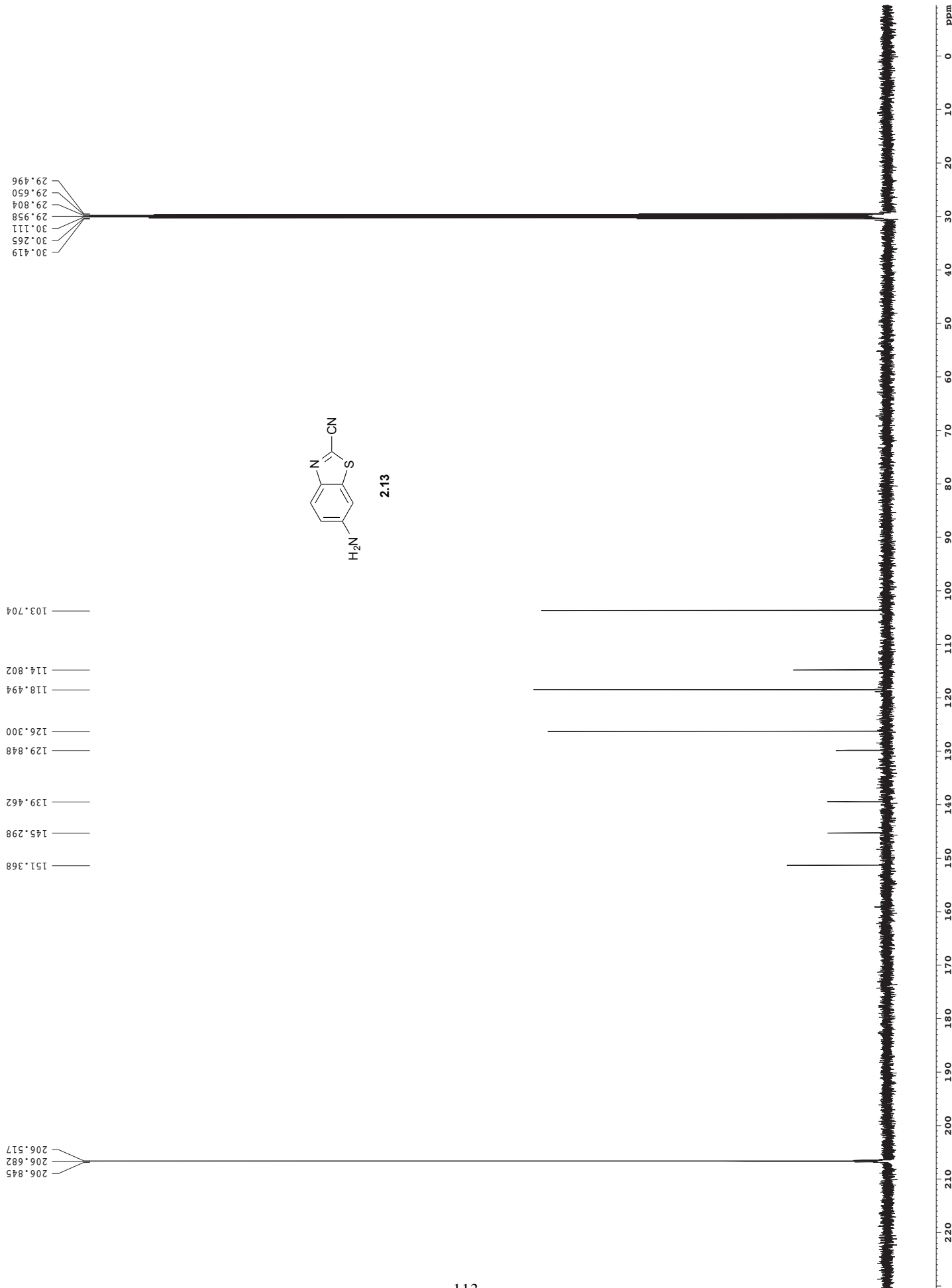
2.1

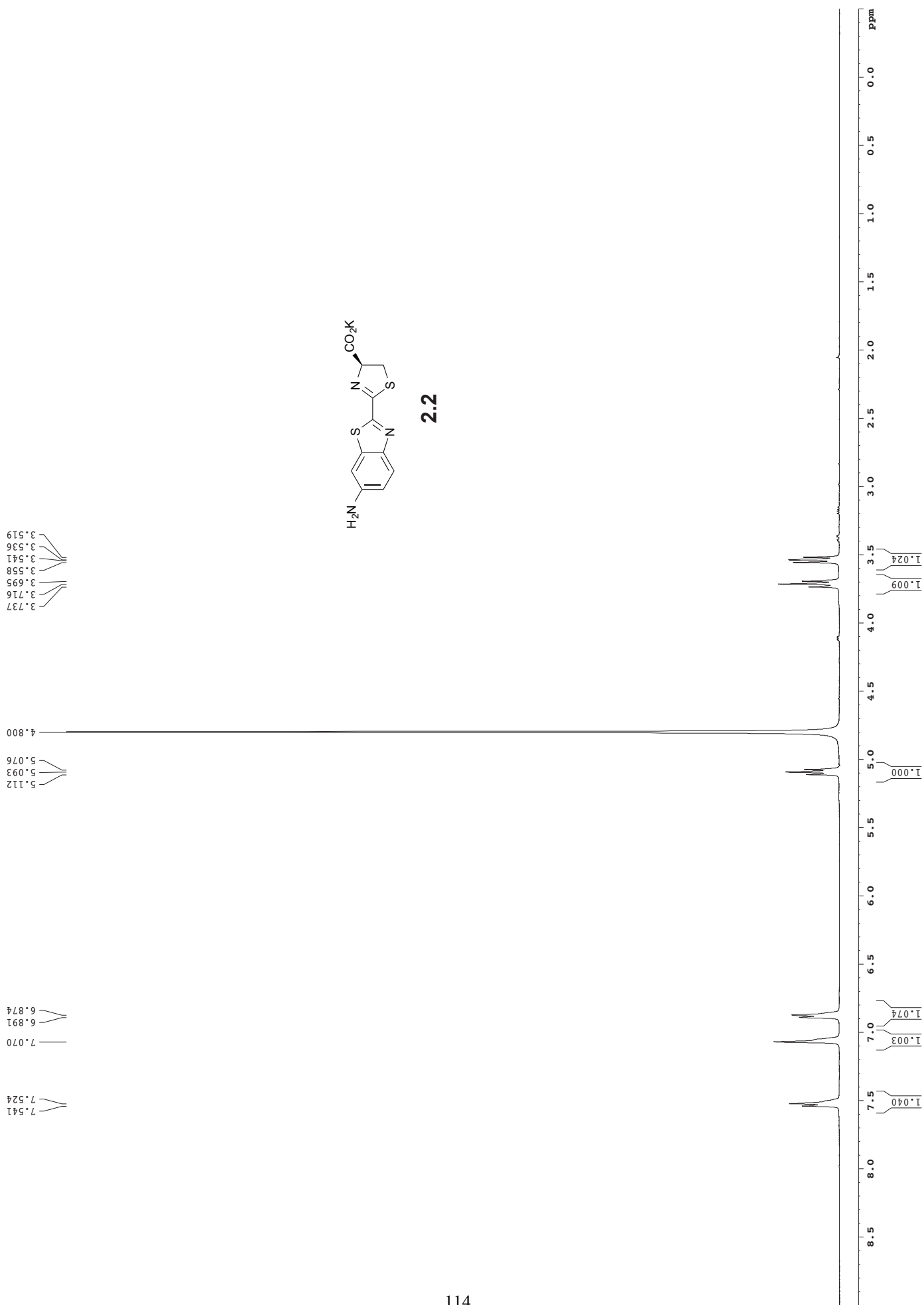


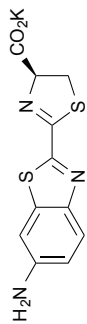




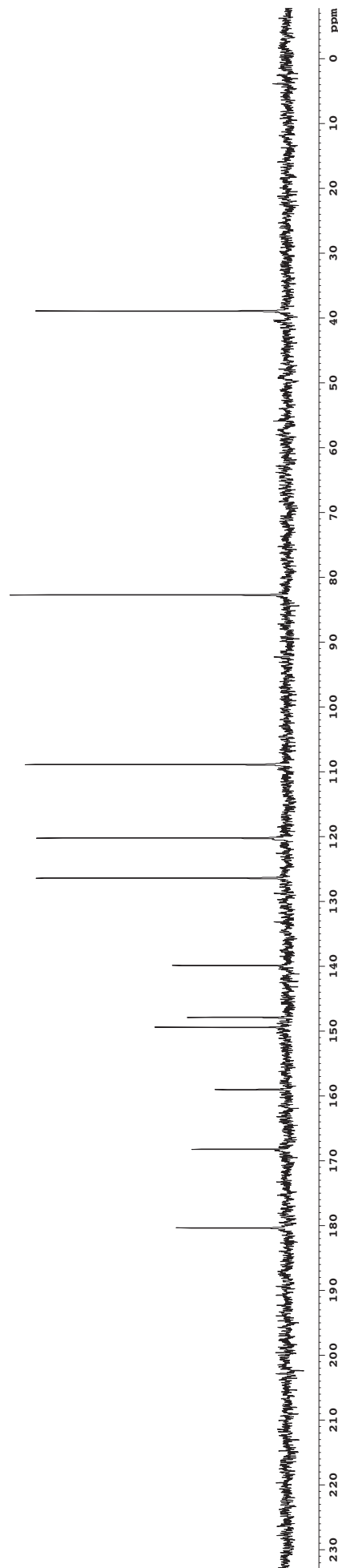




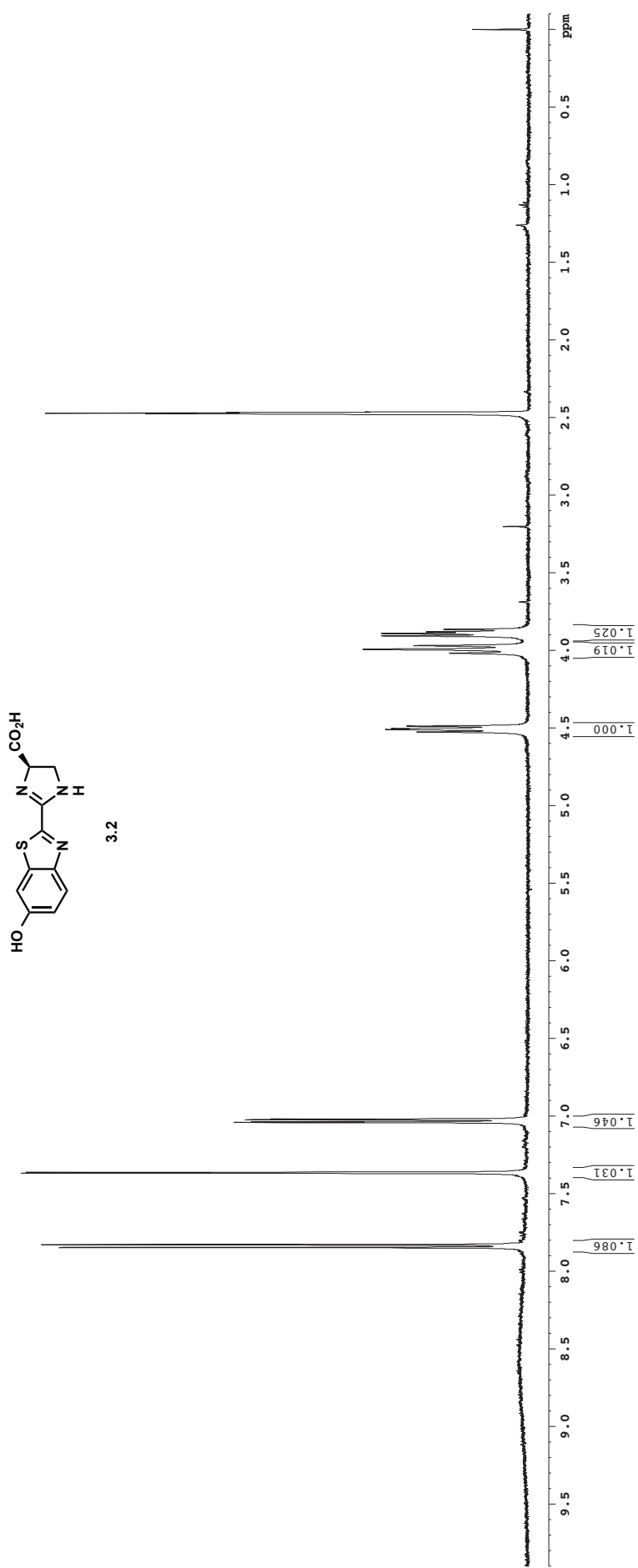




2.2



S24



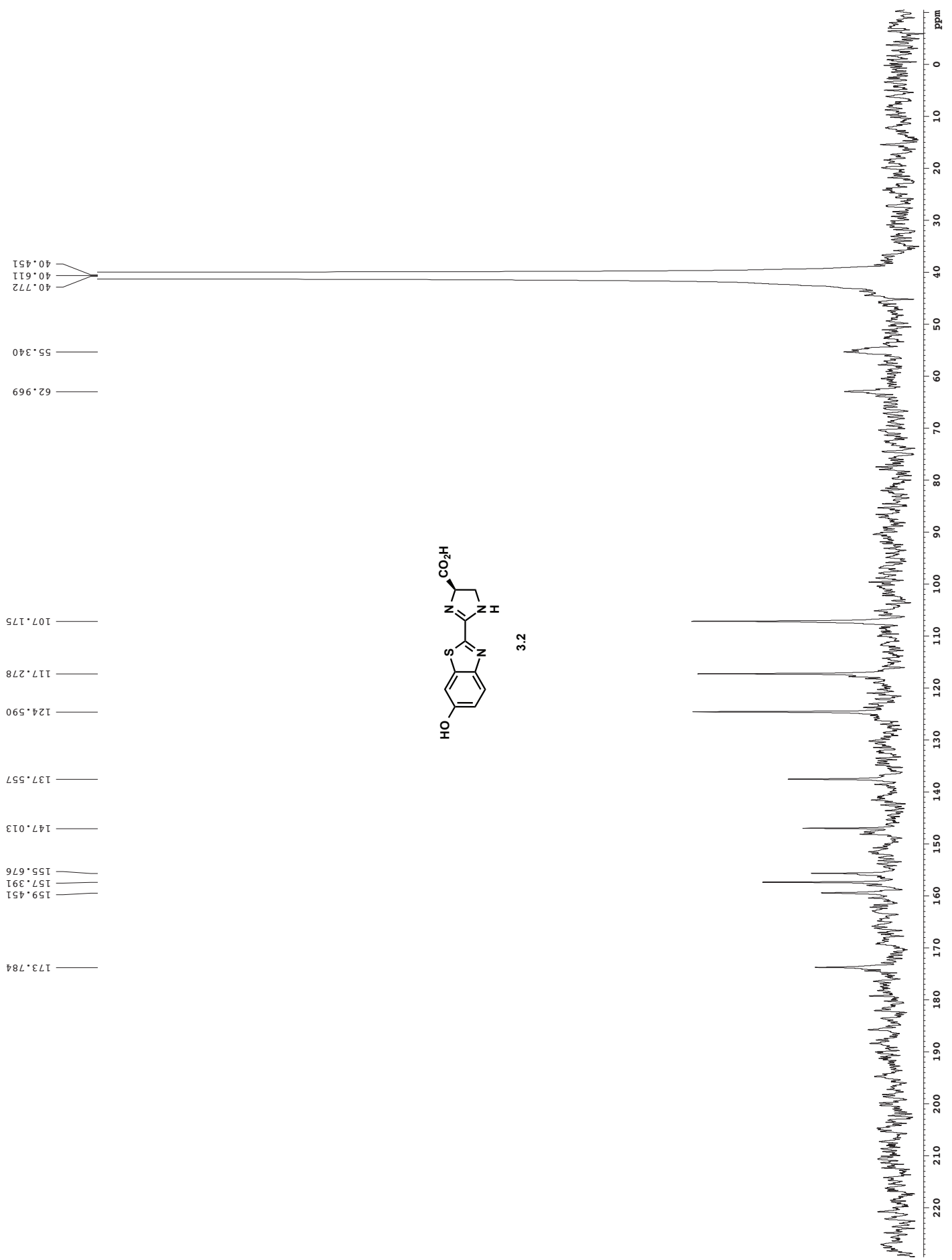
0.000

2.480
2.476
2.473
2.469
2.466

4.527
4.511
4.489
4.019
3.994
3.971
3.907
3.892
3.881
3.866

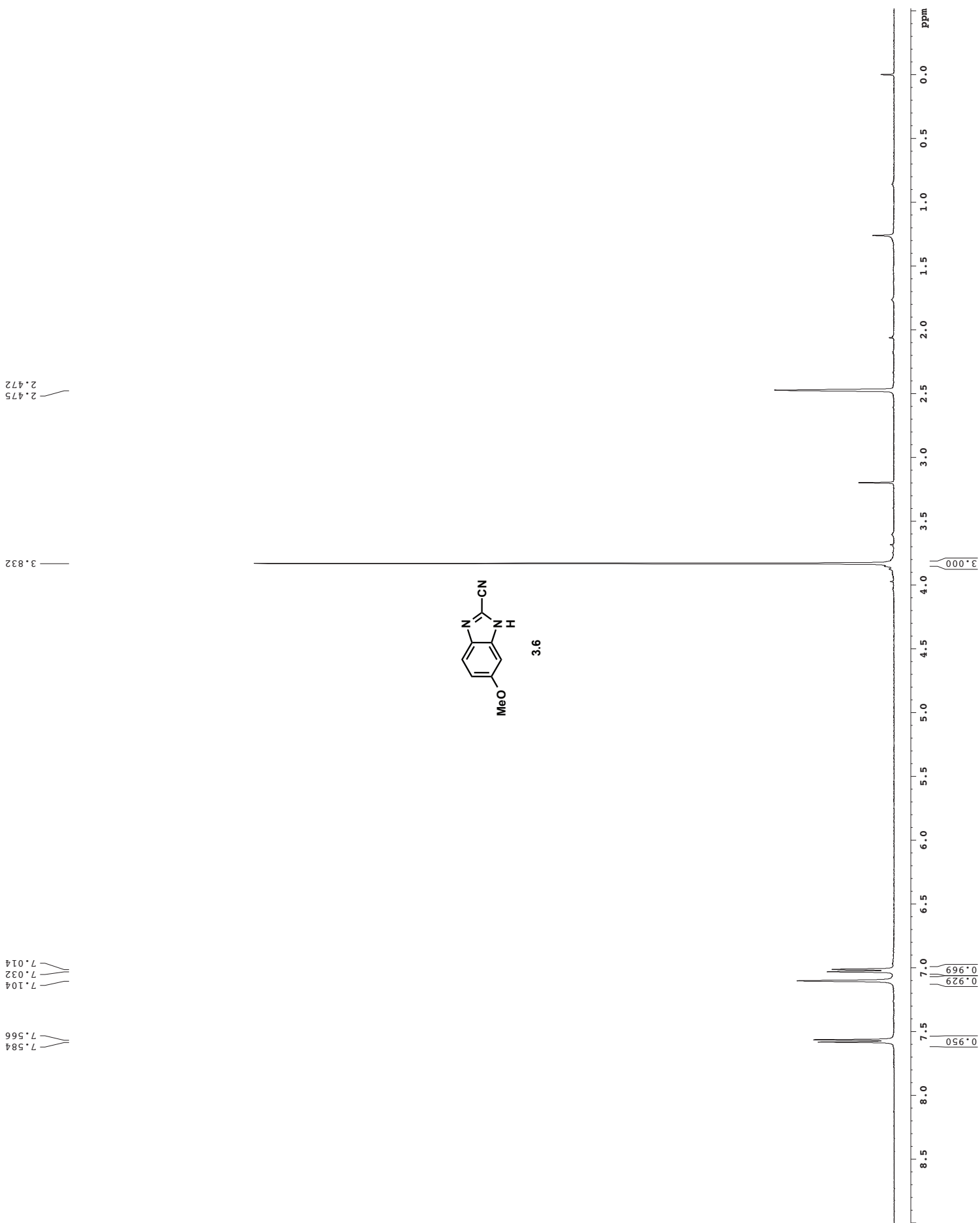
7.369
7.364
7.043
7.038
7.025
7.020

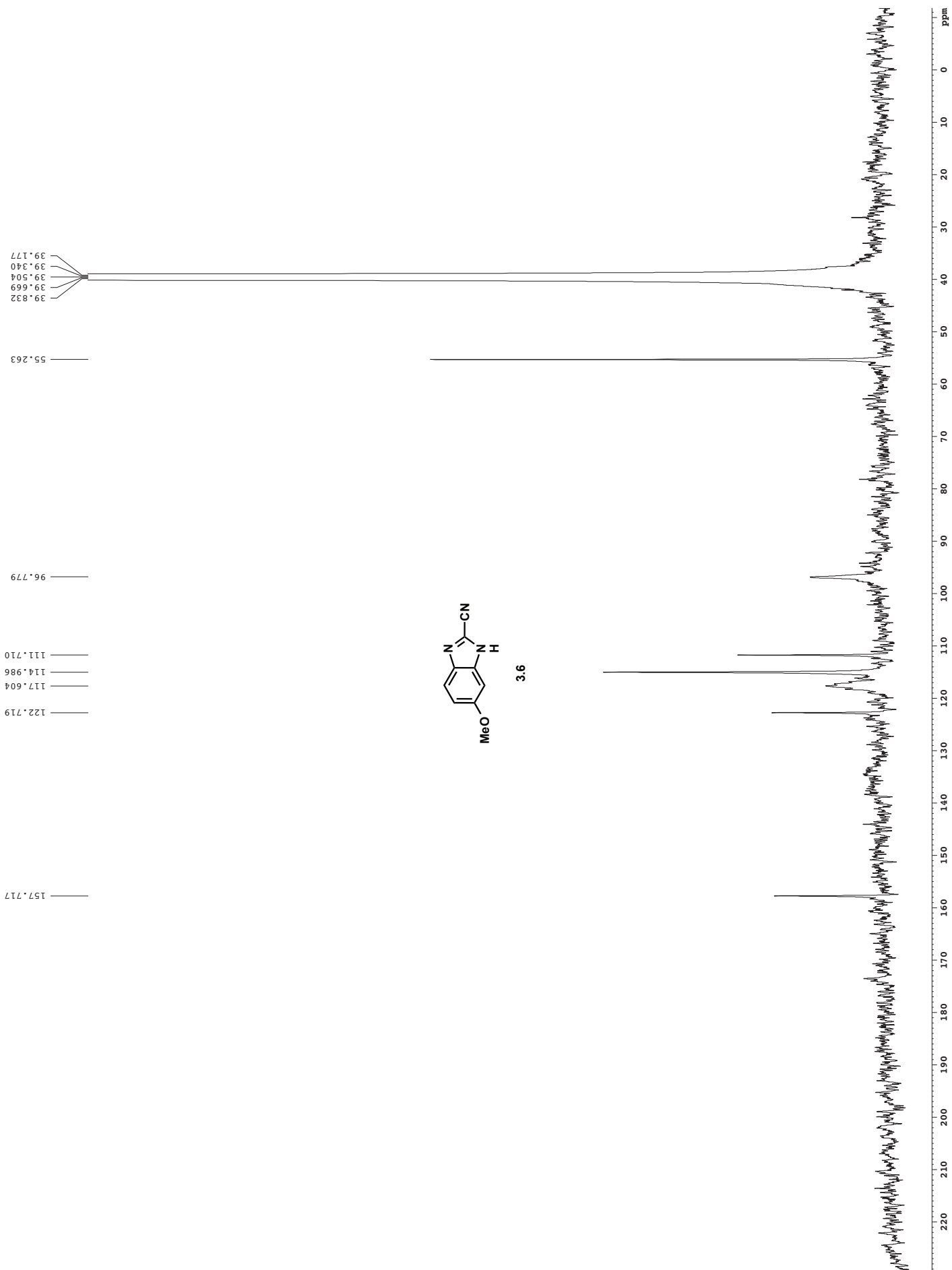
7.848



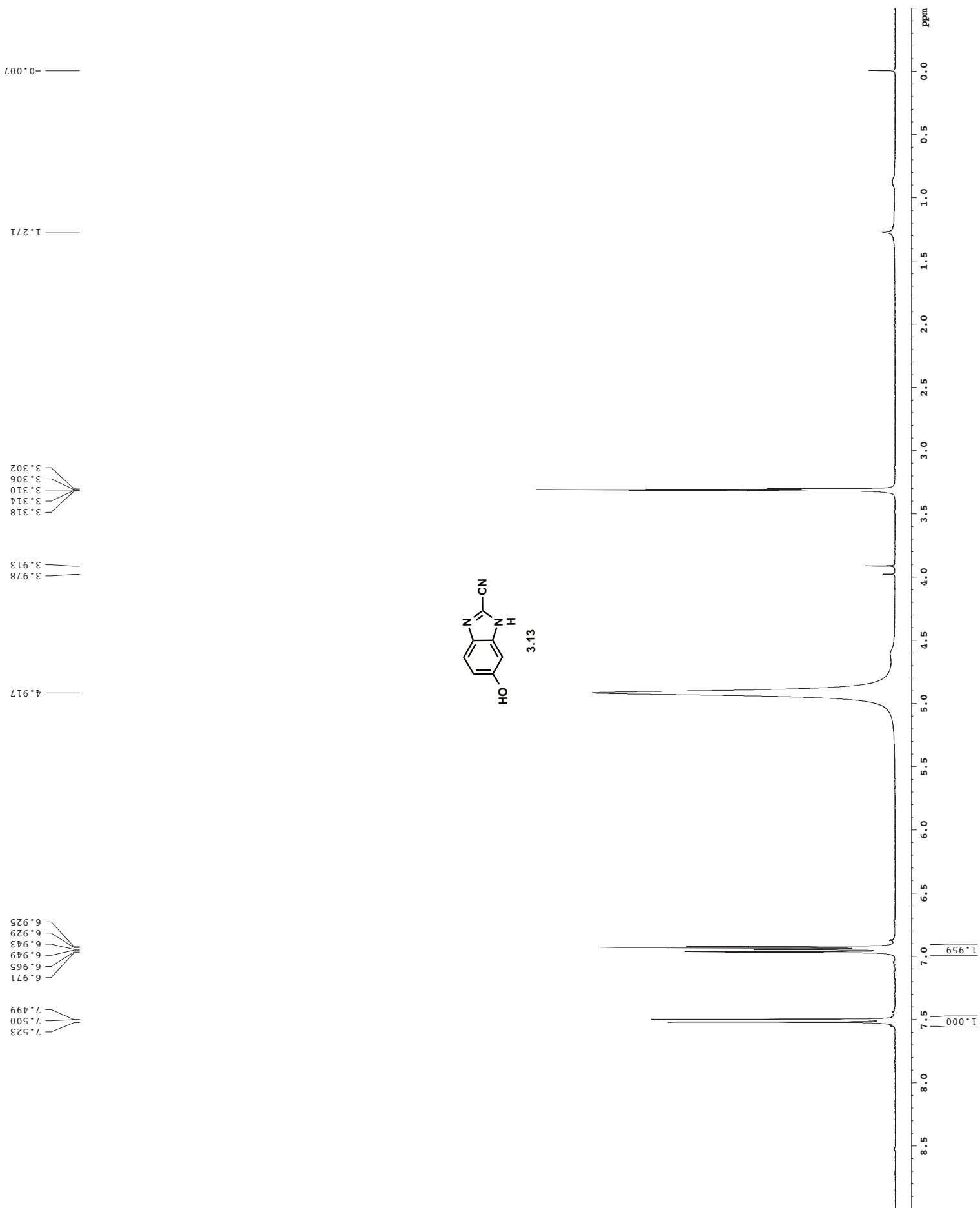
S25

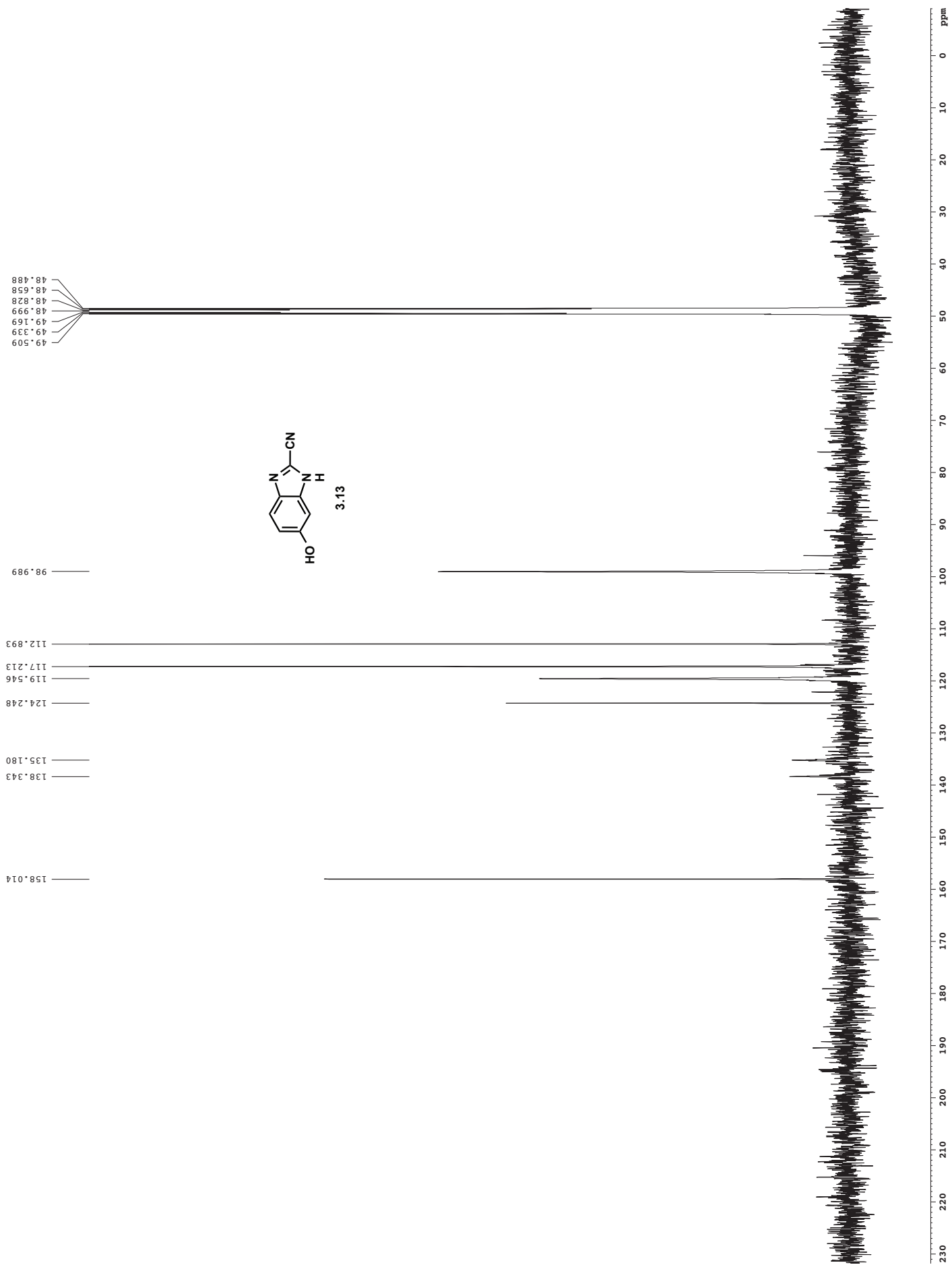
S26



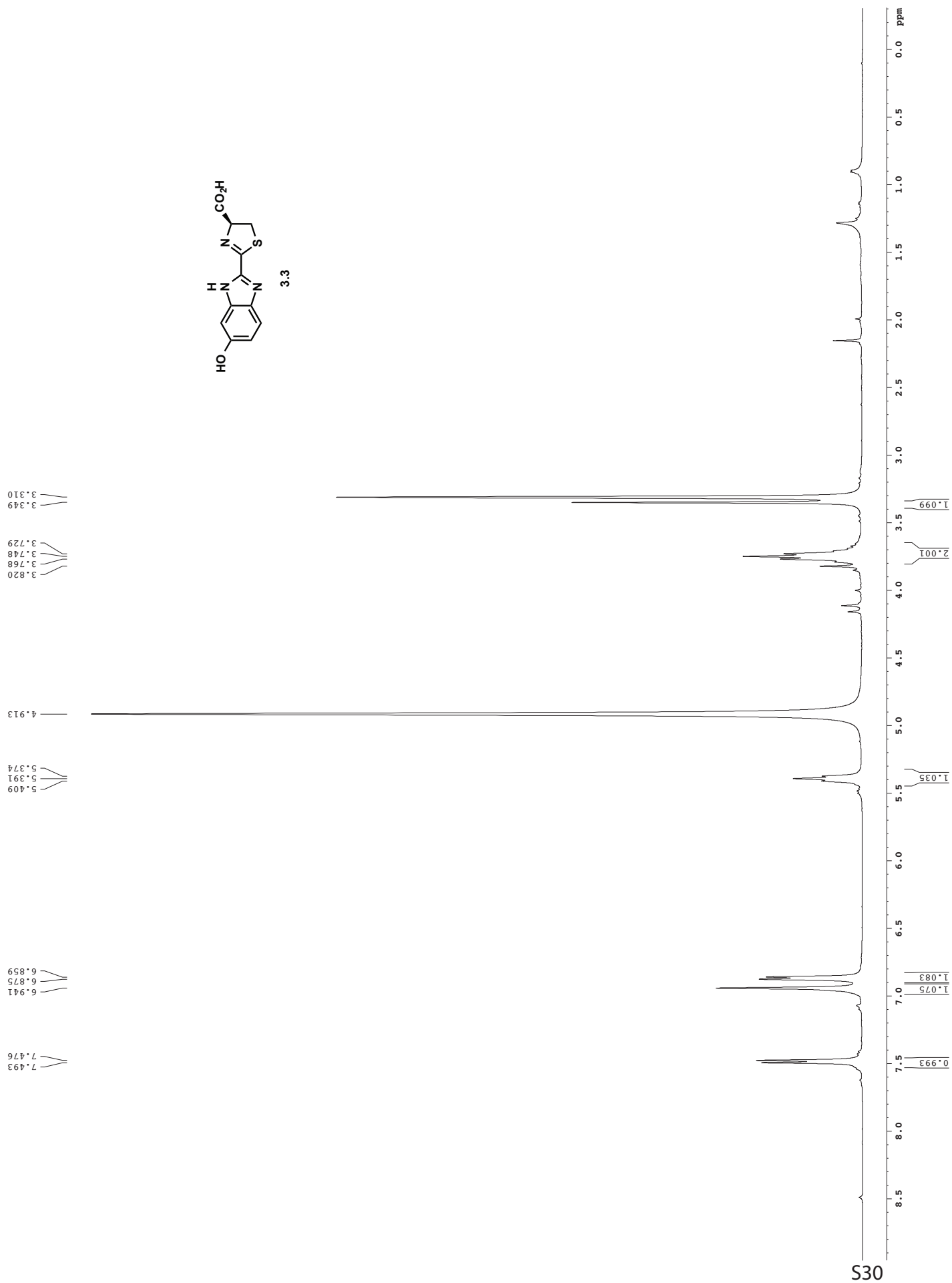


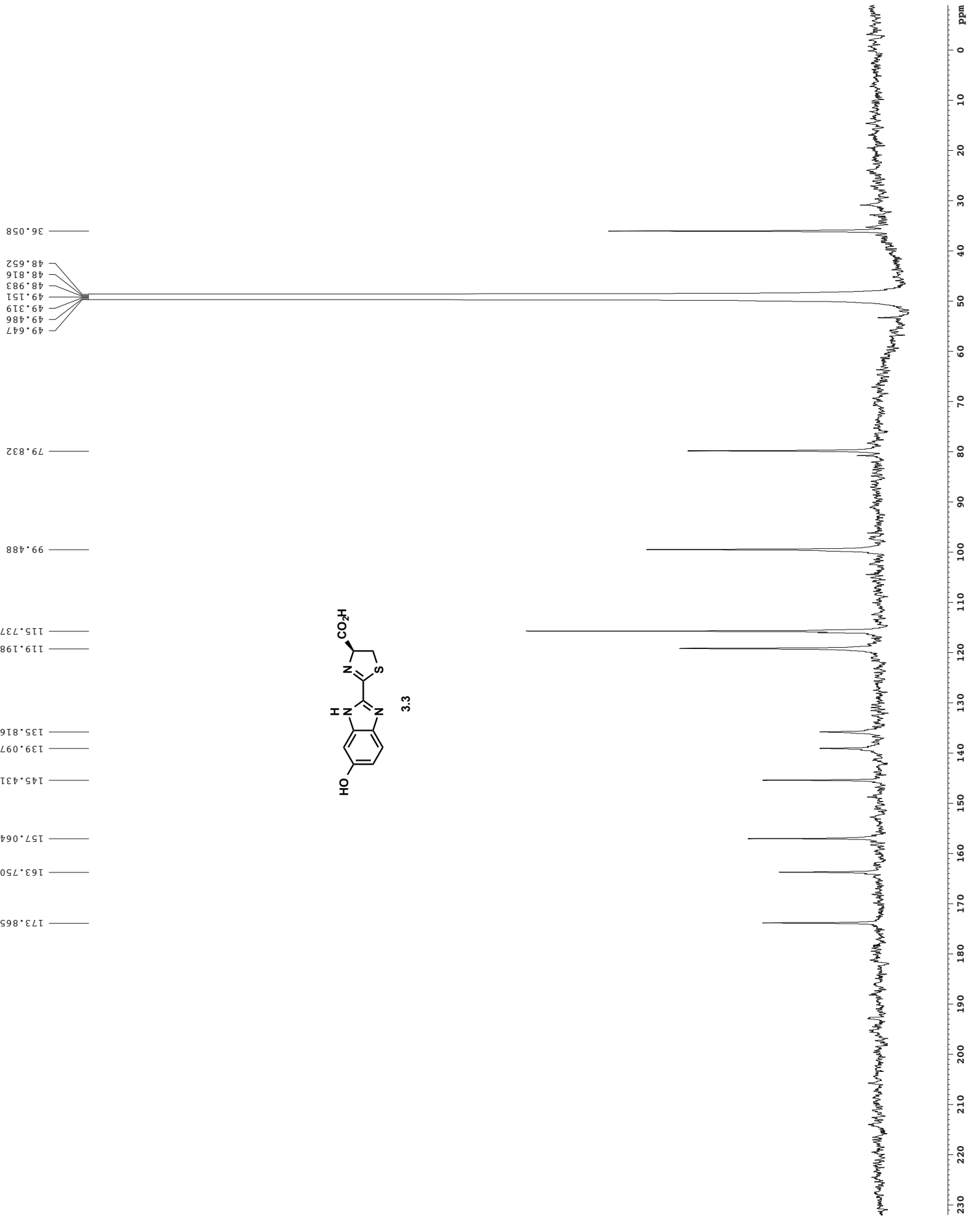
S27



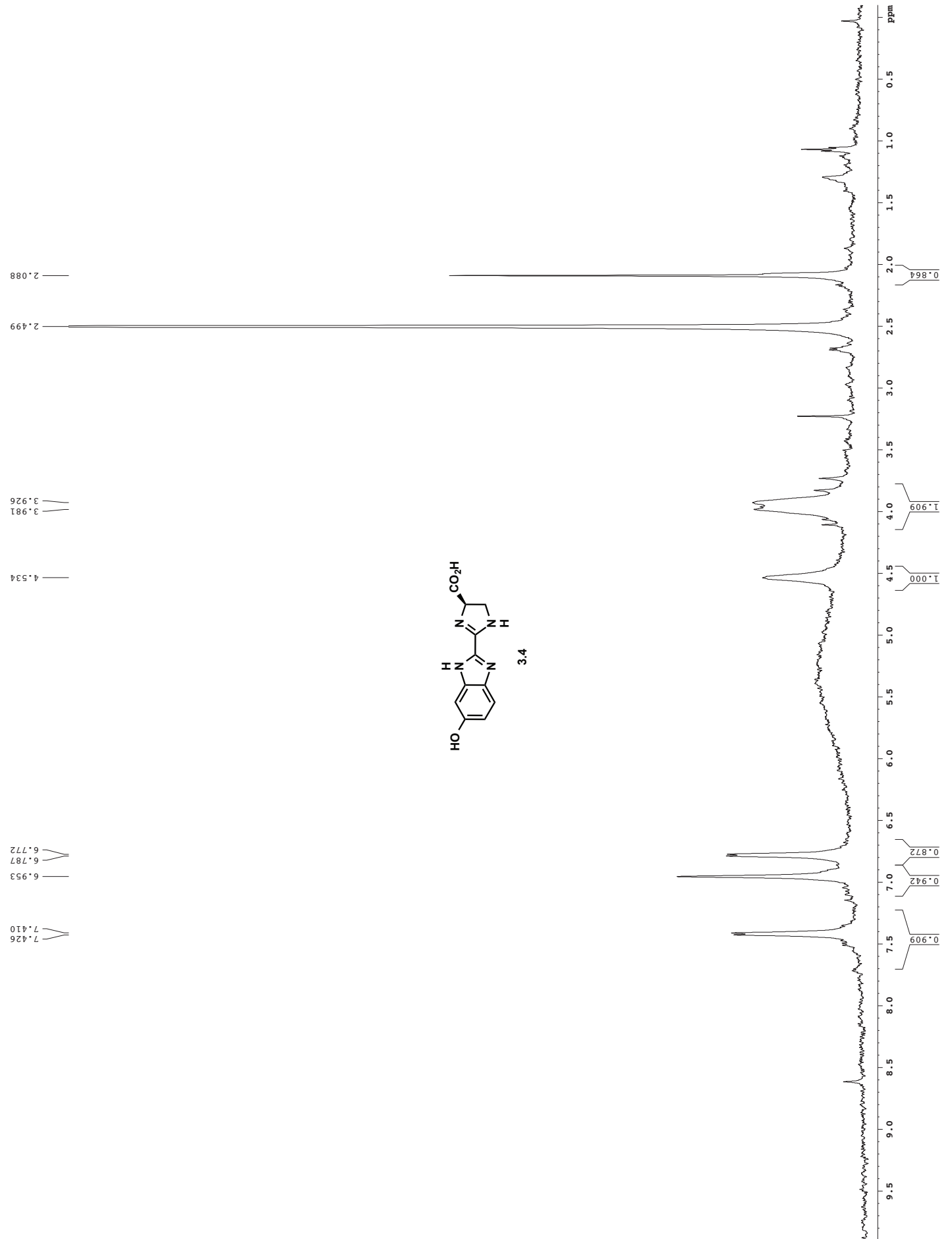


S29

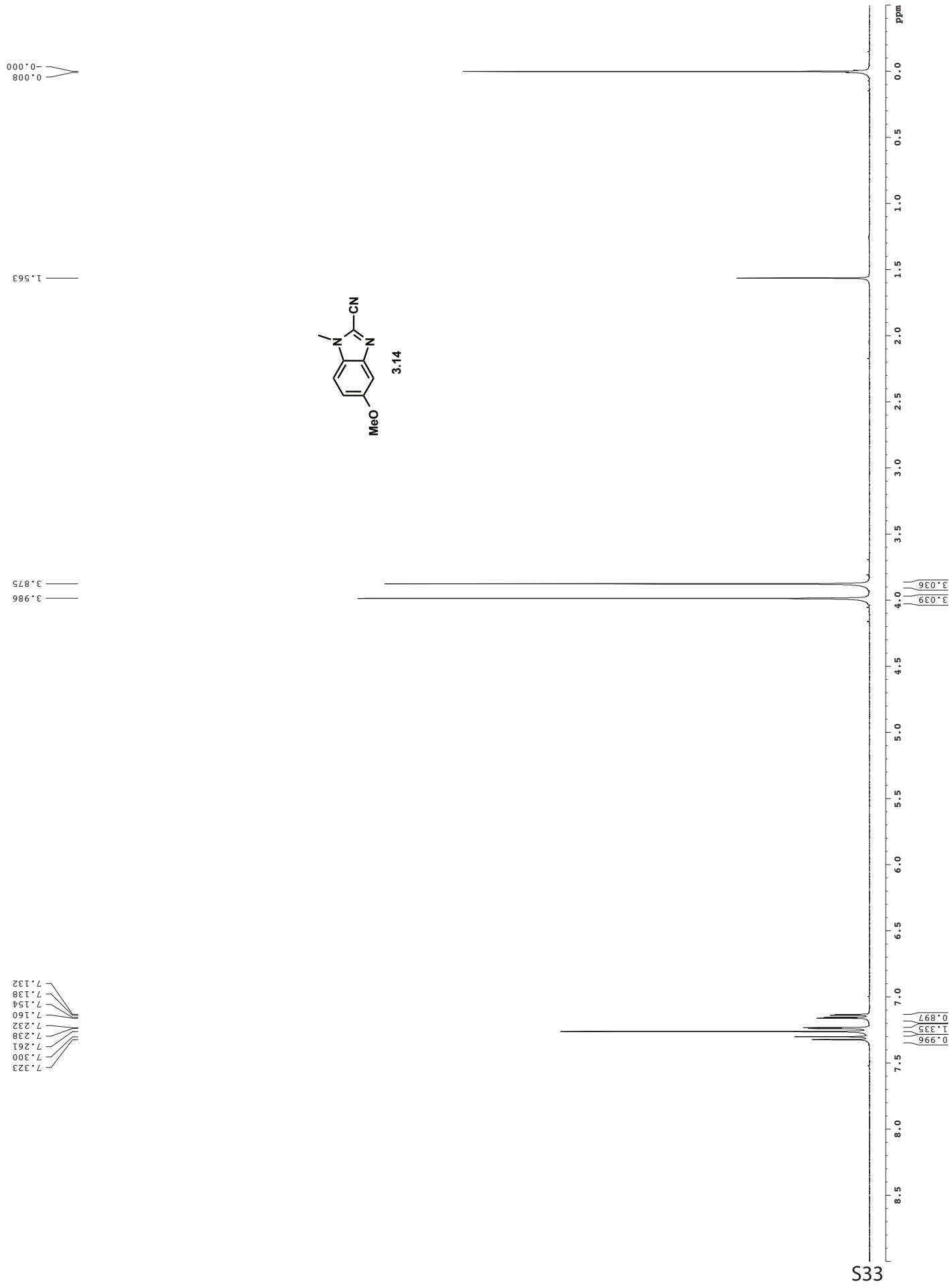




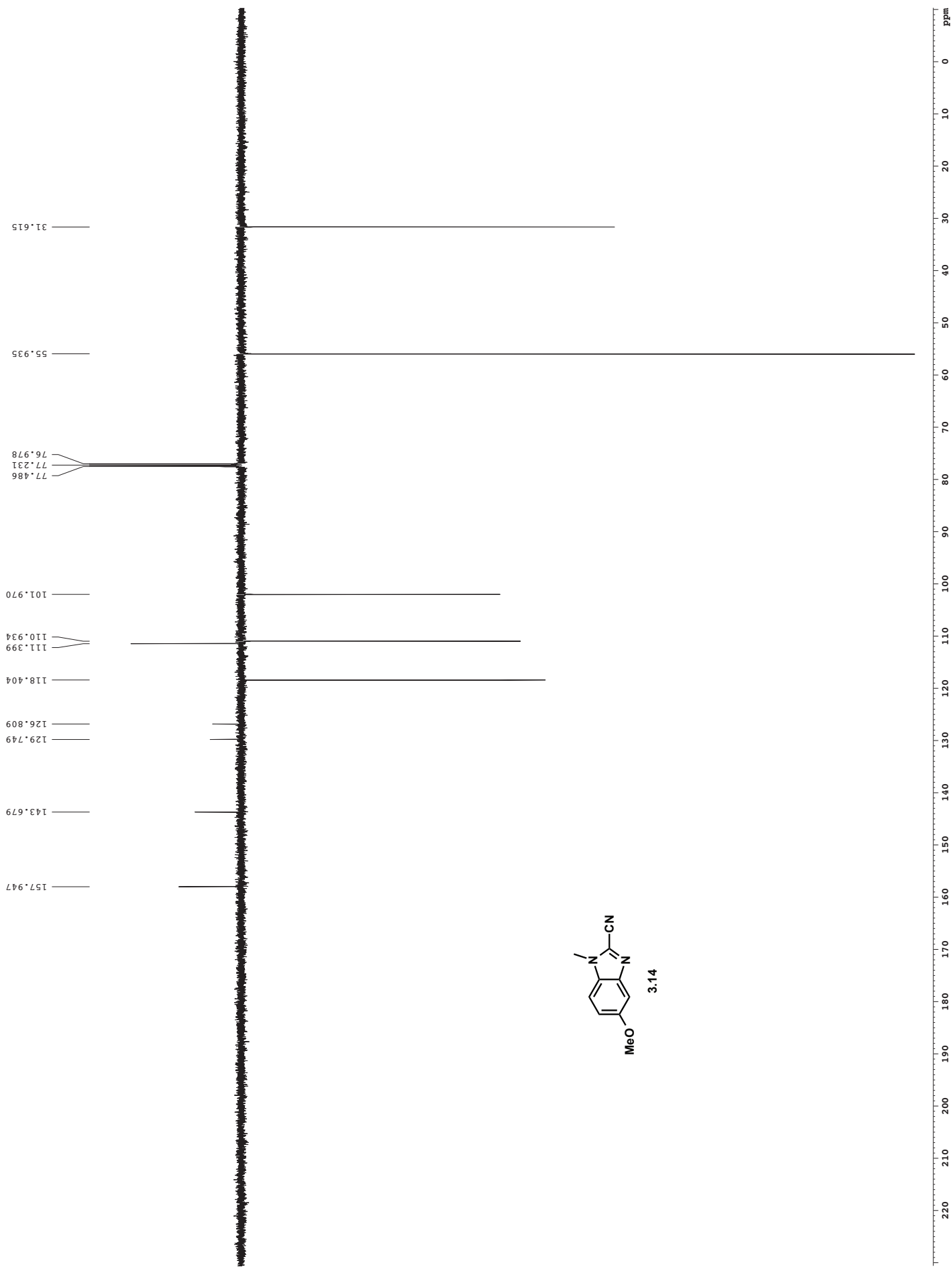
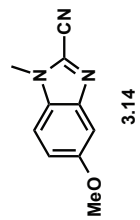
S31

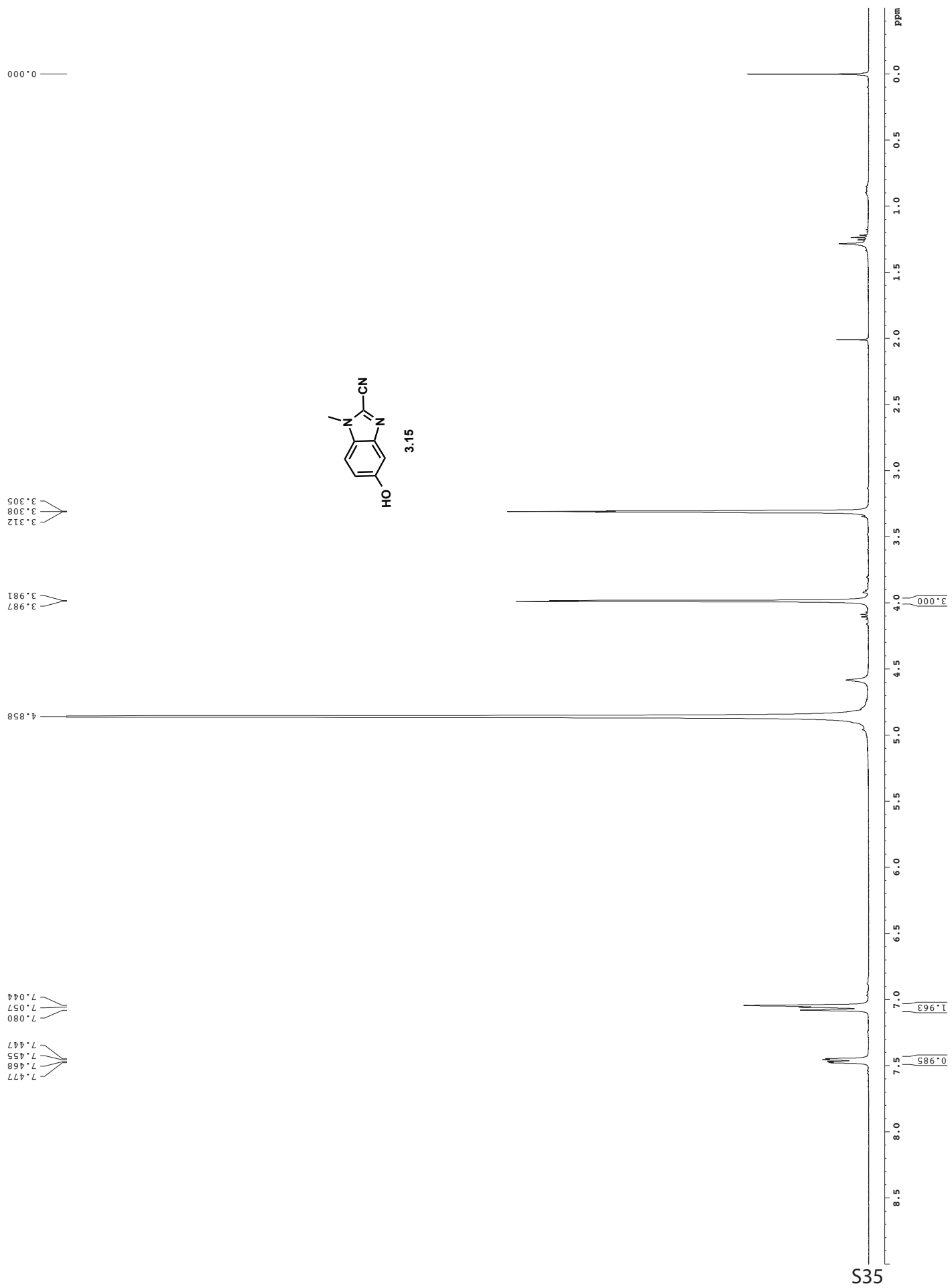


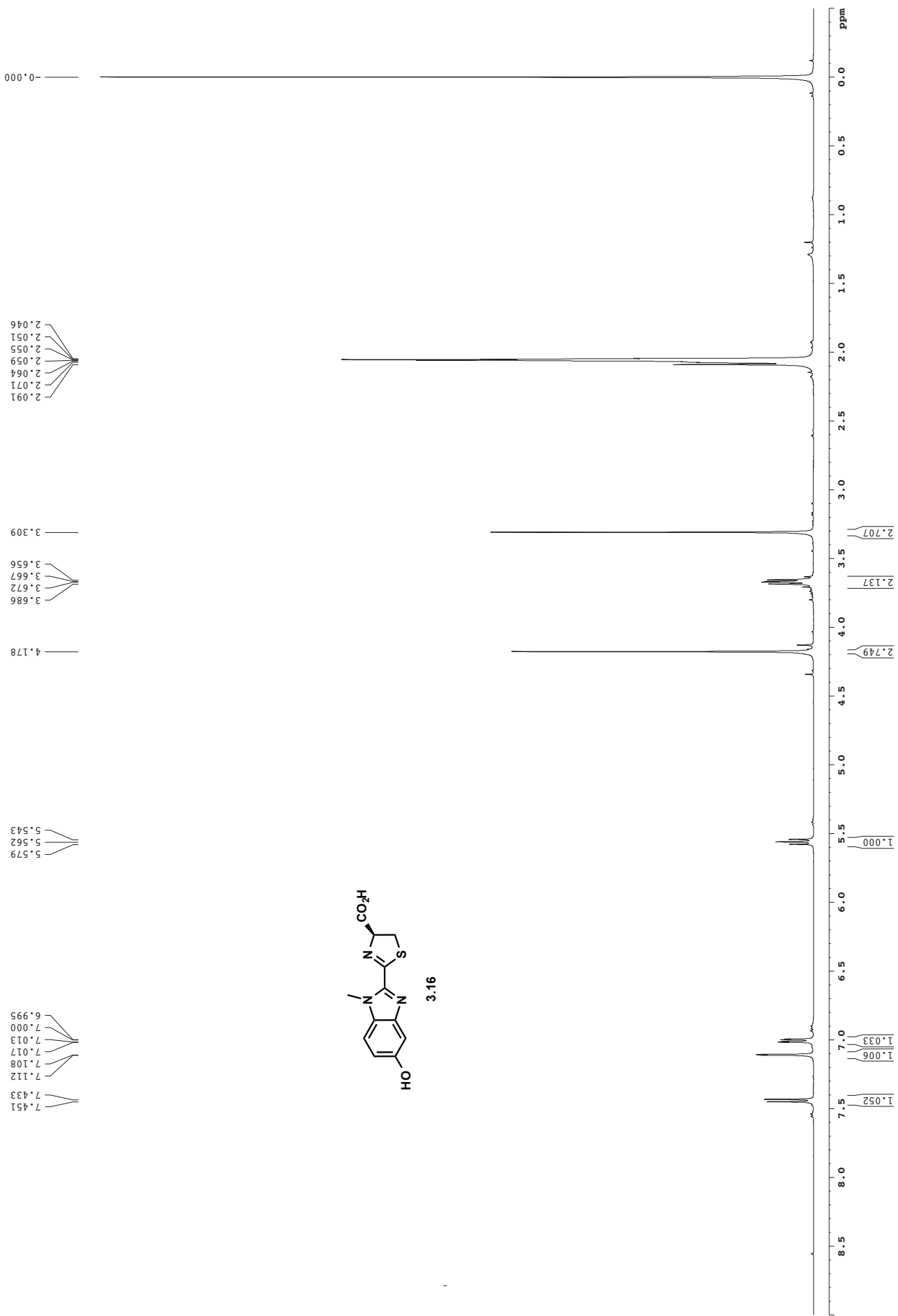
S32

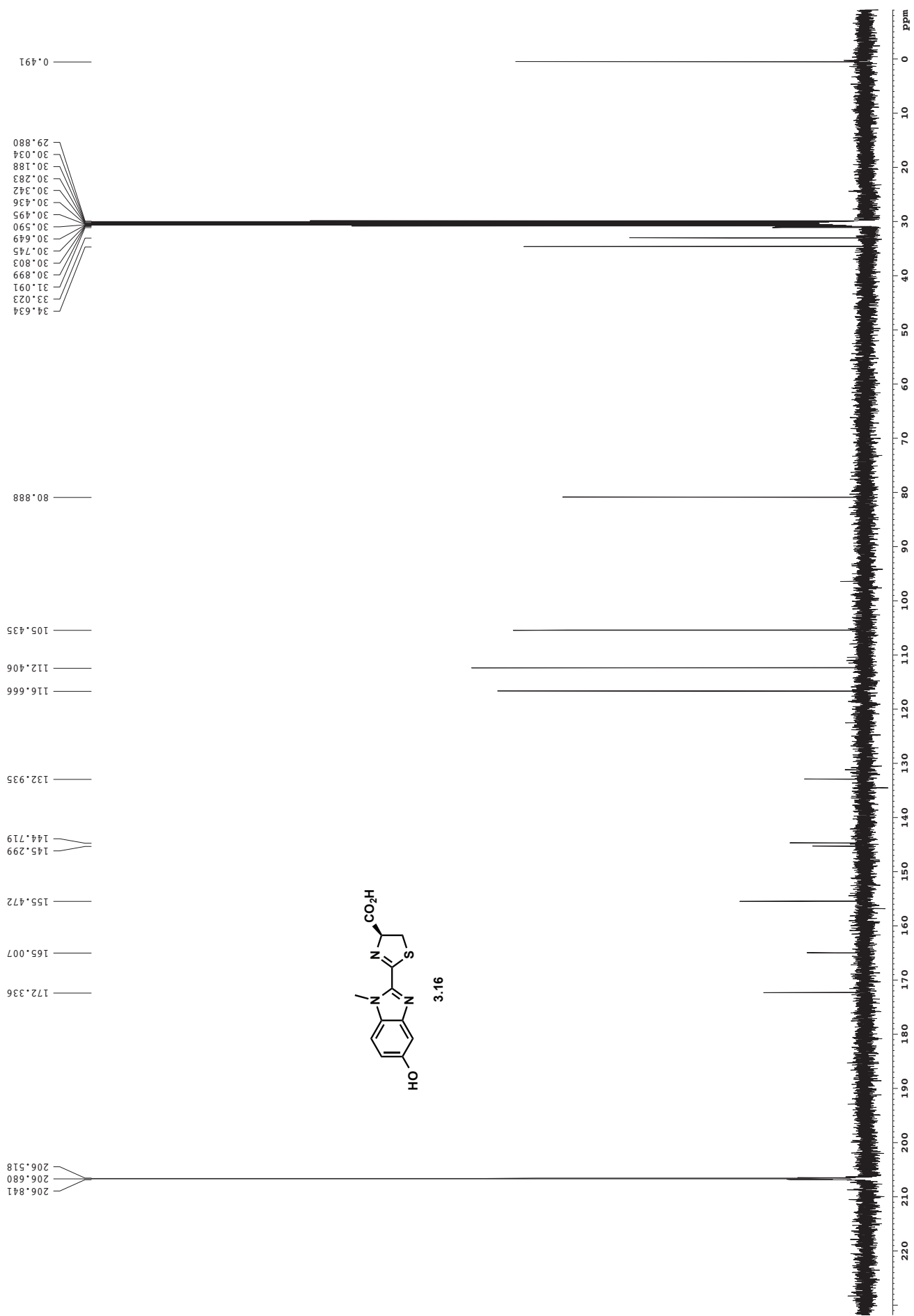


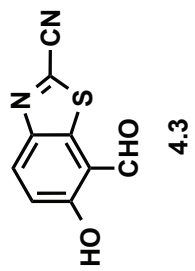
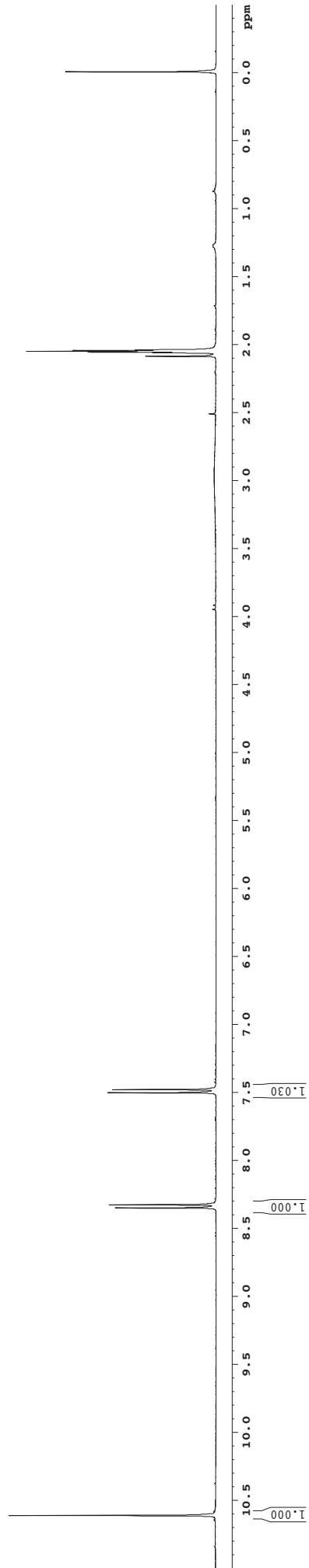
S33





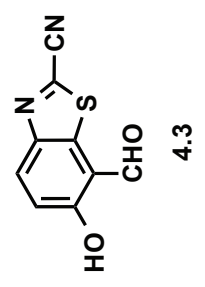


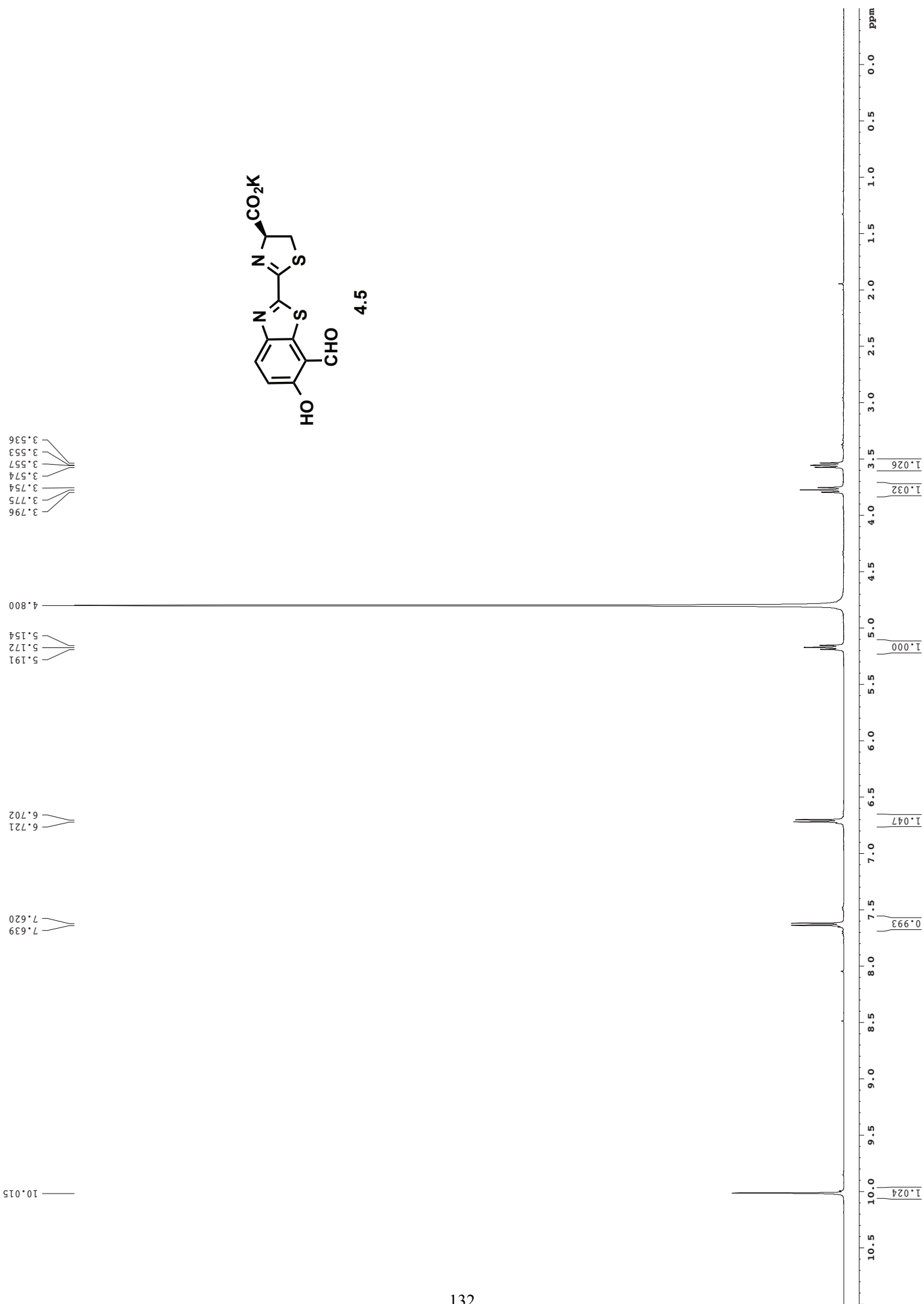


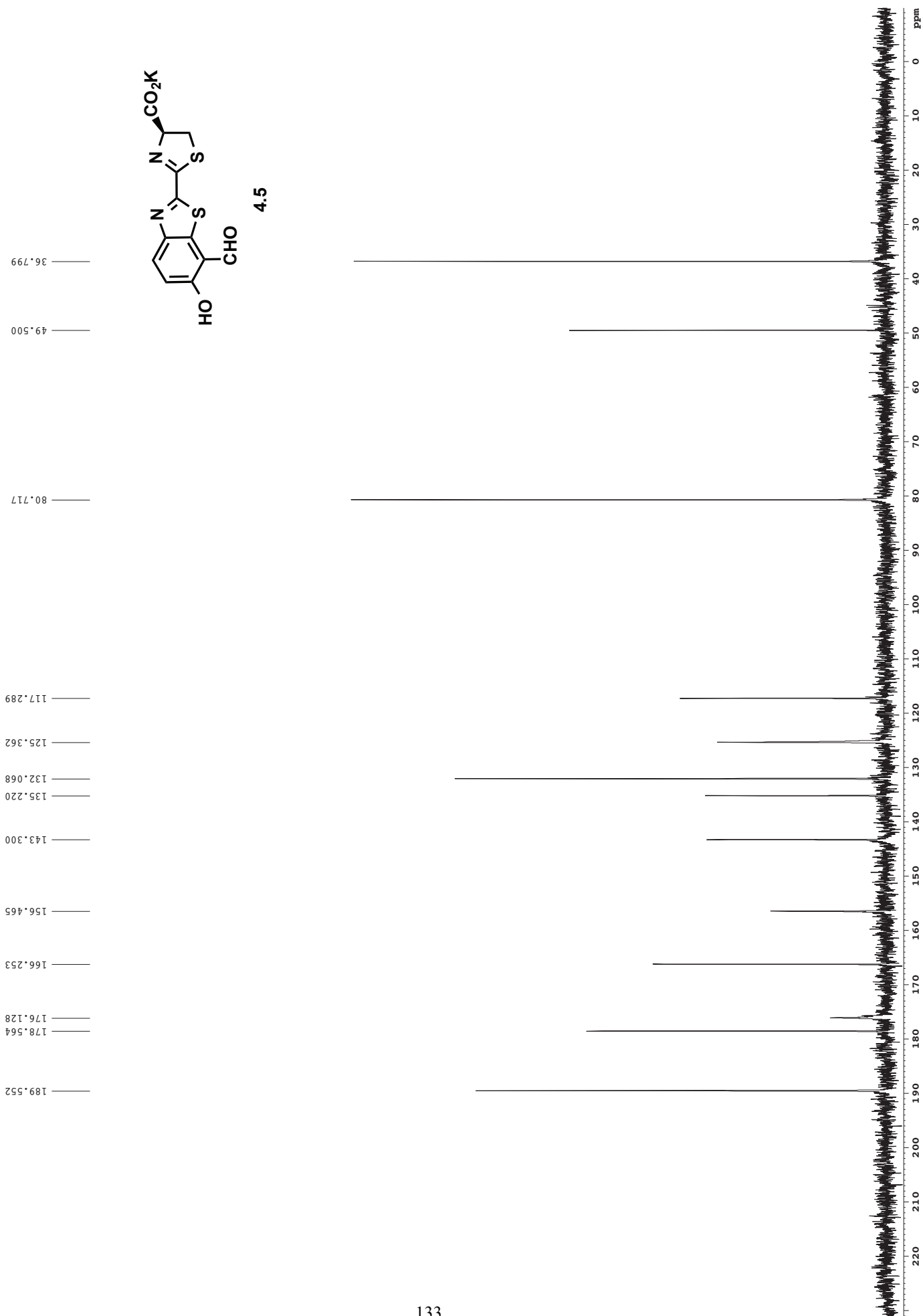


30.791
30.637
30.578
30.484
30.330
30.176
30.022
29.868

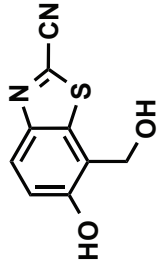
206.833
206.679
206.511
188.116
163.967
148.394
138.718
135.208
133.590
120.812
117.689
114.690







2.086
2.056
2.050
2.045

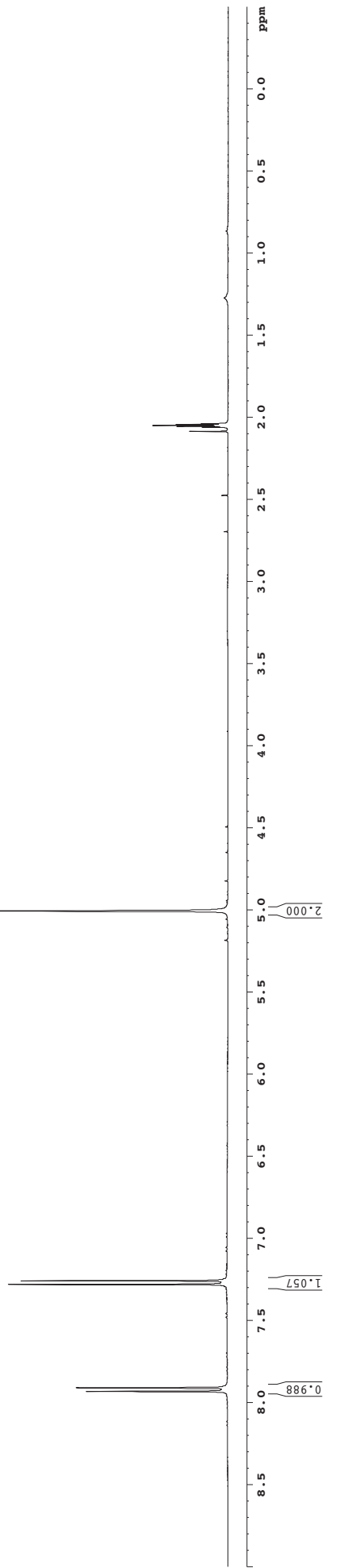


4.6

5.008

7.282
7.260

7.931
7.909



30.611
30.457
30.303
30.149
29.995
29.841
29.688

59.147

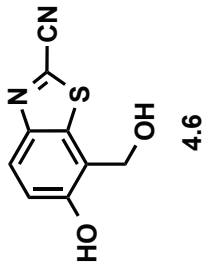
114.857
118.792
122.001
124.850

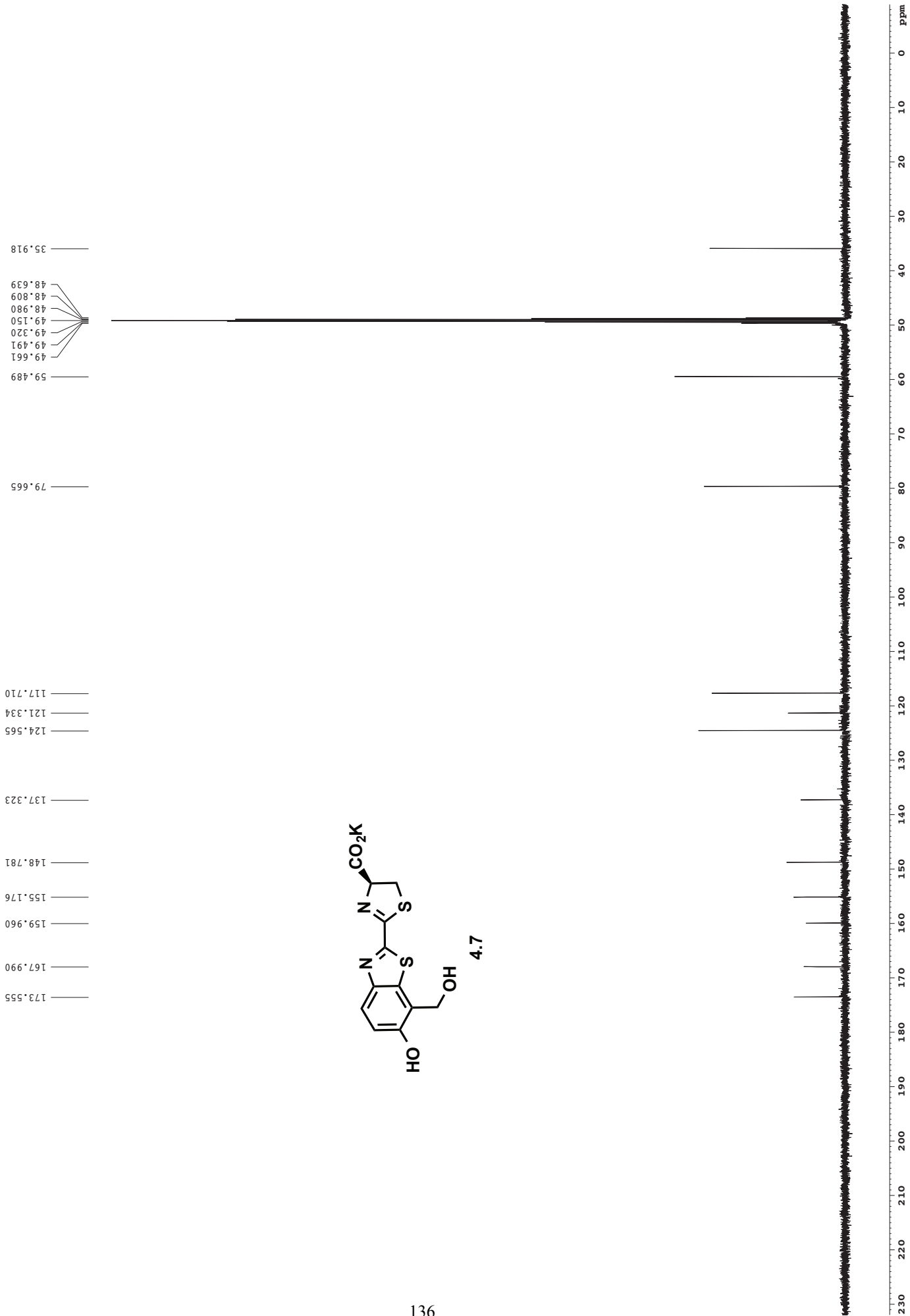
135.282
136.346

148.346

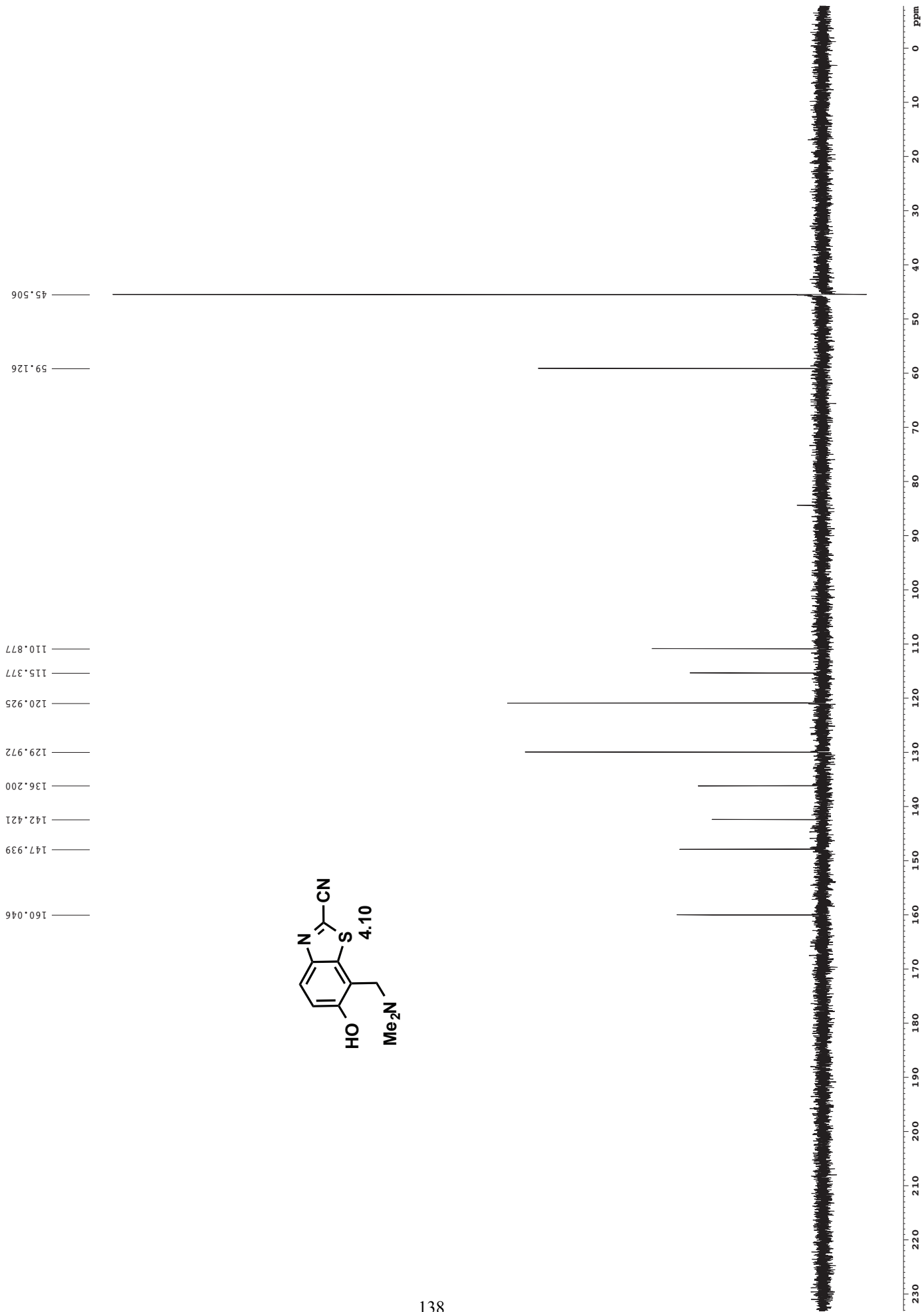
154.816

206.678







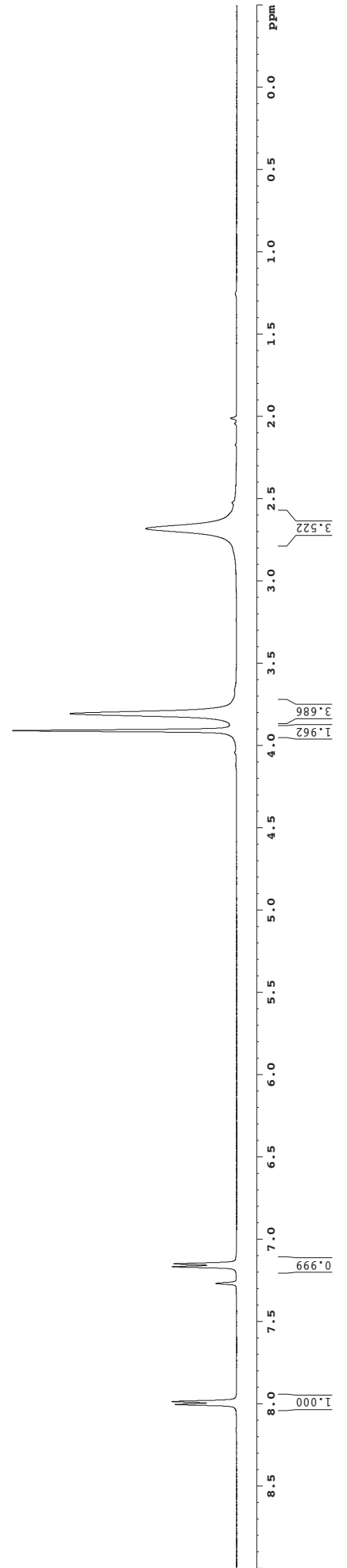
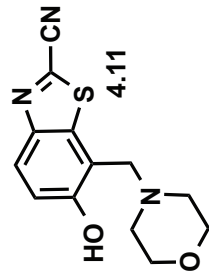


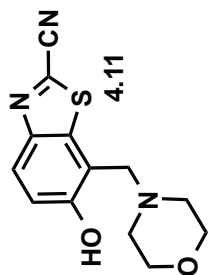
2.683

3.807
3.911

7.151
7.169
7.270

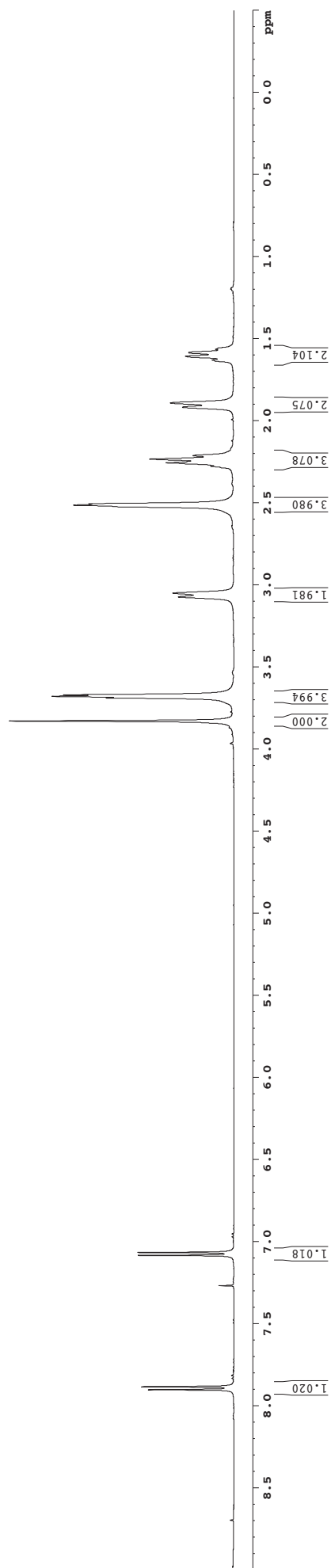
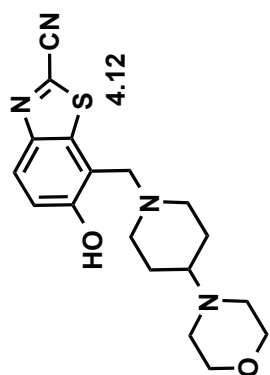
7.985
8.003





158.700
146.353
136.780
132.130
125.508
119.701
113.452
111.612
77.482
77.228
76.974
66.714
61.238
53.189





1.586
1.608
1.631
1.893
1.918
2.213
2.235
2.257
2.279
2.507
2.515

3.051
3.075

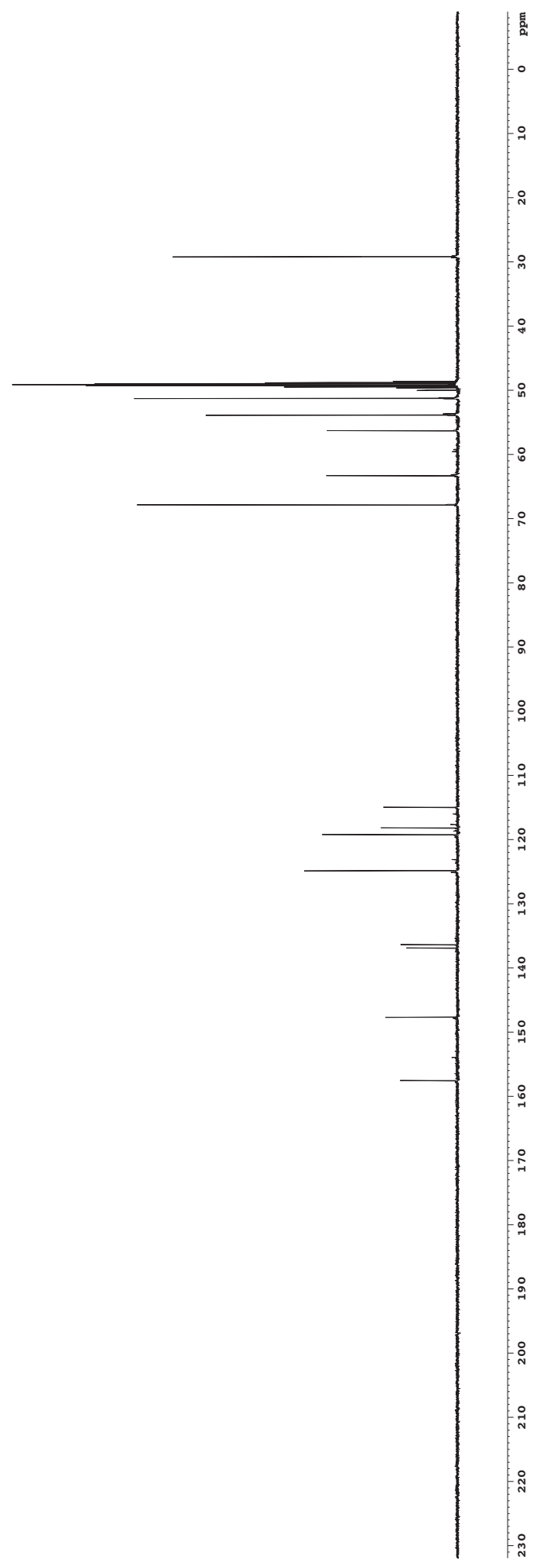
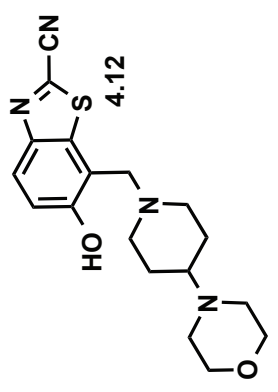
3.671
3.680
3.689
3.830

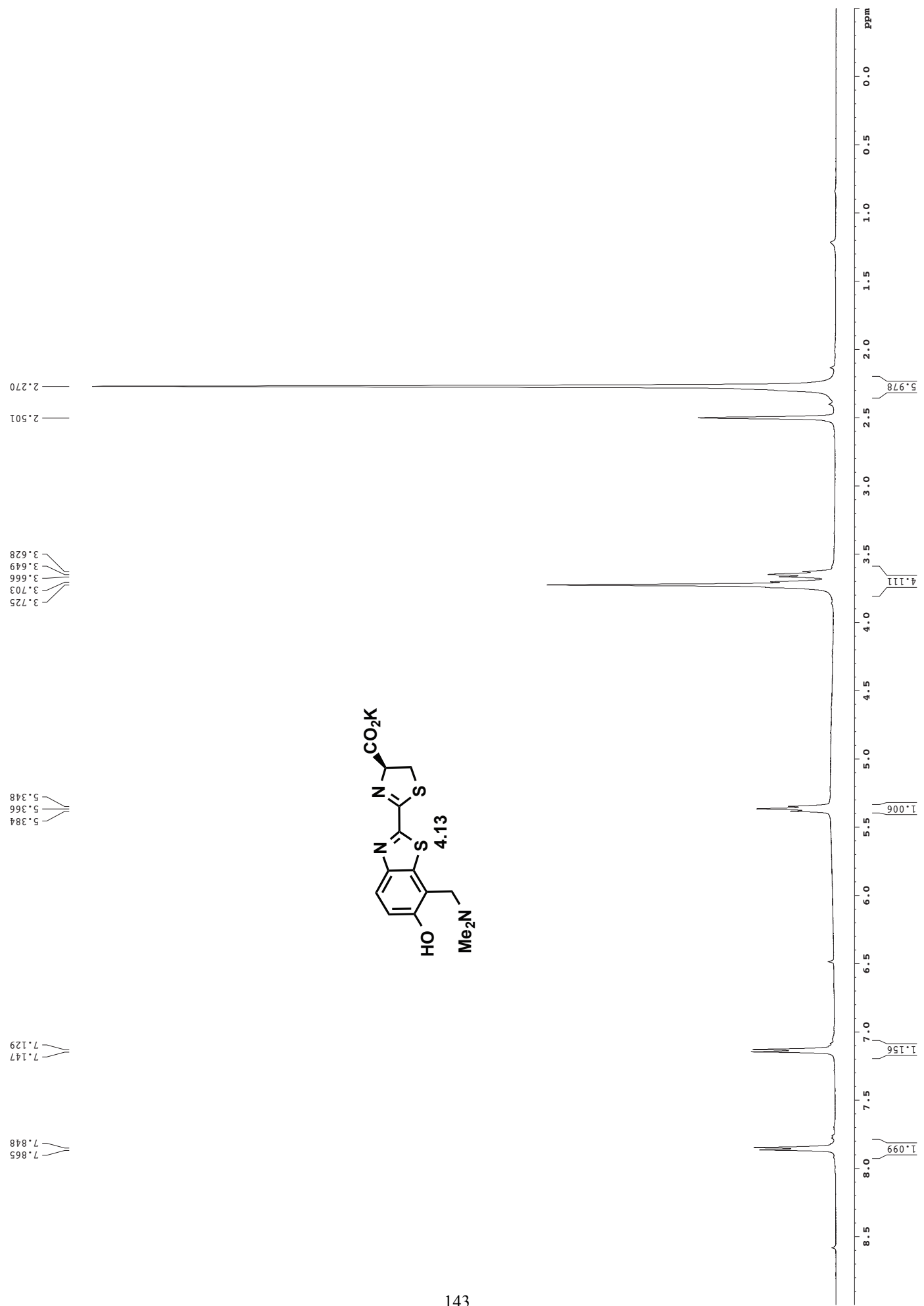
7.068
7.086
7.270

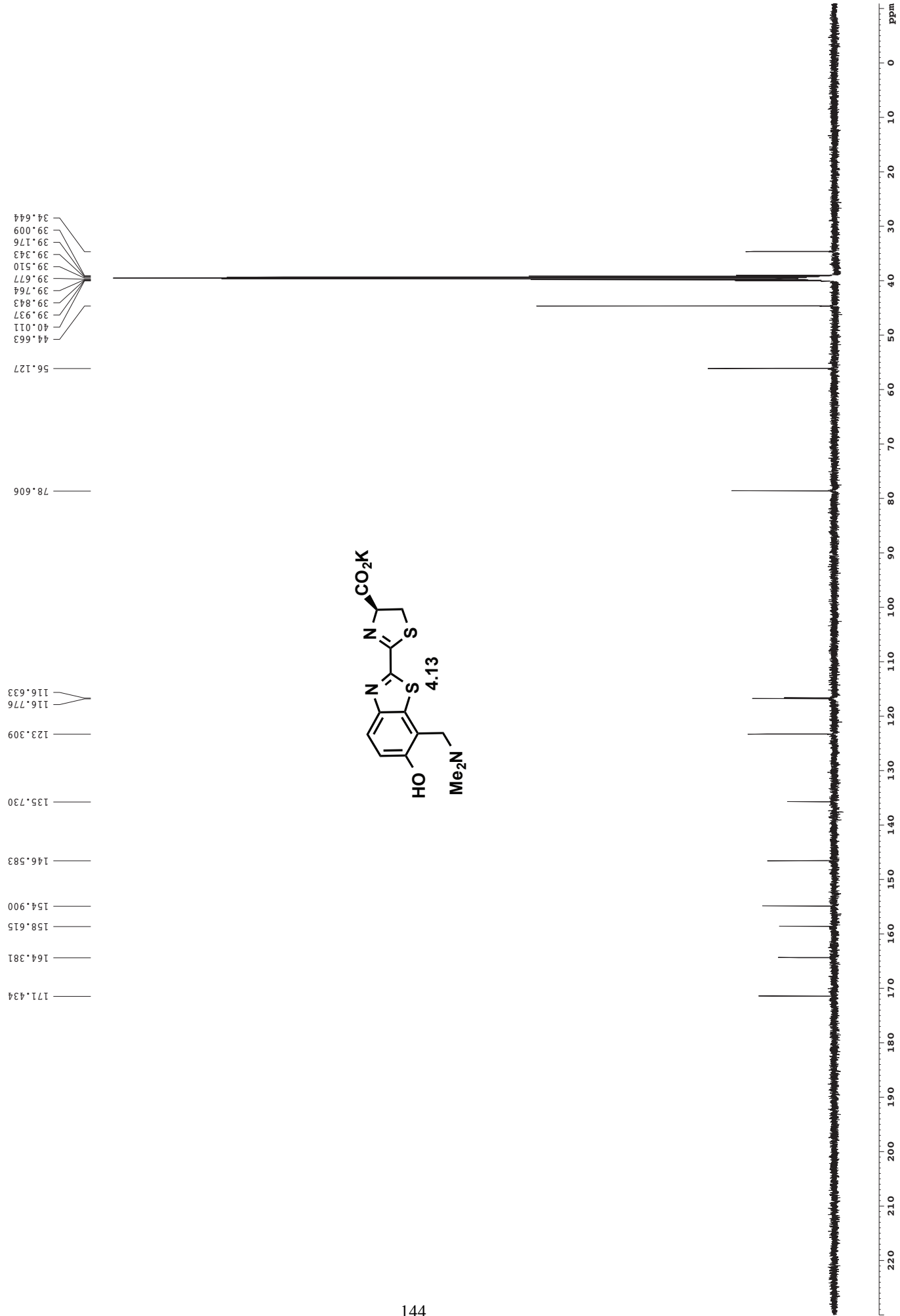
7.886
7.904

67.861
63.322
56.315
53.907
53.673
51.308
51.186
49.999
49.660
49.490
49.320
49.150
48.979
48.809
48.639
29.207

157.572
147.700
136.921
136.396
124.872
119.254
118.205
114.975

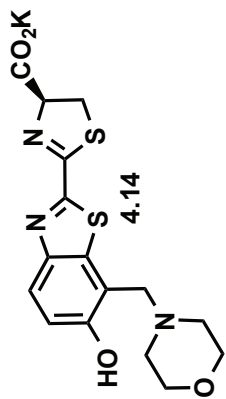




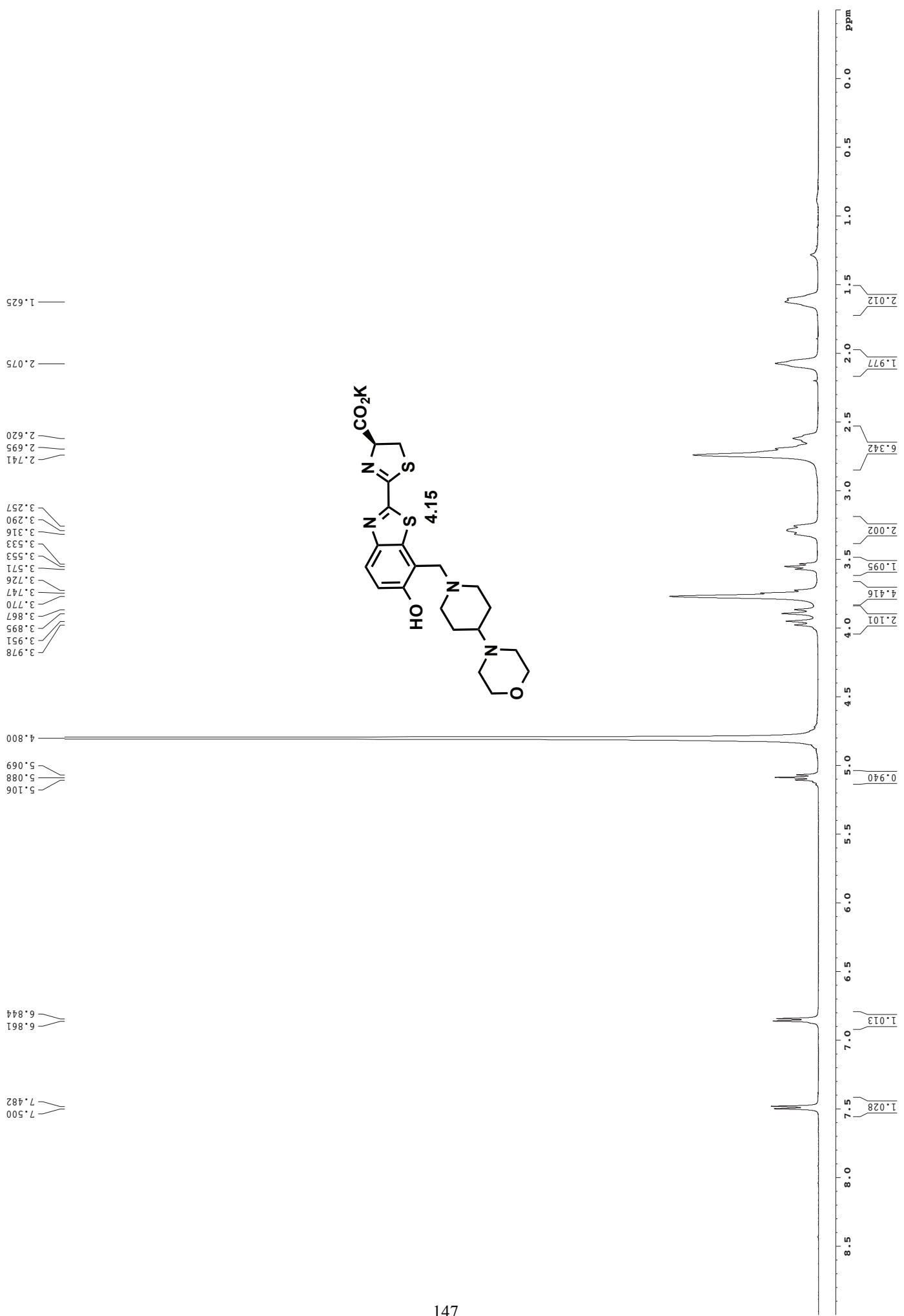


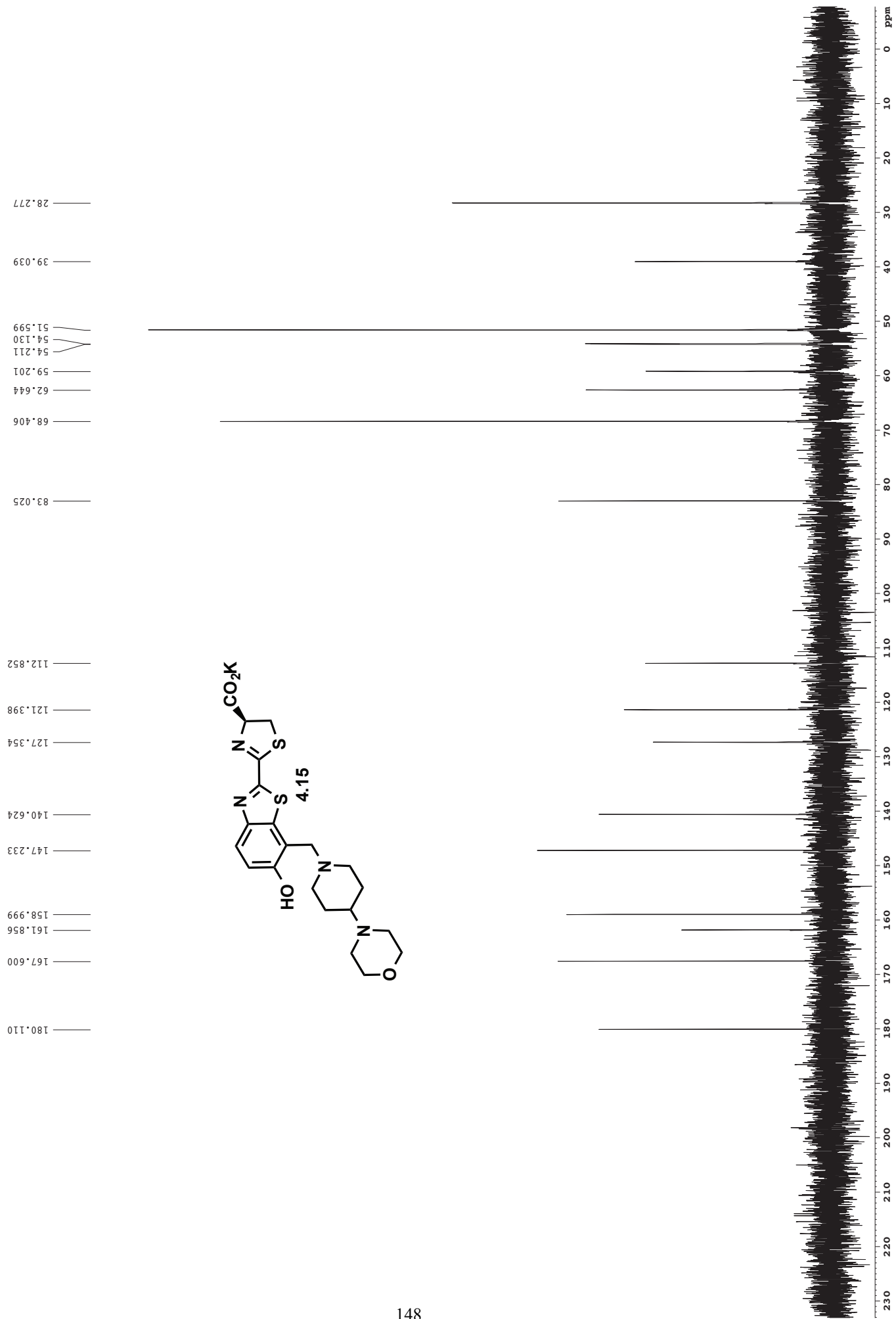


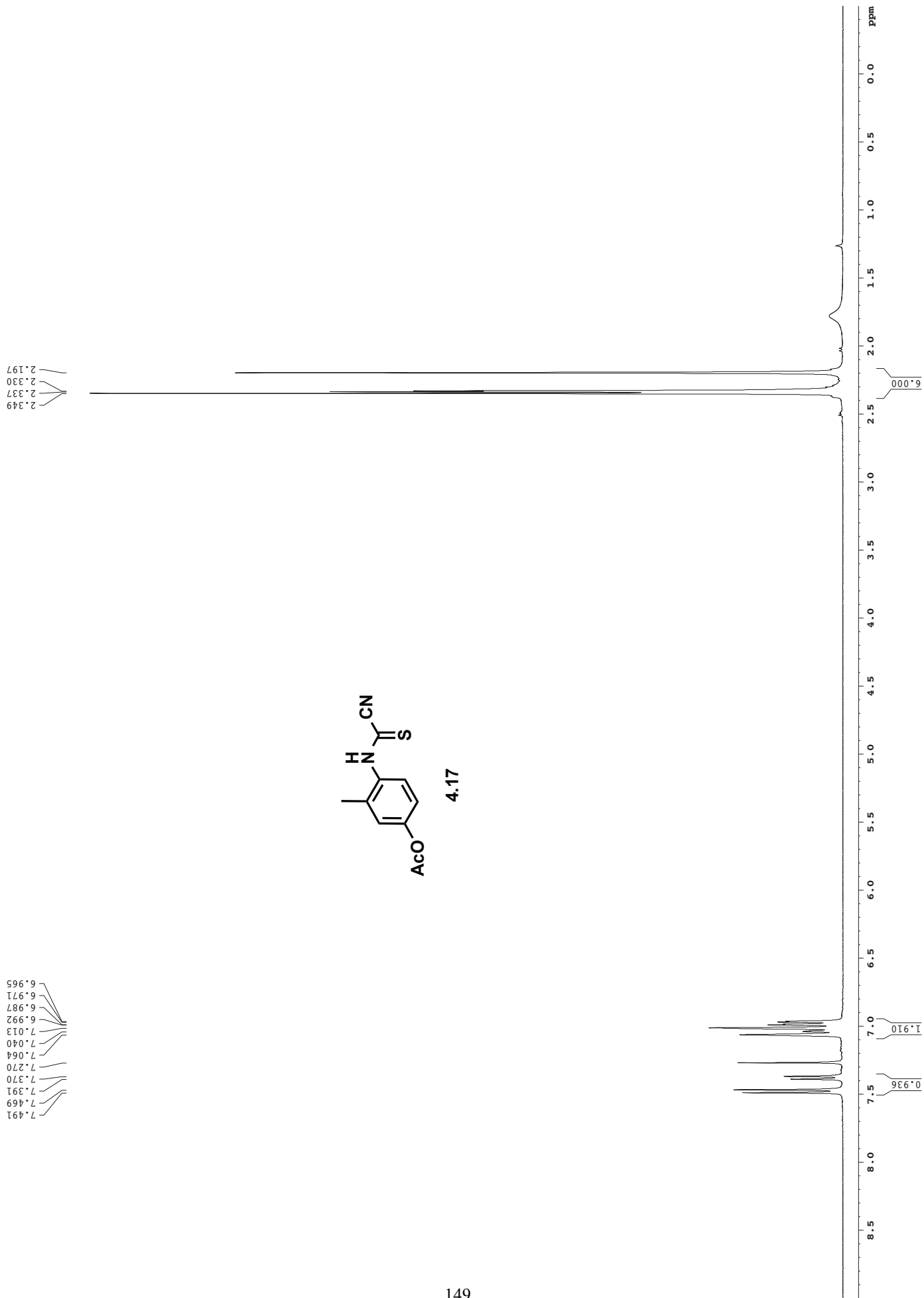
180.237
167.857
160.133
158.616
148.121
139.652
126.455
120.342
115.052
83.008
68.450
60.147
55.003
39.055



230 220 210 200 190 180 170 160 150 140 130 120 110 100 90 80 70 60 50 40 30 20 10 0 ppm







17.965
21.317

76.975
77.229
77.483

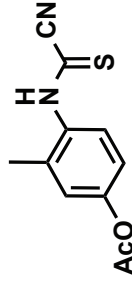
116.828
120.183
124.320

132.556

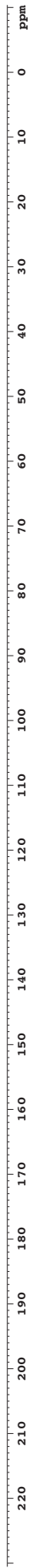
147.578
148.107
148.664

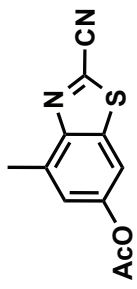
158.337

169.642



4.17

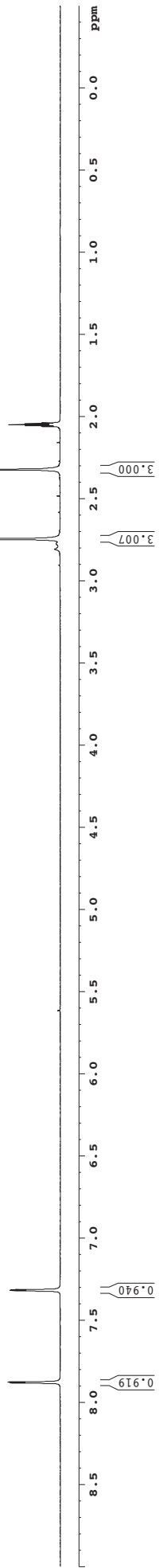


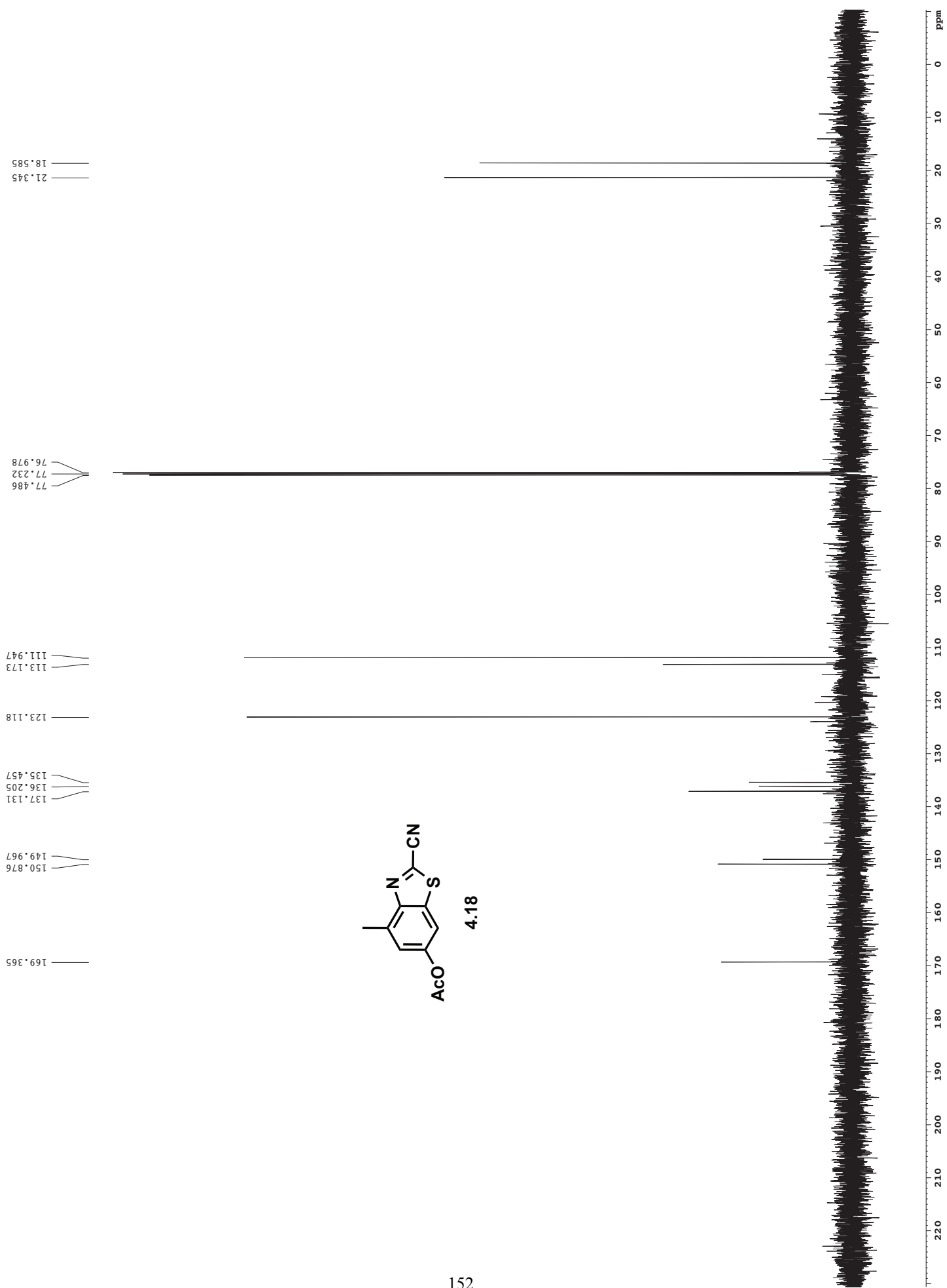


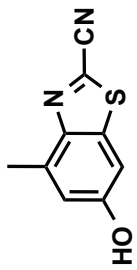
4.18

2.045
2.050
2.055
2.324
2.745
2.747
2.748

7.315
7.318
7.321
7.323
7.877
7.878
7.882
7.884







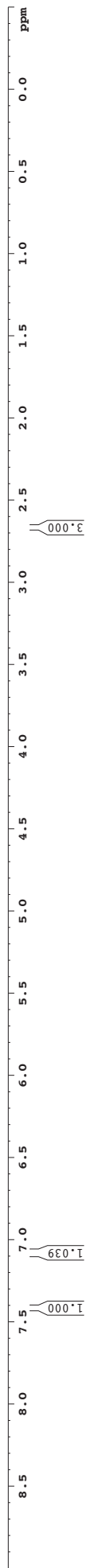
4.21

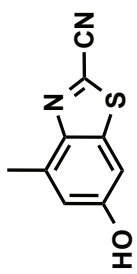
2.086
2.054
2.050
2.046

2.666

7.077

7.418
7.414





4.21

18.651
29.845
29.999
30.153
30.307
30.460
30.614
30.768

105.185

114.844

119.815

132.700

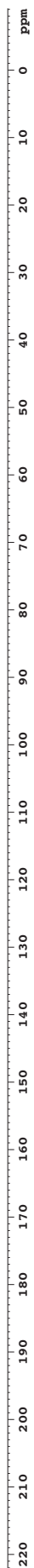
137.613

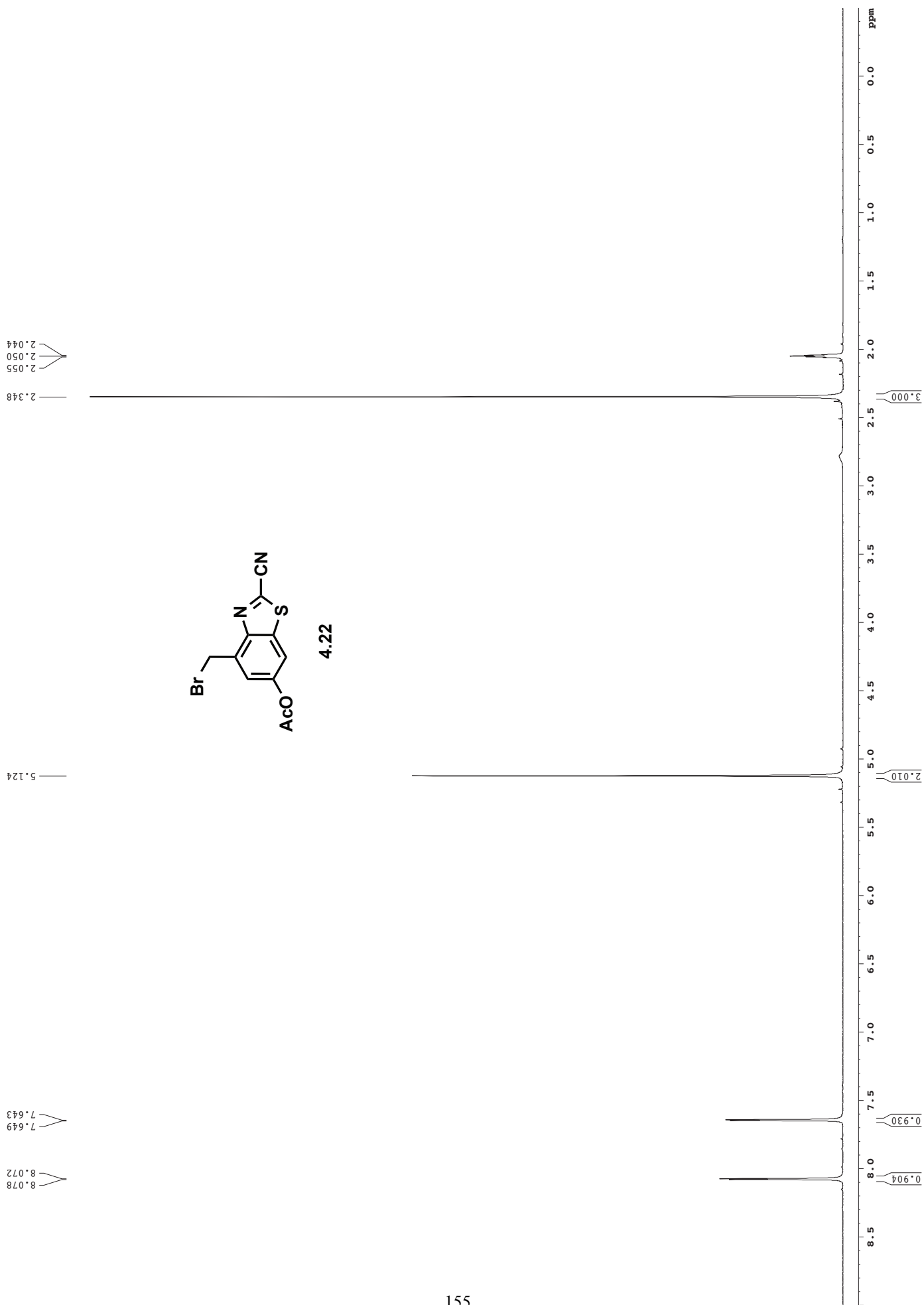
139.054

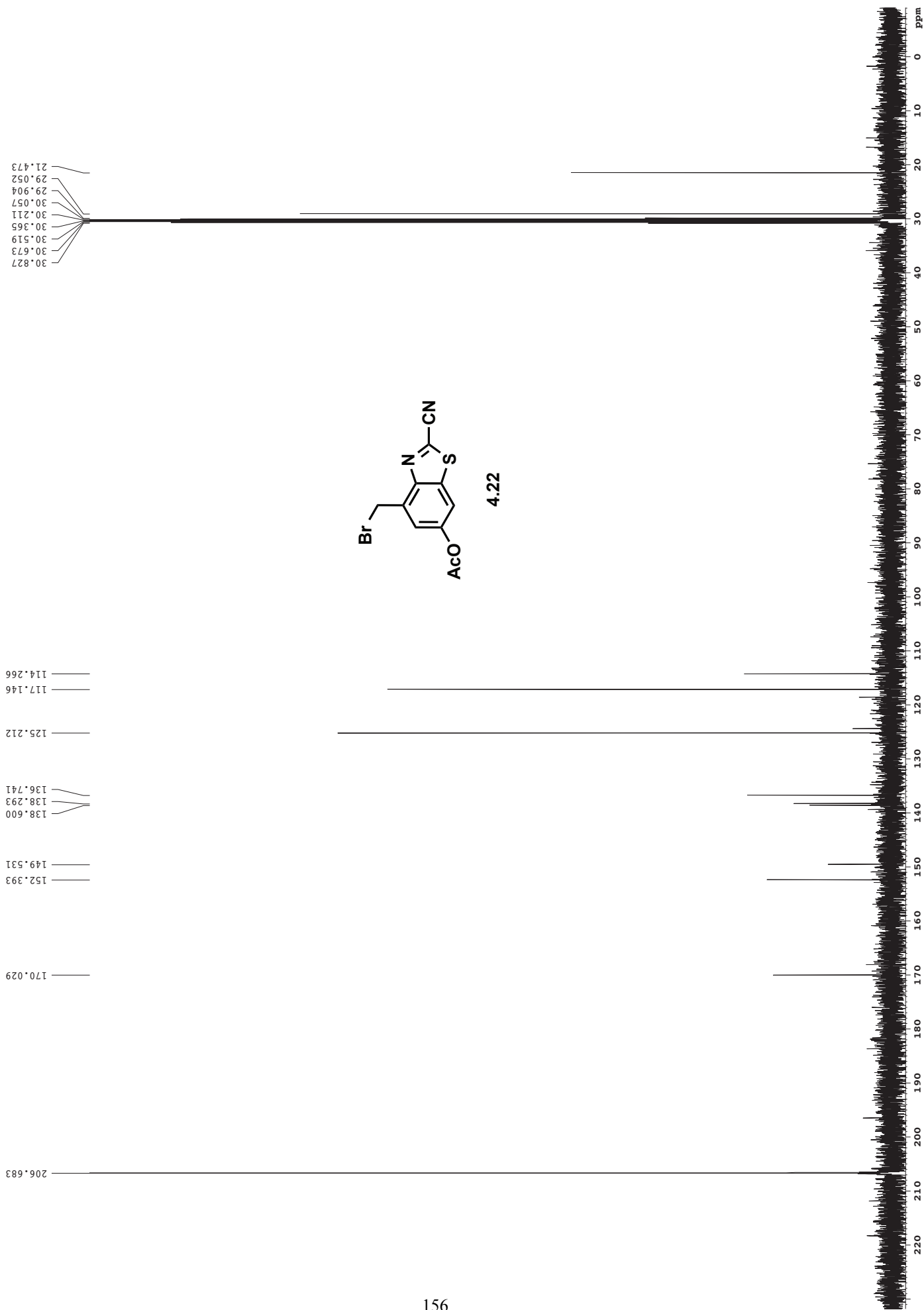
147.355

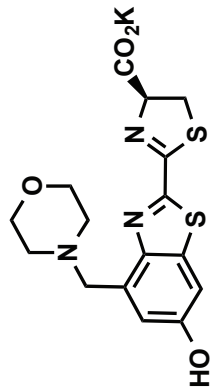
159.947

206.678









- 3.933
- 3.907
- 3.854
- 3.828
- 3.750
- 3.741
- 3.731
- 3.709
- 3.593
- 3.576
- 3.571
- 2.630
- 2.622

- 4.800
- 5.186
- 5.168
- 5.150

- 6.862
- 7.088

